Development of Highly Sensitive and Portable Nanofiber Biosensor for On-site Toxicant Detection

by

CUNYI ZHAO
DISSERTATION

Submitted in partial satisfaction of the requirements for the degree of

DOCTOR OF PHILOSOPHY

in

Agricultural and Environmental Chemistry

in the

OFFICE OF GRADUATE STUDIES

of the

UNIVERSITY OF CALIFORNIA

DAVIS

Approved:

_____

GANG SUN, Chair

_____

YOU-LO HSIEH

_____

CHARLIE LI

Committee in Charge

2022

Acknowledgements

First and foremost, I would like to express my sincere gratitude to my supervisor, Dr. Gang Sun, for providing consistent supports, dedicated guidance and comprehensive insights during my Ph.D. studies. His immense knowledge and great experience have inspired me in all the time of my academic research. His patient encouragement has helped me get through a hard time. And his professional behaviors and scientific thinking have deeply affected me. I cannot finish my Ph.D. training journey without his patience and inspiration.

I would also like to appreciate Drs. Dean Tantillo (Chair), Charlie Li, Peter Green, Tingrui Pan and Gary Smith serve as my Qualifying Exam committee members. They gave me invaluable suggestions, feedbacks and comments. I would also like to thank Drs. You-Lo Hsieh and Charlie Li for serving as my dissertation committee.

Specifically, I would like to express gratitude to Dr. Yang Si for his treasured support, invaluable advice, encouragement and inspiration. Besides, I would also like to appreciate colleagues and visiting scholars, Dr. Jingyuan Zhuo, Dr. Abolfazl Aghanouri, Dr. Maryam Tamizifar, Ms. Sanaz Ghanbari, Dr. Aiqin Hou, Ms. Hao Dong, Dr. Bolin Ji, Dr. Peixing Tang, Dr. Huan Qi, Dr. Zheng Zhang, Dr.Yue Ma, Mr. Kevin Bradley, Mr. Bofeng Pan, Ms. Jiahan Zou, Dr. Jiwei Li, Dr. Yuehan Wu, Dr. Shixiong Yi, Dr. Qiongzhen Liu, Dr. Ahmed El-Moghazy, Dr. Noha Amaly, Dr. Zehong Wang, Dr. Yuan Yu, Dr. Shaoju Fu, Dr. Songsong Tang, Ms. Minyuan Wang for providing valuable discussion and support for my research projects. And I would also like to thank all my friends, lab mates, colleagues in Dr. Sun’s Lab for a cherished time spent together in the lab.

Besides, I would like to acknowledge the Graduate Studies and Agricultural and Environmental Chemistry Graduate Group at the University of California, Davis, for providing me graduate admission fellowship. And I appreciate the financial support from the United States Department of Agriculture and the National Institute of Environmental Health Sciences.

Finally, I would like to express my gratitude to my families. Without their tremendous understanding and encouragement in the past few years, it would be impossible for me to complete my study. Especially, I appreciate my mother, Yi Li, for her selfless love and support, and my wife, Wenhui Ren, for her understanding and encouragement.

Abstract

Biosensors are highly selective and sensitive towards target molecules and should be convenient for on-site toxicant detection. However, the conventional biosensors, including enzyme-linked immunoassay (ELISA), are lacking high sensitivity and hard to reveal a significant colorimetric signal for detecting a trace amount of toxicant. Thus, the detection requires analytical instruments, which limit the application of biosensors for on-site detection. In this dissertation, highly sensitive and portable colorimetric biosensors for the detection of trace amounts of toxicants were designed and fabricated by covalently immobilizing antibodies onto controlled microporous and nanofibrous membranes. The high specific surface of the nanofibers significantly increased the number of immobilized antibodies and the binding capacity with the target toxicant. Thus, the sensitivity of the nanofibrous membrane biosensor was dramatically increased, and a trace number of toxicants could reveal a naked-eye detectable color. Additionally, the diffusion of large biomolecules inside nanofibrous membranes was investigated, revealing the heterogeneous structures of electrospun nanofibrous membranes significantly hinder the diffusion of antibodies into the membrane and dramatically limit the sensitivity of nanofibrous membrane biosensors. Such structural drawbacks of regular electrospun nanofibrous membranes could be overcome by increasing hydrophilicity and controlling microporous structure. Moreover, an ultra-highly sensitive and portable biosensor was fabricated after optimization.

Specifically, chapter 1 summarizes the background information of biosensor and toxicant detection. Chapter 2 reviews the conventional toxicant detection methods, the

technique of fabricating electrospun nanofibrous membrane, and the development of biosensors. In chapter 3, the nanofibrous membrane ELISA biosensors were fabricated for the detection of residual antibiotics in foods. The biosensors exhibited a significant naked-eye distinguishable color at chloramphenicol at 0.3 ng/mL, revealing the potential for on-site detection applications. The novel nanofibrous membrane ELISA biosensors revealed several times increased sensitivities. However, the sensitivity was lower than the expectation based on the design of nanofibrous membrane sensors, which could be attributed to the hindered diffusion behavior of antibodies inside nanofibrous membranes. In chapter 4, the diffusion and partition behavior of proteins inside nanofibrous membranes were studied. Different from other micro-porous materials, electrospun nanofibrous membranes possess layer-by-layer accumulative heterogeneous structures. The effective pore sizes of the nanofibrous membranes were much smaller than the measured pore sizes, affecting the diffusion of proteins through the system and limiting the sensitivity of the biosensors. The results provided insights into the design of proper nanofibrous materials for optimizing the performance of biosensors. In chapter 5, an ultra-highly sensitive and portable colorimetric biosensor was fabricated by controlling microporous structure and increasing hydrophilicity. The protein could rapidly diffuse through the membrane, and the sensitivity of the membrane-based ELISA was dramatically improved. Lastly, chapter 6 summarizes the achievements of the dissertation.

Table of Contents

List of Tables

List of Schemes

List of Figures

Chapter 1. Introduction

1.1 Introduction

Toxicant is a harmful substrate produced by synthesis or naturally occurring. The naturally produced toxicant is also called a toxin, including small molecules, peptides, or proteins. Although toxin residues occur naturally, anthropogenic toxicants are more toxic than others to cause serious environmental concerns. (Ames, Profet et al. 1990) The synthesized toxicants are increasingly used in agricultural and industrial activities, resulting in toxicant residues in air, water, soils, food, and industrial products. (Rossignol, Genuis et al. 2014) The majority of synthesized toxicants in agriculture are pesticides and antibiotics. (Anani, Mishra et al. 2020) The arable lands in high population areas may have high pesticide residues because the pesticides and fertilizers have been over-used in such areas to increase the yield of agricultural products and control pests. In the USA, 1.2 billion pounds of pesticides were used in 2016, and these pesticides may accumulate in corps. (Donley 2019) In a report from the United States Environmental Protection Agency (EPA) in 2016, 0.46 percent of crop samples contained pesticides. Among them, over 55% of samples were domestic, and the rest were imported from foreign countries. (Donley 2019) Meanwhile, when pesticide gets into the soil, it sticks strongly to soil particles and take weeks to years to break down, resulting in chemical residues in soils. Then, the pesticide residues could enter surface or ground waters by either leaching from soil or soil runoff after rain events and volatilizing into the atmosphere days or weeks after application. (Majewski and Capel 2019) In a review from Van Dijk et al., over 80 pesticides

were detected in the rain, and 30 pesticides were detected in the atmosphere. (Van Dijk and Guicherit 1999) In addition to the agricultural products, livestock and seafood products also have the issue of abuse of veterinary drugs such as antibiotics. In stock farming, the antibiotics are administered via injection or feed additives to heal the illness, prevent healthy animals from infections, control the spreading of bacteria and promote the growth of the animals. (Gothwal and Shashidhar 2015) According to a report from the Union of Concerned Scientists (UCS), over 16 million kilograms of antibiotics are used in the U.S. annually, and approximately 80% of antibiotics are used for livestock. Among the veterinary antibiotics, over 70% of antibiotics are used as feed supplements for growth promotion, and only 20% of veterinary antibiotics are used for therapeutic purposes. (Mellon, Benbrook et al. 2001) Some antibiotics may be slowly or poorly metabolized by animals and accumulate in the tissues, resulting in antibiotics residues in livestock. The antibiotic residues in livestock frequently happen at inappropriate antibiotic usage, failure to withdraw drugs, or poor livestock production practices. (Mellon, Benbrook et al. 2001) As the surveys exhibited, 0.78% of milk samples were confirmed containing antibiotic residue at high concentration; and 5 out of 47 antibiotics were detected in shrimp, salmon, tilapia and trout. (Done and Halden 2015, Sachi, Ferdous et al. 2019) Meanwhile, the use of some antibiotics was not optimized in the pharmacokinetics, leading to poorly adsorbed by the animal gut and extraction with the urine and feces, consequently resulting in antibiotic residues in the environment. (Luo, Chen et al. 2019) In a federal survey of pharmaceutical compounds, various antibiotics were detected in 27% of 139 rivers with concentrations higher than 0.7ppb. (Kolpin, Furlong et al. 2002)

Exposure to harmful natural or anthropogenic toxicant residue may cause acute or chronic diseases. For instance, organophosphorus pesticides, the most used insecticides, could inhibit the function of acetylcholinesterase, leading to the accumulation of the neurotransmitter acetylcholine in synapses with consequent neurotoxicity. (Carr, Chambers et al. 2001) Sudden exposure to a large dose of organophosphorus pesticides may cause health problems such as vomiting, irregular heartbeat, paralysis, difficulty breathing and weakness. Chronic exposure to a small dose of organophosphorus pesticides may lead to persistent health effects, including memory and attention deficits, anxiety, depression and irritability. (Choi, Joo et al. 2006) Another example, antibiotic residues could increase the frequent occurrence of resistant genes and develop the antibiotic-resistance from microorganisms. These “super bacteria” may spread to other microbial populations and become a challenge to human health. (Kadri 2020) As a report exhibited, antibiotic resistance causes more than 2 million infections and over 23 thousand deaths in the USA each year. Worldwide, antibiotic resistance has already exceeded 50 percent in some main bacteria groups, including Escherichia coli (E. coli) and Staphylococcus aureus (S. aureus). (Kadri 2020)

For controlling and monitoring the toxicant residues, U.S. federal agencies have established strict regulations for each toxicant. For pesticides, EPA studies the toxicity, evaluates both non-occupational exposure and cumulative effects, inspects the toxic effect to infants and children, and sets maximum residue limits (MRLs). (EPA 2020) Meanwhile, to ensure the safety of food supply and maintenance, the U.S. Department of Agriculture (USDA) enforces the Maximum Residue Limits (MRLs) of pesticides for meat, poultry and egg, and the Food and Drug Administration (FDA) enforces the tolerance for

seafood and milk. (USDA 2020) Besides, each state enforces pesticide regulations to protect the urban environment and ensure local food safety. For instance, the California Department of Pesticide Regulation (DPR) enforces regulation for the usage of organophosphorus pesticides with lower MRLs. Especially, pesticide chlorpyrifos was prohibited from use in California after December 2020, but it is allowed to use in federal with MRLs at a level of 0.1ppm. (DPR 2020) Similarly, the FDA and veterinary feed directive (VFD) establish regulation for each antibiotic, set the classification as toxicity and prohibit the usage of some antibiotics for animal production. (FDA 2019) For example, chloramphenicol (CAP), an extensive spectrum antibiotic with remarkable penetration into the tissues, was prohibited from feeding animals in the USA. (FDA 2020) For ensuring the concentration of toxicant residue at MRLs, sensitive and selective detection methods are necessary to monitor the toxicant residue in the environment.

The common and standard analytical methods for detecting varied toxicants include gas chromatography (G.C.), high-performance liquid chromatography (HPLC) and enzyme-linked immunosorbent assay (ELISA). (Sullivan, Simon et al. 1983, Sharma and Whiting 2005, Costa, Baugh et al. 2009) Chromatography is a technique for separating mixtures and purifying analytes. Then, the purified analytes could be monitored and quantitated by computerized detectors. The chromatography methods are sensitive and reliable but have limitations at on-site detection. The samples need to be sent to a modern laboratory and analyzed by trained personnel via specific instruments. For simplified operation, an alternative is ELISA which can detect varied analytes based on the specific interaction between antibodies and analytes. The concentration of analytes could be quantified by measuring the intensity of the colorimetric signal and comparing the

intensities of the colorimetric signal to the calibration curves. The ELISA could be applied in quantifying a wide spread of analytes, including pesticides, antibiotics, biomarkers and bacteria. The conventional ELISA is easy to operate and selective to specific analytes but still has many challenges. It still requires specific and expensive lab instruments, such as plate reader, bio-incubation oven and shaker, which make it hard for on-site detection, point-of-care detection and home use. (Pang, Zhao et al. 2018) Meanwhile, the sensitivity of conventional ELISA is not high enough for detecting trace analytes with concentrations below the sub-ppb level. (Zhou, Wang et al. 2012)

Due to potential daily exposure to toxicant residues, it is necessary to design a field-developable or on-site use analysis method for unprofessional users. The ideal analysis method should have merits, including easy operation, independence from instruments, and desired sensitivity. Especially, it should exhibit a significant signal when the concentration of toxicant is at MRLs from government regulations. The current standard detection methods, both chromatography and ELISA, are not suitable for the on-site detection of toxicants.

For achieving a highly sensitive on-site detection, an alternative biosensor is designed based on the affinity binding between antibody and antigen and can measure the concentration of analytes by using different types of signals such as electric signals and fluorescent signals. (Verma, Bhardwaj et al. 2015) Since the electric signals in the presence of analytes are easy to be recorded by a transducer, such biosensors usually have higher sensitivity than the conventional colorimetric ELISA. Meanwhile, the biosensors could be used as point-of-care detection with a portable device, such as micro-fluid chips. (Uniyal, Sharma et al. 2018) However, since the electric signal is not

directly visible, the analysis still requires specific and expensive instruments to measure the electric signal. Based on the requirements of on-site detection and personal use, an ideal biosensor should be a colorimetric biosensor exhibiting a significant colorimetric signal which could be qualitatively analyzed by naked eyes or measured by a smartphone, even while the concentration of analytes is low.

Colorimetric biosensors, such as paper-based ELISA, lateral flow assay and micro-fluid-based ELISA, have been designed and fabricated for on-site detection independent from specific instruments. (Nery, Kubota et al. 2013) The microplates of conventional ELISA are substituted by a low-cost filter paper, and the expensive detectors, such as plate readers, are not necessary for paper-based ELISA. The paper-based ELISA system could be applied at on-site detection or home use because of low cost, easy operation, naked-eye distinguishable signal and independence from instruments. For instance, pregnancy test strips are one type of lateral flow assays, which transfer the concentration of human chorionic gonadotropin to a colorimetric signal. (Zhang, Ma et al. 2019) However, since the bioreceptors have less affinity to the filter paper than the micro-plate wells, the sensitivity of paper-based colorimetric biosensors is even lower than the conventional plate ELISA. (Gwyn, Cooley et al. 2017) Thus, the paper-based colorimetric biosensors are not suitable to detect toxicants whose MRLs are at ppb level. (Zhang, Ma et al. 2019)

The sensitivity of colorimetric biosensors could be remarkedly improved by using a nanofibrous membrane as a support material for loading bioreceptors. Nanofibers are one-dimensional fibrous material with diameters at hundreds of nanometer ranges, which could be fabricated by various organic or inorganic materials, including metal, silicon,

carbon and polymers. (Şimşek, Rzayev et al. 2016) Because of the ultra-small diameter of nanofiber, the nanofibers media always have an ultra-high specific surface area which could be calculated by the surface area-to-volume ratio. (Roco 2003) More bioreceptors could be loaded on the surface or inside nanofibrous media, leading to the improvement of sensitivity. Thus, the sensitivity of nanofiber ELISA could be dramatically improved, and a significant colorimetric signal could be exhibited when detecting trace toxicants at a sub-ppb level. Besides, nanofibrous membranes also have unique properties, including high porosity, micro-pore size, proper mechanical strength, and flexibility in surface modification. (Li and Xia 2004) Given above, nanofibrous membrane-based ELISA has the potential to be applied for on-site detection with high sensitivity.

1.2 References

Aldeek, F., Hsieh, K. C., Ugochukwu, O. N., Gerard, G., & Hammack, W. (2017). Accurate quantitation and analysis of nitrofuran metabolites, chloramphenicol, and florfenicol in seafood by ultrahigh-performance liquid chromatography–tandem mass spectrometry: method validation and regulatory samples. Journal of agricultural and food chemistry, 66(20), 5018-5030.

Ames, B. N., Profet, M., & Gold, L. S. (1990). Nature's chemicals and synthetic chemicals: comparative toxicology. Proceedings of the National Academy of Sciences, 87(19), 7782-7786.

Anani, O. A., Mishra, R. R., Mishra, P., Enuneku, A. A., Anani, G. A., & Adetunji, C. O. (2020). Effects of Toxicant from Pesticides on Food Security: Current Developments. In Innovations in Food Technology (pp. 313-321). Springer, Singapore.

California Department of Pesticide Regulation. (2020). Chlorpyrifos Cancellation. https://www.cdpr.ca.gov/docs/chlorpyrifos/index.htm

Carr, R. L., Chambers, H. W., Guarisco, J. A., Richardson, J. R., Tang, J., & Chambers, J. E. (2001). Effects of repeated oral postnatal exposure to chlorpyrifos on open-field behavior in juvenile rats. Toxicological sciences, 59(2), 260-267.

Choi, K., Joo, H., Rose, R. L., & Hodgso, E. (2006). Metabolism of chlorpyrifos and chlorpyrifos oxon by human hepatocytes. Journal of biochemical and molecular toxicology, 20(6), 279-291.

Costa, P. R., Baugh, K. A., Wright, B., RaLonde, R., Nance, S. L., Tatarenkova, N., ... & Lefebvre, K. A. (2009). Comparative determination of paralytic shellfish toxins (PSTs) using five different toxin detection methods in shellfish species collected in the Aleutian Islands, Alaska. Toxicon, 54(3), 313-320.

Done, H. Y., & Halden, R. U. (2015). Reconnaissance of 47 antibiotics and associated microbial risks in seafood sold in the United States. Journal of hazardous materials, 282, 10-17.

Donley, N. (2019). The USA lags behind other agricultural nations in banning harmful pesticides. Environmental Health, 18(1), 1-12.

Gothwal, R., & Shashidhar, T. (2015). Antibiotic pollution in the environment: a review. Clean–Soil, Air, Water, 43(4), 479-489.

Gwyn, S., Cooley, G., Goodhew, B., Kohlhoff, S., Banniettis, N., Wiegand, R., & Martin, D. L. (2017). Comparison of platforms for testing antibody responses against the Chlamydia trachomatis antigen Pgp3. The American journal of tropical medicine and hygiene, 97(6), 1662-1668.

Kadri, S. S. (2020). Key Takeaways From the US CDC's 2019 Antibiotic Resistance Threats Report for Frontline Providers. Critical care medicine.

Kolpin, D. W., Furlong, E. T., Meyer, M. T., Thurman, E. M., Zaugg, S. D., Barber, L. B., & Buxton, H. T. (2002). Pharmaceuticals, hormones, and other organic wastewater contaminants in US streams, 1999− 2000: A national reconnaissance. Environmental science & technology, 36(6), 1202-1211.

Li, D., & Xia, Y. (2004). Electrospinning of nanofibers: reinventing the wheel?. Advanced materials, 16(14), 1151-1170.

Luo, W., Chen, D., Wu, M., Li, Z., Tao, Y., Liu, Q., ... & Xie, S. (2019). Pharmacokinetics/Pharmacodynamics models of veterinary antimicrobial agents. Journal of veterinary science, 20(5).

Majewski, M. S., & Capel, P. D. (2019). Pesticides in the atmosphere: distribution, trends, and governing factors. CRC Press.

Mellon, M., Benbrook, C., & Benbrook, K. L. (2001). Hogging it. Estimates of antimicrobial abuse in livestock, 7-9.

Nery, E. W., & Kubota, L. T. (2013). Sensing approaches on paper-based devices: a review. Analytical and bioanalytical chemistry, 405(24), 7573-7595.

Pang, B., Zhao, C., Li, L., Song, X., Xu, K., Wang, J., ... & Li, J. (2018). Development of a low-cost paper-based ELISA method for rapid Escherichia coli O157: H7 detection. Analytical biochemistry, 542, 58-62.

Roco, M. C. (2003). Nanotechnology: convergence with modern biology and medicine. Current opinion in biotechnology, 14(3), 337-346.

Rossignol, D. A., Genuis, S. J., & Frye, R. E. (2014). Environmental toxicants and autism spectrum disorders: a systematic review. Translational psychiatry, 4(2), e360-e360.

Sachi, S., Ferdous, J., Sikder, M. H., & Hussani, S. A. K. (2019). Antibiotic residues in milk: Past, present, and future. Journal of advanced veterinary and animal research, 6(3), 315.

Sharma, S. K., & Whiting, R. C. (2005). Methods for detection of Clostridium botulinum toxin in foods. Journal of food protection, 68(6), 1256-1263.

Simşek, M., Rzayev, Z. M., & Bunyatova, U. (2016). Multifunctional electroactive electrospun nanofiber structures from water solution blends of PVA/ODA–MMT and poly (maleic acid-alt-acrylic acid): effects of Ag, organoclay, structural rearrangement and NaOH doping factors. Advances in Natural Sciences: Nanoscience and Nanotechnology, 7(2), 025009.

Sullvan, J. J., Simon, M. G., & Iwaoka, W. T. (1983). Comparison of HPLC and mouse bioassay methods for determining PSP toxins in shellfish. Journal of food science, 48(4), 1312-1314.

U.S. Environmental Protection Agency. (2020). Regulatory and Guidance Information by Topic: Pesticides. https://www.epa.gov/pesticides

U.S. Food and Drug Administration. (2019). New Drug and Antibiotic Regulations. https://www.fda.gov/science-research/clinical-trials-and-human-subject-protection/new-drug-and-antibiotic-regulations

U.S. Food and Drug Administration. (2020). CFR - Code of Federal Regulations Title 21. https://www.accessdata.fda.gov/scripts/cdrh/cfdocs/cfcfr/cfrsearch.cfm?fr=216.24

United States Department of Agriculture. (2020). Pesticide Regulatory Policy. https://www.usda.gov/oce/pest/about

Uniyal, S., & Sharma, R. K. (2018). Technological advancement in electrochemical biosensor based detection of organophosphate pesticide chlorpyrifos in the environment: a review of status and prospects. Biosensors and bioelectronics, 116, 37-50.

Van Dijk, H. F., & Guicherit, R. (1999). Atmospheric dispersion of current-use pesticides: A review of the evidence from monitoring studies. Fate of Pesticides in the Atmosphere: Implications for Environmental Risk Assessment, 21-70.

Verma, N., & Bhardwaj, A. (2015). Biosensor technology for pesticides—a review. Applied biochemistry and biotechnology, 175(6), 3093-3119.

Zhang, Y., Ma, C. B., Yang, M., Pothukuchy, A., & Du, Y. (2019). Point-of-care testing of various analytes by means of a one-step competitive displacement reaction and pregnancy test strips. Sensors and Actuators B: Chemical, 288, 163-170.

Zhou, F., Wang, M., Yuan, L., Cheng, Z., Wu, Z., & Chen, H. (2012). Sensitive sandwich ELISA based on a gold nanoparticle layer for cancer detection. Analyst, 137(8), 1779-1784.

Chapter 2. Literature Review

2.1 Detection techniques for toxicants

2.1.1 Gas chromatography / High Performance Liquid Chromatography – Mass spectrometry

Gas chromatography (GC) is used for separating different components of a mixture, purifying a particular analyte, and analyzing vaporized compounds. In a GC analysis, a gaseous or liquid sample is injected into a temperature-controlled glass or metal column, mixes with a carrier gas (mobile phase), and passes through the solid particles filled columns (stationary phase). The mobile phase consists of an inert gas such as helium, argon and nitrogen, and the stationary phase is a layer of viscous liquid on the surface of inert solid particles. (Harris 2010) The analyte molecules could be adsorbed either on the solid particles or column walls. Since the chemical molecule has a different rate of progression, the various components of the analytes reach the end of the column at different retention times. Thus, each particular analyte could be separated by the GC column. A computerized detector, such as a flame ionization detector or thermal conductivity detector, is connected to the end of the column for monitoring the retention time at which each analyte reaches the outlet of the column. (Harris 2010) For GC quantitative analysis, there are many requirements for the samples. In general, the analytes are required to be vaporized below 300 °C without decomposition. The samples are also required to be salt-free, and a reference standard is necessary to be measured at the same time.

If the samples are less volatile or samples contain salts, high-performance liquid chromatography (HPLC) is required. In an HPLC, pumps are commonly required to mix analyte samples with varied solvents and pass the mixture through a column. The mobile phase of HPLC is a liquid made up of organic solvents, ultrapure water and other ingredients which are compatible with the sample, and the stationary phase is made by solid, porous and surface-active small particles. The separation of various components is based on their differential partitioning and various interactions with the stationary phase. These interaction forces include dispersion interaction, hydrophobic interaction, dipole-dipole interaction, hydrogen bonding, ionic interaction, and π-π interaction between the substrates and the stationary phase. (Snyder and Ritchie 2010) Sample retention time depends on the interactions with the stationary phase, the analyte molecules, and the solvent. Analytes that have weak interaction with the stationary phase and strong interaction with the mobile phase would reach the outlet of the column rapidly. Based on the different separation mechanisms, the HPLC could be categorized as partition chromatography, normal–phase chromatography, displacement chromatography, reversed-phase chromatography, size-exclusion chromatography, ion-exchange chromatography, and aqueous normal-phase chromatography. Reversed-phase chromatography is the dominant HPLC mode, especially for detecting analytes from mixtures of organic compounds. In reversed-phase chromatography, the column is packed with non-polar silica particles, such as octadecyl, octyl and phenyl-hexyl, acting as a stationary phase; and the mobile phase consists of mid to high polar organic solvents, such as acetonitrile, isopropanol, tetrahydrofuran, and methanol. The relatively hydrophobic and less polar analytes could be adhered to the silica surface by the

hydrophobic alkyl ligands, resulting in a longer retention time. (Mallik, Qiu et al. 2018) On the contrary, in normal–phase chromatography, the stationary phase is made by polar silica particles, and the mobile phase consists of the non-polar and non-aqueous solvent. Normal–phase chromatography is effective and efficient for separating analytes dissolved in non-polar solvents. (Abbott 1980) Besides, the size-exclusion chromatography could separate compounds on the basis of molecular size, which is effective for protein separation and detection. In ion-exchange chromatography, retention is based on the attraction between analyte ions and charged silicas on the column. In the partition chromatography, the stationary phase is made by loading retained solvent on the surface of the fibers, leading to separate analytes by differences in their polarity. (Kim, Ryu et al. 2018)

A mass spectrometry (MS) is usually combined with GC and HPLC for providing a structural identity of each separated component and dramatically improving the detection sensitivity. MS is used to measure the mass-to-charge ratio (m/z) of ions and export a mass spectrum. The mass spectrum could be used to calculate the exact molecular weight of the sample components, identify unknown compounds via molecular weight, quantify known analytes, and determine the structure and chemical properties of molecules. (Sparkman 2000) In general, an MS consists of three components: ionization source, mass analyzer, and ion detection system. First, the analyte molecule is converted to gas-phase ions, which can transport in external electric and magnetic fields. Electrospray ionization and matrix-assisted laser ionization are two techniques for solid or liquid. (Fenn, Mann et al. 1989) And chemical ionization and electron ionization are two common techniques for gaseous analytes. (McNaught and Wilkinson 1997) In the

chemical ionization source, the analyte molecule is ionized by ion-molecule reactions during collisions; and in the electron ionization source, an energetic electron interacts with analyte molecules to produce ions. Once ionized, the ions are separated according to m/z ratios in electric and magnetic fields in a vacuum because the motion of the charged particle is determined by the m/z ratio. The commonly used mass analyzers include time-of-flight analyzer, quadrupole mass filter, ion trap analyzer, and so on. Each analyzer type has its merits and limitations, but all have the same mechanism. (El-Aneed, Cohen et al. 2009) The final component of MS is the detection system. The m/z ratios and relative abundance of each separated ion would be recorded. Then, a mass spectrum exhibits the m/z ratios against relative abundance. Each peak in the mass spectrum represents a component of the analytes, and the structure of analytes could be identified by analyzing the relative abundance of components.

Since the HPLC/GC-MS is a reliable, sensitive, and selective technique, it is widely used for detecting varied toxicant residues. For example, HPLC-MS is the standard technique for detecting antibiotic residues. Hammack et al. (Hammack, Carson et al. 2003) determined chloramphenicol (CAP) residues in shrimp with a liquid chromatography tandem mass spectrometer. The LOD was found at 0.3 ug /kg, which met the confirmation criteria recommended by the U.S. Food and Drug Administration. Rønning et al. developed an LC-MS method for detecting CAP residues in several food matrices. The critical concentrations were found with decision limit and detection capability values of 20 and 40 ug/kg for the 321 →152 ion transition and 20 and 30 ug /kg for the 321 → 194 ion transition, respectively. (Rønning, Einarsen et al. 2006) Recently, Veach et al. optimized and improved the sensitivity of HPLC-MS methods for CAP detection with LOD at 0.01

ug/kg. (Veach, Baker et al. 2015) Similarly, Kaufmann et al. developed an ultra-high performance liquid chromatography combined with high-resolution mass spectrometry for detecting nitrofuran and chloramphenicol residues in fish. The technique could achieve a low LOD at 0.05 ug/kg. (Kaufmann, Butcher et al. 2015)

2.1.2 Enzyme-linked immunosorbent assay

Enzyme-linked immunosorbent assay (ELISA) is a plate-based immunoassay for detecting and quantifying specific analytes, including peptides, antibiotics, proteins, and bacteria. (Walker 2009) In an ELISA analysis, the antigen specifically reacts with antibody-forming a bioconjugation, and the bioconjugation is incubated with the appropriate dyes to produce a detectable colorimetric signal. Before ELISA was developed, the commonly used immunoassay was radioimmunoassay, where radiolabeled antigen or antibody provides a radioactive signal. (Yalow and Berson 1960) As radiolabeled molecule has a potential health threat, researchers spent around decades to develop a suitable alternative with a nonradioactive signal. The first ELISA technique was introduced by Engvall and Perlman in the 1970s. The IgG analytes were captured by microplate wells where antibodies were pre-coated, and chromogenic reporters were employed to produce colorimetric signals. (Engvall and Perlmann 1971; Nassau, Parsons et al. 1976) Recently, new ELISA techniques also employ fluorescent, phosphorescent, chemiluminescent, and electrochemiluminescent reporters to create quantifiable signals, which could produce a high intensity of the signal and improve sensitivity. (Leng, McElhaney et al. 2008) In 2012, Roberto et al. developed an ultra-sensitive ELISA, where gold nanoparticles were used as chromogenic reporters. The

aggregation of gold nanoparticles could change the optical properties of nanoparticles, and the ultra-sensitive ELISA could give a naked-eye color change from red to blue with the presence of analytes.

Various ELISA technologies have been developed for different types of analytes and used with different detectors. Based on the types of analytes, the ELISA methods have several formats, including direct, indirect, sandwich and competitive ELISA. (Crowther 2001) In the direct ELISA, the analyte antigens are coated on the plates, and enzyme-modified antibodies are captured by the loaded antigen. In the indirect ELISA, firstly, the analyte antigens are coated on the plates; secondly, primary antibodies are added and captured by the antigens; then, enzyme-modified second antibodies are captured by the primary antibodies. In the sandwich ELISA, firstly, primary antibodies are coated on the plates; then, analytes are added; lastly, enzyme-modified second antibodies are added and captured by the analyte antigens. When the analytes are small molecules such as antibiotics, a competitive ELISA is required, where analytes and enzyme-linked analytes are added to the antibodies coated plates at the same time. The advantages and shortcomings of each ELISA are listed in Table 2.1. (Crowther 2001)

The commercial ELISA method consists of five main procedures: 1) the bioreceptors, including antigens or antibodies, are coated onto polystyrene microplate wells by physically adsorption; 2) block agents, such as bovine serum albumin (BSA) and milk whey, are added into the pre-coated microplate for blocking the unsaturated surface reactive sites; 3) the analyte samples are added into the as-prepared microplate and incubated at a specific temperature so that analytes could bind to the pre-loaded bioreceptors; 4) after incubation, the microplate is washed to remove all unbonded

analytes, and a dye substrate is added to each microwell to produce color change; 5) the intensity of the colorimetric signal is analyzed by a detector, such as a plate reader. (Lin 2015) Developing a high binding plate is the first step for building an ELISA system. The micro-plates of all ELISAs are made by polystyrene, which is a hydrophobic polymer and could adsorb the proteins by non-specific hydrophobic force. If the antigen is a small molecule, the antigen needs to be linked with a protein, such as BSA, to be coated on the plates. The common method for coating is adding a 2–100 μg/mL of antibodies or antigen phosphate-buffered saline (PBS) solution into the plate wells. Then, the coated plates are incubated for several hours at room temperature or overnight at 4 °C. (Gardas and Lewartowska 1988) The hydrophobic adsorption could arise many issues, including poor immobilization efficiency, binding of contaminants, and denaturation of protein. Especially, the antibodies may be loaded with improper orientation: the antigen-binding sites on the antibody could be blocked to the plates, resulting in false-negative results. (Lee, Park et al. 2012) Thus, a surface-modified plate is employed for avoiding passive adsorption. The plates could be pre-coated with protein A, protein G, glutathione and metal-chelate, which could capture antibodies with proper orientation and preserve the antigen-binding affinity. (Chen, Chen et al. 2018) In some ELISA systems, the bioreceptors are small molecules such as peptides or nucleic acids, which could not be passively adsorbed on the polystyrene. In this case, the plates are pre-coated with streptavidin which could efficiently bind with the biotinylated peptides or nucleic acids. (Bockstahler, Li et al. 2002)

The bioreceptors could be biological molecular species, such as antibodies, enzymes, peptides, and nucleic acids, or a living biological system, including cells, tissues or organisms. A proper bioreceptor requires strong interaction with analytes, high selectivity,

stability and durability. (Vo-Dinh and Cullum 2000) Among bioreceptors, antibodies are currently the most commonly used bioreceptors because antibodies have a stable structure and highly specific affinity to analytes. An antibody is a Y-shaped protein generated by the immune system to identify antigens such as bacteria and viruses. Antibodies include polyclonal, monoclonal or recombinant, depending on the synthesis methods. (Huang, Garcia-Carreras et al. 2020) Polyclonal antibodies are the most common ones, which are produced by conventional immunization procedures. The monoclonal antibodies are produced by cloning a unique white blood cell. Since monoclonal antibodies have monovalent affinity binding to one antigen, the monoclonal antibodies are more selective. Recombinant antibodies, such as nanobodies, are antibody fragments. Unlike polyclonal and monoclonal antibodies, which need hybridomas and animals in the production process, recombinant antibodies are generated in vitro using synthetic genes. (Khongorzul, Ling et al. 2020) Currently, various antibodies, such as anti-antibiotics and anti-pesticides, are now commercially available. However, the antibody ELISA also has some limitations. Since the antigens only bind to the antibodies which have correct conformation, the antibody ELISA could not be applied in high temperature, organic solvents or high salty solvents, which could denature the 3rd or 4th structure of antibodies. (Goode, Rushworth et al. 2015) Thus, the ideal working environment is PBS solvents.

After the plates are coated by bioreceptors, a blocking buffer is added to each well. Since the number of binding sites on each microplate well is higher than the number of loaded proteins. It is necessary to block the remaining binding sites to prevent the non-specific adsorption of analytes during subsequent steps. (Crowther 2001) The blocking

solution is made up by adding inert proteins, such as BSA or milk whey protein, into a PBS solution. When selecting blocking proteins, there are two requirements: 1) the signal-to-noise ratio needs to be improved after blocking, and 2) the blocking protein would not sterically inhibit the affinity binding between antibody and antigen. (The signal-to-noise ratio is represented by the ratio between the signal obtained from the analyte sample and signal obtained from the non-analyte sample.) The inadequate amounts of blocking solution would result in high background signal, low signal-to-noise ratio, and low sensitivity. On the other hand, excessive amounts of blocking solution may inhibit the antibody-antigen interactions or inhibit the affinity between antibody-antigen bioconjugation and enzyme reporters, resulting in a reduction of the signal intensity. The ideal blocking solution would precisely bind to all the remaining reactive sites, eliminating background signal, increasing the signal-to-noise ratio and improving the sensitivity consequently. (Steinitz 2000, Xiao and Isaacs 2012) Thus, preliminary empirical testing is necessary for optimizing the blocking parameters for each ELISA analysis.

After blocking, the varied analytes and enzyme reporters would be added to the coated plates subsequently. The commonly used enzyme reporters include horseradish peroxidase (HRP), alkaline phosphatase, β-galactosidase and acetylcholinesterase. (Tighe, Ryder et al. 2015) Then, the corresponding dye substrates are selected for performing ELISA based on the types of enzyme reporters. The enzyme reporters could convert the substrate to a detectable signal, and the intensity of the signal is directly proportional to the number of analytes captured by the coated plate. The substrates determine the types of signals and signal intensity. Generally, the common types of substrates include a chromogenic substrate, fluorescent substrate and chemiluminescent

substrate. The common colorimetric substrates include 3,3',5,5'-tetramethylbenzidine, o-phenylenediamine, and 2,2'-azino-bis (3-ethylbenzothiazoline-6-sulfonic acid), which could work as hydrogen donors for the reduction of hydrogen peroxide by peroxidase enzyme reporters. The colorimetric ELISA may have lower sensitivity than fluorescent or chemiluminescent ELISA but could reveal a visualized signal and enable the kinetic study. Fluorescent ELISA is more sensitive and has a wider dynamic range than colorimetric ELISA, but a fluorometer with proper excitation and emission filters is required. Chemiluminescence is a chemical reaction that generates a light signal. The common chemiluminescent substrate is luminol, which is oxidized and reaches the excited state in the presence of a peroxidase enzyme and peroxide solution. Since the detector could record the accumulation of emission light, the chemiluminescent ELISA is the most sensitive ELISA, but its signal would decay when the substrate is exhausted. (Crowther 2001, Ma and Shieh 2006)

As a selective and convenient analysis technique, ELISA has also been widely applied in toxicant detection and compared with HPLC/GC-MS methods. Scortichini et al. established an ELISA qualitative screening method for measuring CAP in muscle, eggs, honey and milk. The detection capability values are below the minimum required performance limit (0.3ppb) for all the samples. (Scortichini, Annunziata et al. 2005) Impens et al. developed and validated a method to detect CAP in seafood tissue. In this analysis method, ELISA was used for screening CAP, and GC-MS or LC-MS was used for confirmation. The ELISA screening was carried out directly on the aqueous extract of the seafood, and confirmation was performed after extraction. This selective technique could detect CAP residue at the 0.1ppb level. (Impens, Reybroeck et al. 2003) Zhang et

al. developed a chemiluminescent ELISA to detect CAP in chicken muscle. The luminol solution was used as the substrate, and horseradish peroxidase was used as the enzyme reporter. The chemiluminescent ELISA was found at 10 times more sensitive compared to the colorimetric ELISA. (Zhang, Zhang et al. 2006)

Table 2.1. Comparison of different ELISA formats

ELISA format	Advantages	Disadvantages
Direct ELISA	Rapid detection Fewer incubation steps	Low sensitivity Less commercial antibodies
Indirect ELISA	Increased sensitivity Commercial antibodies	Cross-reactivity
Sandwich ELISA	Highly sensitive Commercial antibodies	More incubation steps
Competitive ELISA	Small analytes	Limited sensitivity Low accuracy

2.1.3 Biosensors

Although HPLC/GC-MS and plate ELISA have many merits, such as sensitive and precisive detection of targets, they have many limitations such as requiring expensive instruments, complicated operations, and long extraction and preparation time, which limit their applications in point-of-care inspections. Contrarily, various biosensors could be applied as the relatively convenient analytical technique for rapid detection. The biosensor is an analytical device that can specifically detect chemical or biological

components with high sensitivity. Similar to plate ELISA, bioreceptors, such as antibodies, enzymes, peptides, etc., are required to be pre-loaded on a solid support material for fabricating a biosensor. Then, the bioreceptors could interact with the specific analytes to produce a bioconjugation which could combine with a specific enzyme to produce a signal for recording. (Bondavalli 2019) However, there are two main differences between plate-ELSIAs and biosensors: 1) ELISAs are on a micro-plate, but biosensor could be fabricated on varied solid media, including fiber, film and electrode; 2) ELISAs usually exhibit an optical signal, but biosensors exhibit different signal, such as electric signal. (Gaudin, Cadieu et al. 2005; Campbell, Huet et al. 2009)

The biosensors could be categorized by the types of transducers. A wide variety of transducers have been designed and fabricated in the past decade. In general, electrochemical, mass sensitive, thermometrical and optical transducers are the commonly used transducers for the detection of toxicant residues. Among these transducers, the electrochemical biosensors are the most frequently developed biosensors, and these techniques were introduced in the 1950s. (Pohanka and Skládal 2008) In the electrochemical biosensor analysis, varied bioreceptors are immobilized onto the surface of an electrically conductive material, such as carbon electrode or conductive fiber. The basic mechanism for electrochemical biosensors is converting chemical information to an electrical signal. The chemical reactions between immobilized bioreceptors and analytes could produce or consume ions and electrons, which affect the electrical properties (such as electric current, impendent or potential) of the biosensor. The first developed electrochemical biosensor is an amperometric biosensor where the current is proportional to the analyte concentration. (Thévenot, Toth et al. 2001) Montiel

et al. developed an amperometric biosensor to detect three different types of antibiotic residues in milk. The antibodies were immobilized on the magnetic beads, and HRP was employed to enhance the signal. Compared with HPLC and LC-MS, the amperometric biosensor could exhibit a low LOD at 0.8ng/mL with a rapid detection time at 5mins. (Montiel, Campuzano et al. 2015) Recently, the most popular electrochemical biosensor is the impedimetric electrochemical biosensor which measures the variation of resistance and interfacial capacitance between the electrode surface and a solution. The impedimetric electrochemical biosensor has many merits, including the highest sensitivity, no labelling and rapid detection. (Kim, Iezzi Jr et al. 2019) Thavarungkul et al. fabricated an impedimetric label-free immunosensor for detecting penicillin in milk. Anti-penicillin G was immobilized on a gold working electrode, and the impedance was carried out at the optimum frequency of 160 Hz. The impedimetric immunosensor system provided an ultra-low LOD at 3.0 × 10−15 M and a short detection time at 45mins. (Thavarungkul, Dawan et al. 2007) Wu et al. immobilized an anti-neomycin antibody on a nanotube to fabricate a paper-support impedimetric biosensor for neomycin detection, which has a low LOD at 0.04ng/mL. (Wu, Kuang et al. 2012)

Thermometric biosensors could measure the released or adsorbed heat from biological reactions. The thermometric biosensors have merits, including simple operation and convenience. Xu et al. developed a flow-injection thermometric biosensor for rapidly quantifying diazepam and verified the detected results by HPLC. Each sample only needs 15 min to generate an entire heat signal, and the cycle time, including regeneration and retrimming, is shorter than 45 min. The thermometric biosensor has a linear range at 45.37 - 726.71 ng/mL and a corresponding LOD at 33.71 ng/mL. The sensitivity is not

outstanding, but it meets the requirement of diazepam detection for the patient. (Xu, Bai et al. 2017)

Mass-sensitive transducers, also called gravimetric biosensors, could detect the mass change after bio-conjugation formed. The common mass-sensitive biosensors include piezoelectric crystals, quartz crystal microbalances, and surface acoustic waves. A piezoelectric biosensor could record the oscillators on piezoelectric effect due to analytes bound on the piezoelectric crystal surface. (Pohanka 2017) The quartz crystal microbalance biosensor could record the mass change by measuring the change in frequency of quartz crystal resonators. (Vo-Dinh and Cullum 2000) Surface acoustic wave biosensors could record the acoustic wave travelling along the surface of materials after analytes interact with bioreceptors. (Länge, Rapp et al. 2008) However, the sensitivity of mass-sensitive transducers is lower than the sensitivity of electrical biosensors. Karaseva and Ermolaeva developed a quartz crystal microbalance biosensor for the detection of CAP from meat, milk and egg. However, the announced detection of limitation is 5-10ng/mL, which is higher than the minimum required performance level of CAP (0.3ng/mL). (Karaseva and Ermolaeva 2012) Another team developed a novel quartz crystal microbalance biosensor based on a molecularly imprinted polymer for the detection of CAP in meat, milk, honey and shrimp. The LOD is lower than the minimum required performance level only when detecting CAP in honey and shrimp. (Marx, Zaltsman et al. 2004)

Optical biosensors are based on the optical signal when a dye molecule reacts with the enzymes. The optical biosensors have a large number of subclasses based on the different light types. Colorimeters or fluorescence biosensors measure the absorbance or

emission light of dye molecules; flow cytometric immunoassay biosensors measure the light scatter when an analyte passes through the light beam; surface plasmon resonance biosensors measure the change of refractive index on the surface of solid, and chemiluminescent biosensors measure the optical signal from a chemical reaction catalyzed by enzymes. (Damborský, Švitel et al. 2016) The first article on developing an optical biosensor was published in the 1990s, but the optical biosensors were widely applied for toxicant detection after the 21st century. Chu et al. employed a fluorescence biosensor for aminoglycosides detection in milk; Song et al. fabricated a polymer nanobelt based fluorescence biosensor to detect sulfadimethoxine in milk; Chen et al. developed a multiplex biosensor based on fluorescence for the detection of varied antibiotics and compared the results with those from the conventional ELISA; and Fernández et al. developed a portable surface plasmon resonance biosensor, which contains three parallel channels, for evaluation of toxicant in milk. (Chu, Wu et al. 2008; Song, Jeong et al. 2012; Chen, Wang et al. 2009; Fernandez, Pinacho et al. 2011) Among optical biosensors, the most common one is paper-based ELISA, which is fabricated by adapting a conventional ELISA on nitrocellulose and filter papers to establish a diagnostic tool. (Hawkes, Niday et al. 1982) Paper-based ELISA was first documented by Whitesides at Harvard University in 2010, where hydrophobic polymer was patterned on the hydrophilic filter paper to fabricate a platform for interacting with antigens. (Cheng, Martinez et al. 2010) Since the paper-based ELISAs have merits, including low cost, direct visualization, and easy operation, they have been widely used in on-site detection, point-of-care detection and qualitative detection. Shih et al. applied a paper-based ELISA to rapidly detect Escherichia coli in 5 hours. The research provided a fast, easy to perform, and less

expensive method for detecting bacteria in low- and middle-income areas. (Shih, Chang et al. 2015) Nilghaz and Lu fabricated a paper-based microfluidic device for detecting antibiotic residues in pork. The paper had both filtration and detection function, and the device had a LOD at 1ppm for detecting norfloxacin residues. (Nilghaz and Lu 2019) Zhang et al. developed a low-cost and simple paper-based microfluidic device for multiplex determination of different types of chemical contaminants in food. The device was fabricated by physically adsorbing fluorescence-labelled DNA on filters. (Zhang, Zuo et al. 2015) The optical biosensors have many merits, such as portable devices, low cost and visible signal. But optical biosensors are less sensitive than electrochemical biosensors.

2.2 Electrospun nanofiber and their application

2.2.1 Electrospun Nanofiber

The most common materials for producing nanofiber are natural and synthetic polymers. Examples of natural polymers include protein (such as silk fibroin, gelatin and collagen) and polysaccharides (such as cellulose, alginate and chitosan). (Vasita and Katti 2006) Examples of synthetic polymers include polycaprolactone, poly (vinyl alcohol-co-ethylene), polyurethane, poly(3-hydroxybutyrate-co-3-hydroxyvalerate) and polystyrene. (Khajavi, Abbasipour et al. 2016) The fabricating methods are determined by the types of raw materials. The techniques for fabricating nanofibers include thermal-induced phase separation, drawing, template synthesis, self-assembly, sea-island methods, and electrospinning. Among them, electrospinning is the most commonly used

technique to fabricate nanofibers. (Li and Xia 2004, Sarbatly, Krishnaiah et al. 2016) Electrospinning is the process of applying electrostatic forces to fabricate fibers from polymer solutions. At four centuries ago, William Gilbert, an English physicist, first found that the liquid could warp into a cone shape and form a spherical drop when the solution was held under electrostatic attraction. (LF Nascimento, S Araujo et al. 2015) In the late 19th century, scientists found that the liquid could be ejected in a tiny jet stream at the equilibrium between electrostatic force and liquid surface tension. (Rayleigh, Magazine et al. 1882) After the first patent about electrospinning was published in the early 20th century, scientists spent much effort and time attempting nanofiber production. (Cooley 1900; Simons 1966; Tucker, Stanger et al. 2012) In the 1930s, Formals had designed and fabricated polymer filaments under an electric field. (Huang, Zhang et al. 2003) In the 1950s, Vonnegut successfully applied an electric field on a small volume of liquids and produced droplets with micrometre diameter, which was a precursor for electrospinning nanofiber. (Vonnegut and Neubauer 1952) In the 1960s, Simons designed and optimized an electrospinning instrument to produce electrospun non-woven fabrics. (Huang, Zhang et al. 2003) In the 1970s, Baumgarten successfully created a modern electrospinning process and developed modern electrospinning instruments. (Baumgarten 1971) At the same time, hundreds of polymer solutions had been applied in the electrospinning, and more than one hundred ultrafine fibers had been successfully obtained. (Huang, Zhang et al. 2003) In the 1980s, the electrospinning process has been widely applied in varied applications, including bio-engineering, drug delivery and filtration. But none of the above research could be applied in industrial manufacture for fabricating fiber in nanometer size. Only in the 1990s, electrospinning had been rediscovered by D. Reneker. (Doshi and

Reneker 1995) Then, electrospinning became popular among scientists and researchers and continues to be researched and developed even today.

The mechanism of electrospinning had also been studied and analyzed in the 20th century. Briefly, electrospinning begins with a charged polymer solution and a grounded electrode which is placed at some distance away from the polymer solution droplet. An electric field is applied between polymer solution and ground electrode, resulting in the accumulated charge on the surface of the solution. Then, the polymer solution deforms, and a liquid droplet with accumulated charge is generated. When a sufficient electric field is applied, the electrostatic repulsion force is equal to the liquid surface tension forces. Then, the interaction of the charges in the droplet and the external electrical field stretch liquid droplet into a conical shape liquid droplet, which is called Taylor cone. (Kessick, Fenn et al. 2004) In 1964, Sir Geoffrey Ingram Taylor firstly documented the Taylor cone and theoretically studied the factors affecting the formation and size of a liquid cone under an electric field. He found the cone would be stretched with the increase of the intensity of the electric field. Finally, the semi-vertical angle of the Tylor cone will reach 49.3°. (Taylor 1964) When the electrical potential keeps increasing, the Tylor cone becomes unstable, resulting in that a jet stream is emitted from the Taylor cone and moving toward the grounded electrode. Since the discharged fluid jet is unstable, the polymer fluid is elongated under an electric field, resulting in a long and thin jet. The jet moves straight at a short distance and starts a whipping path at a certain distance. The initial straight path is controlled by Rayleigh instability, and the whipping path is controlled by bending and whipping instabilities. (Reneker, Yarin et al. 2000) During the whole process, the solvent would be evaporated, resulting in forming a small diameter fiber.

Based on the above mechanism, various configurations were developed and used for electrospinning. The majority of instruments for electrospinning include four main components: 1) a high voltage supply for generating electric potential, 2) a small diameter tube (such as a syringe) with a needle for storing polymer solution, 3) a pump for extruding polymer, and 4) a metal collector for collecting nanofibers. (Bhardwaj and Kundu 2010) The electrode is attached to the tips of the needle, and the ground electrode is connected with the metal collector. As the mechanism explains, when the applied repulsive electrostatic force overcomes the surface tension of polymer solution, the jet stream of polymer solution is ejected from the tip of the needle, transports toward ground electrode collectors, solidifies with the evaporation of solvent and forms nanofibers at the meal collector.

2.2.2 Parameters that affect the morphology of electrospun nanofibers

The morphology of nanofibers formed by electrospinning is shown in microporous nanofibrous structures and is influenced by many factors and parameters. The majority of factors include: 1) the solution properties, 2) the process parameters, and 3) environment factors. (Bhardwaj and Kundu 2010)

The polymer concentration is the most critical solution property for electrospinning. Beads or discontinuous electrospun fibers are generated when polymer concentration is lower than the concentration that can cause polymer chain entanglement; contrarily, bands and micrometre diameter fibers form when the polymer concentration is too high. (Almetwally, El-Sakhawy et al. 2017) The fiber diameter and pore size increase with the

increase of the polymer concentration. (Greiner and Wendorff 2007) The solution viscosity should also be considered when electrospinning polymers. The continuous fibers could not be generated when solution viscosity is too low, but the Taylor cone could not form in a highly viscous solution because of the high surface tension. Besides, the molecular weight of polymer has a significant effect on both the rheological and electrical properties of the polymer solution. Low molecular weight polymer solution would cause the instability of the polymer solution jet, resulting in beads and discontinuous fibers. Contrarily, the fiber cross-section changes from circular to flat when the molecular weight of the polymer is too high. (Bhardwaj and Kundu 2010; Mohammadian and Haghi 2014)

The process parameters include the intensity of applied voltage, flow rate, the distance between needle and collector, and types of collectors. As the mechanism explained, the jet could only be ejected from the Taylor cone when the threshold voltage reached. A higher applied voltage could increase the repulsive force between each charge located on the jet, resulting in a longer whipping path. With more solvent evaporation in the patch, a thinner fiber is fabricated in the process. (Pillay, Dott et al. 2013) The flow rate has a dramatic influence on the diameter of fiber. Slow flow rates reduce the size of the Taylor cone and volume of polymer jets, ensuring the evaporation of solvent during the whipping path and resulting in a smaller diameter fiber. Meanwhile, when flow rates are high, and the size of the Taylor cone is large, more fiber beading would form due to insufficient evaporation. (Shin, Hohman et al. 2001) Similarly, the working distance also affects the diameter of fibers by controlling the evaporation time. Short distances limit the solvent evaporation and drying of polymer jet, resulting in a wet nanofiber. But the long-distance could reduce the intensity of the electric field, resulting in beads and discontinuous fibers.

(Pillay, Dott et al. 2013) Lastly, the collector is critical to determine the orientation and alignment of fibers. Nanofibers are homogenously distributed and less oriented on a static plate collector. The oriented nanofibers need be collected by a rapidly rotating drum or a rotating disc which could mechanically stretch the fiber and help the alignment of the fibers. (Zander 2013)

Environment factors, including relative humidity and temperature, also have a dramatical influence on the morphology of electrospun fibers. The temperature affects the evaporation rates of polymer solution jets by controlling the vapour pressure of solvents. A thinner fiber could be produced at a higher room temperature. The influence of relative humidity is complicated. For water-based solvents, the increase of relative humidity would increase vapor pressure of the solvent and slow down its evaporation, resulting in an increase of diameter, porosity, and pore size nanofiber mats. Such electrospun nanofibers have an ideal surface feature for specific applications, including tissue engineering and drug delivery. However, high relative humidity may cause a thinner fiber for non-polar solvents because moisture could help the solidification of polymers. (Casper, Stephens et al. 2004) Generally, the nanofiber needs to be fabricated at low relative humidity (10-40%). However, when relative humidity is too low, solvents may evaporate rapidly, and the solidified polymer could block the needle tips. Besides, for fabricating a thin nanofibrous membrane, hot air is commonly used to increase the evaporation rates, and a vacuum pump could be applied to remove solvents. When the oxygen-sensitive nanofiber is fabricated by electrospinning, inert gases, such as nitrogen or argon, are necessary to fill the spinning chamber to prevent the oxidization of the polymer at extremely high voltage.

2.2.3 Applications of electrospun nanofibers

Due to the unique as-mentioned properties, nanofiber could be employed in a broad scope of applications in nanoscale devices, including water or air filtration, clinical use, energy storage, and protein adsorption. (Venugopal, Ramakrishna et al. 2005; Martins, Araújo et al. 2007) Filtration is the major application of nanofibrous membranes. The pore size of the nanofibrous membrane is varied from nanometer to micrometer range, compactible to filters for removal of submicron particles from air or water. Meanwhile, the hydrophilicity and ionic charge of the nanofiber surface contribute to adsorbing and dissolving chemical elements from air or water. Thus, nanofibrous membranes with proper pore sizes and proper chemical properties could be employed as mechanical and chemical filters. (Schreuder-Gibson, Truong et al. 2003) These nanofibers incorporated with nonwoven fabrics have been widely used in filtration products, such as facemasks, aerosol filters, personal care fabrics, defensive clothing, wastewater filters, water/oil separation film and heavy metal adsorption film. (Kumar and Nahm 2011; Zhang, Chae et al. 2012; Li, Wang et al. 2013; Wang, Si et al. 2014; Si, Fu et al. 2015; Wang, Yu et al. 2016)

Nanofibers are widely used in clinical textiles and biological applications because the pore size of nanofibrous media is compatible with the size of cells. The nanofibers have been used as drug delivery substrates, artificial organs, artificial blood vessels, and tissue engineering. (Pham, Sharma et al. 2006; Nisbet, Forsythe et al. 2009) Synthetic biocompatible nanofibers such as poly (lactic acid), polycaprolactone and poly (lactic-co-glycolic acid) have been applied as scaffold production. (Azimi, Nourpanah et al. 2014)

The diameter of such nanofibers varies from 50nm to 500 nm, the porosity of these nanofibrous membranes is above 90%, and pore size is controlled at micrometer range. These nanofiber scaffolds have an ideal morphology and micro-structure for cellular recognition, attachment, and differentiation. (Khajavi, Abbasipour et al. 2016) Due to proper cellular recognition, biocompatible polymers initiate immune responses rarely. (Cheng, Jun et al. 2017) Meanwhile, they also have other merits, including low toxicity, biodegradation, and proper mechanical properties. (Hejazi and Mirzadeh 2016) The biocompatible and biodegradable nanofibers also could be used as drug delivery and drug-releasing substrate. The nanofibers possess high drug-loading capacity due to the ultra-high specific area. Then, since the diffusion of drug molecules inside nanofibrous material is extremely slower than the diffusion of such molecules inside other porous material, the drug could release slowly for the exertion of long-term therapy. (Sharifi, Sooriyarachchi et al. 2016)

Since some polymers have proper electric conductivity, these nanofibers could be applied in energy materials, including semiconductors, battery separators, fuel cells and supercapacitors. (Zhang and Pan 2015) For an instant, polyaniline nanofiber and their composites, prepared by polymerization of aniline monomer under acid conditions, have high conductivities and high specific capacitance. Such nanofiber composites could be used as supercapacitor electrodes. (Zhang, Zhang et al. 2010; Yanilmaz, Dirican et al. 2019) Compared with conventional capacitance material, nanofiber-based capacitors have many merits, including flexibility, wearability, fast charge and discharge rates, high power densities, and long lifetime. Besides, carbon nanofiber is widely used as a substrate material for metal oxides in rechargeable lithium-air batteries. Carbon

nanofibers could be made into open macro-porous structures, providing ideal support for the oxygen reduction reactions. (Yang, He et al. 2009)

Besides, the surface of nanofibers could be modified by functional chemical compounds for specific applications. (Wang, Yu et al. 2016) For instance, the surface of nanofibers could be modified with chelating groups for heavy metal adsorption and purification. (Zhu, Yang et al. 2011; Foong, Wirzal et al. 2020) Nanofibers could be functionalized by N-halamine or photoactive agents for anti-bacterial and antifouling applications. (Zhang, El-Moghazy et al. 2020; Ma, Ramos et al. 2021; Ma, Wisuthiphaet et al. 2021) Especially, nanofibers could be modified with proper biological groups such as peptides and antibodies. Such biological functionalized nanofiber could be used for protein adsorption, detection and purification. (Zhu, Sun et al. 2012) Zhu et al. modified poly (vinyl alcohol-co-ethylene) nanofibrous membranes by eight different bio-functional linking agents and immobilized protein A/G onto the modified membranes for selectively recognizing and capturing IgG. Among all of these linking agents, disuccinimidyl carbonate was found to be the most effective agent for immobilizing protein A/G. However, since its high reactivity toward amine groups, multiple binding sites may form between nanofibers and protein A/G, subsequently changing the conformation of the protein A/G and eventually resulting in less captured IgG. Glutaraldehyde was found to have the highest IgG binding capacity because it has high efficiency for immobilization of protein A/G and would not affect the conformation of protein A/G. The results indicate that the nanofibrous membranes are flexible to be modified by different linking agents and the modified nanofibrous membranes have the potential to be applied as biosensors. (Zhu and Sun 2015)

2.3 Nanofiber-based biosensors

2.3.1 The merits of nanofiber-based biosensors

The nanofiber biosensor is fabricated by coating various bioreceptors on an electrospun nanofibrous substrate for specific analyte detection. Compared with conventional biosensor systems, the nanofiber biosensors have the following merits: 1) high sensitivity, 2) proper mass transfer, 3) convenient operation process, and 4) less false positive or negative results. These advantages of nanofiber biosensors could be attributed to the unique properties of electrospun nanofibers, including ultra-high specific surface area, high porosity, portability and flexibility for surface modification, respectively.

The ultra-large surface area of electrospun nanofibers could improve the antibody capacity, leading to high sensitivity. As the mechanism of ELISA explained (as shown in the introduction of this dissertation), compared with the conventional biosensor, the nanofiber biosensors could reveal the strong intensity of signal when detecting the same concentrated analytes, resulting in remarkably high sensitivity. Mertz et al. (Mertz, Kunduru et al. 2011) compared the sensitivity of polystyrene nanofiber biosensor and polystyrene bead biosensor for C-reactive protein detection. The sensitivity of the nanofiber biosensor was found around twice higher than the polymer bead biosensor.

The conventional biosensor may have the mass transfer issue, especially when detecting small molecule analytes from a complicated system such as detecting biomarkers from blood plasma. (Qureshi, Gurbuz et al. 2012) The blood plasma contains many large-size components such as exosomes and cells, which may be adsorbed on

the surface of conventional biosensors and sterically block the interaction between biomarkers and bioreceptors, eventually leading to inaccurate and imprecise detection of small size biomarkers. The parallel samples always reveal a huge error bar, resulting in a high signal-to-noise ratio and low sensitivity. Li et al. fabricated a surface-modified mesoporous nanofibrous membrane for biomarker detection from blood plasma samples. In this research, the nanofibers acted in two roles: 1) support solid substrates for loading bioreceptors, 2) filter matrices for blocking and removing large size components. The surface of the nanofibers was modified by hydrophilic agents for reducing non-specific adsorption. Thus, the reaction between biomarkers and bioreceptors is rarely sterically inhibited. Such nanofiber biosensors could increase 6 folds in the sensitivity and 5 times in signal-to-noise for direct blood plasma detection. (Li, Liu et al. 2020)

Besides, nanofibers could be fabricated as the support material of portable biosensors for on-site detection. Since the nanofiber biosensor has a higher sensitivity than the conventional biosensor, a low concentration of analytes could cause a significant signal via a nanofiber biosensor. Thus, a highly sensitive detector is not necessary for nanofiber biosensors. Meanwhile, the micro-porous nanofibrous material is an ideal filtration material that could block impurities. Thus, professional filtration columns and extraction instruments may not be required for nanofiber biosensors. Given the above advantages, the nanofibrous membrane biosensors have the potential to be applied as point-of-care detection with inexpensive commercial devices. Shaibani et al. fabricated a portable nanofiber biosensor for rapid Escherichia coli detection in orange juice. The nanofiber sensor was placed inside a 3D printed microfluid chip for sample transferring, and a LED light was applied for the light source. The LOD of this sensor was found to be 102 CFU/mL.

(Shaibani, Etayash et al. 2018) Çetin et al. fabricated a portable and rapid glucose biosensor based on poly(3,4-ethylenedioxythiophene) nanofibers for glucose detection. The LOD was found to be 2.9 μM with a short response time at 2–3 s. (Çetin and Camurlu 2018) Jiang et al. developed a low-cost and portable electrochemical nanofiber biosensor for rapid detection of milk allergen casein. The substrate material was fabricated by a graphene /carbon nanofiber / gelatin methacryloyl composite which has high conductivity and good biocompatibility. Rat basophilic leukemia (RBL-2H3) mast cells, as bioreceptors, were immobilized on the surface of the biosensor. And a portable electrochemical station was applied as the detector. The LOD was found to be 32ng/mL with a short detection time. (Jiang, Ge et al. 2019)

Lastly, since the bioreceptors are physically adsorbed on the surface of conventional biosensor materials by physical adsorption, the materials are usually hydrophobic polymer materials such as nitrocellulose. The blocking agents hardly cover all the unsaturated reactive sites, and the enzyme reporters could be non-specifically adsorbed, resulting in false-positive results. Contrarily, since the hydrophobic force is not as strong as covalent binding, the adsorbed bioreceptors could be washed off in the washing steps, resulting in false-negative results. (SternesjÖ and Gustavsson 2006) On the contrary, the surface of electrospun nanofiber could be modified by varied linking agents, leading to covalent immobilization of bioreceptors. Thus, the bioreceptors are hardly washed off by PBS solution, resulting in fewer false-negative results. Since some linking agents such as N-hydroxysuccinimide (NHS) ester could be hydrolyzed in the aqueous solution, the enzyme reporters would not be linked with biosensors by non-specific binding, resulting in less false-positive results. Wang et al. electrospun a bioactive and antifouling

nanofibrous membrane for rapidly detecting model target protein (mouse IgG) with no false-positive results. The nanofibrous membrane was made of a poly(oxanorbornene) derivative, which is a hydrophilic polymer and flexible to modify. The biotin (bioactive agents) and triethylene glycol (antifouling agents) were modified on the nanofiber. Since HRP would not be non-specifically adsorbed on the antifouling agent modified nanofiber, no false-positive results were detected by the nanofiber biosensor. (Wang, Yang et al. 2020)

2.3.2 Recent advances in nanofiber biosensors

The commonly developed nanofiber biosensors include an impedimetric biosensor, electrochemical biosensor, optical biosensor, and so on.

Nanofiber-based impedimetric biosensors measure the changes in charge conductance and capacitance on the nanofiber surface as the selective binding of the analytes. (Kim, Iezzi Jr et al. 2019) Migliorini et al. developed a urea impedimetric biosensing by depositing zinc oxide nanoparticles modified by polyamide 6 and polypyrrole electrospun nanofibers onto a fluorine-doped tin oxide electrode. Such a composite material exhibited excellent properties for the immobilization of urease enzyme, resulting in high sensitivity for urea detection with a LOD at 0.011 mg/dL. (Migliorini, Sanfelice et al. 2018) Gokce et al. fabricated an impedimetric DNA biosensor by using polyurethane/poly(m-anthranilic acid) (PU/P3ANA) electrospun nanofibers. The PU/P3ANA nanofiber was deposited on an indium tin oxide polyethylene terephthalate electrode. Then, a probe DNA was immobilized by covalent binding with carboxyl groups

on the nanofibers. The nanofiber biosensor was ultra-sensitive for Salmonella spp detection with a LOD at 0.1 μM. (Gokce, Akalın et al. 2018) Yagati et al. developed an impedimetric aptamer biosensor for detecting tumor marker MUC1 with electrospun core-shell nanofibers. The surface of its carbon electrode was modified with honey and polyvinyl alcohol core-shell electrospun nanofibers, multi-walled carbon nanotubes and gold nanoparticles. Then, MUC1-binding aptamer was immobilized on the surface of the composite material. The resistance of the electrode was measured by electrochemical impedance spectroscopy. The biosensor exhibited a linear range from 5 to 115 nM of MUC1 and a LOD at 2.7 nM. (Yagati, Park et al. 2017) Ye et al. used a functionalized nanoporous alumina membrane to fabricate a rapid and highly sensitive impedance biosensor for detecting histamine from seafood. The biosensor was modified with magnetic nanoparticles for histamine accumulation, impurity filtration, and signal amplification. The LOD was found at 1 μM. Such biosensors showed a potential for rapid detecting histamine to confirm the safety of seafood products. (Ye, Ding et al. 2017)

The electrochemical biosensors are the most common and sensitive biosensors, and their sensitivity could be further improved by incorporating them with nanofibers. Jeong et al. fabricated a high-performance field effective transistor-based biosensor by N-doped carbon nanofibers for cortisol detection. The morphology of the nanofibers was controlled by the vapor pressure conditions during vapor deposition polymerization. After thermal annealing, acid treatment, and antibody attachment, the field-effective transistor transducers exhibited high sensitivity and accurate selectivity to the detection of cortisol molecules with a LOD at 10aM and linear range at 100aM to 10nM. (Jeong, Oh et al. 2019) Wang et al. developed a molybdenum disulfide nanosheet arrays / carbon

nanofibers biosensor for the detection of levodopa and uric acid. The biosensor was fabricated by hydrothermal synthesis and electrospinning. Due to the superior conductivity and high specific surface area of carbon nanofibers, the carbon nanofiber modified biosensor had a low LOD at 0.91 and 0.73 uA/uM for levodopa and uric acid, respectively. The biosensor also displayed good stability and repeatability. (Wang, Yue et al. 2019) Demiroglu et al. fabricated lignin/polyacrylonitrile/graphene-enhanced nanofibers as an electrode material of an electrochemical biosensor for detecting acetaminophen. Biopolymer lignin was blended with polyacrylonitrile and graphene. And nanofibers in sizes less than 100nm were obtained via electrospinning, thermal stabilization, and carbonization. The results indicated that the carbon nanofiber modified electrode exhibited a remarkable improvement in conductivity, resulting in a highly sensitive response to analytes. (Demiroğlu Mustafov, Mohanty et al. 2019) Alim et al. developed a novel glucose biosensor based on polymerized multi-porous tin oxide nanofiber. Multi-porous tin oxide nanofiber was synthesized by the electrospinning method and polymerized with polyaniline. Such nanofiber possesses a high surface area and good electrical conductivity. Then, glucose oxidase and horseradish peroxidase were immobilized on the surface of the nanofibers. The nanofiber biosensor exhibited a longer linear range, low LOD and quick response time. (Alim, Kafi et al. 2019)

Optical biosensors are direct, convenient and portable biosensors for toxicant analysis. The signal of optical biosensors is directly visual and could be measured by a camera or smartphone. A novel optical biosensor for direct and selective detection of serotonin in serum was developed by Ramon-Marquez et al. A commercially available nanofiber was applied to capture serotonin directly from serum. Then, primary and secondary antibodies

were immobilized onto the analytes. Subsequently, serotonin phosphorescent emission was measured from the solid surface. Since the signal was detected by a phosphorescent detector, the interference from emission fluorescence of other molecules in the serum sample could be avoided. Thus, the developed nanofiber biosensor could be directly applied in serum analysis with a simple clean-up protocol. The serum samples from seven healthy volunteers were detected by the device with a correlation coefficient of 0.997. (Ramon-Marquez, Medina-Castillo et al. 2016) Wang fabricated a near-infrared optical nanofiber biosensor for 2,4,6-trinitrotoluene (TNT) explosive detection by directly loading TNT binding peptide to single-walled carbon nanotubes utilizing the π-π interaction between the aromatic amino acids and carbon nanotube. The results showed a highly selective and sensitive detection of TNT explosive targets with a LOD at 0.01ppm and linear range at 0.01ppm-10ppm. (Wang 2018) Chandra et al. developed a label-free ultrasensitive optical sensor by immobilizing antibodies on polyaniline nanofibers. The molecular conformation of polyaniline polymer before and after immunological interactions was studied by various instruments, including proton nuclear magnetic resonance, Fourier transformed infrared and selected area electron diffraction. The spectroscopic properties of the polyaniline polymer changed because the immunological interactions happening on the surface could change the polymer conformation. Based on the optical properties of the polyaniline polymer, an IgG biosensor was developed with a LOD at 37 pM. (Chandra, Bharadwaj et al. 2017)

Nanofiber-based ELISA is the most studied optical biosensor by incorporating the ELISA system on the nanofiber matrix. Due to the ultra-high specific surface area of nanofibers, the bioreceptor capacity and sensitivity of ELISA should be remarkedly

improved accordingly. However, based on published research, the sensitivity of nanofiber ELISA is slightly higher than micro-plate ELISA. Yang et al. developed an electrospun nanofiber ELISA for HIV detection. The track-etched polycarbonate membrane was applied as the solid substrate. Compared with plate ELISA, the antibody capacity of the nanofiber sensor was increased to 10 times, and the sensitivity was increased to 5 times. (Yang, Niu et al. 2008) Mahmoudifard et al. covalently immobilized antibody on polyethersolfone electrospun nanofibrous membrane for biosensing applications. The polyethersolfone nanofibrous membrane was fabricated by electrospinning, activated by an oxygen plasma, modified through 1-ethyl-3-(3-dimethylaminopropyl)-carbodiimide / N-hydroxysuccinimide (EDC/NHS) coupling strategy, subsequently. The antibody capacity was increased to 2.3 times, and the sensitivity was increased to 1.2 times. (Mahmoudifard, Soudi et al. 2016) Falcucci et al. fabricated a poly(ε-caprolactone) electrospun nanofiber ELISA for human papillomavirus (HPV) type 16 detection. The sensitivity was increased to 5-6 times. (Falcucci, Paolini et al. 2021) Sadir et al. compared three different fiber-based ELISAs for C-reactive protein detection. The electrospun poly-L-lactic acid nanofiber, cellulose acetate nanofiber and a microfiber of commercial cotton swabs were selected for testing. The LODs of each fiber-based platform were 13 pg/ml, 53 pg/ml and 27.32 pg/ml, respectively. The nanofiber ELISA did not exhibit improved sensitive detection than the microfiber ELISA in this research. (Sadir, Prabhakaran et al. 2014)

2.4 Research objectives

The progress of conventional and updated analysis techniques in detecting and quantifying toxicants have been reviewed. The regular ELISA methods offer critical perspectives but still have many limitations and challenges. The current commercially available ELISA can provide results with satisfying accuracy and sensitivity. However, conventional ELISA is expensive and not available for on-site detection. The nanofiber-based impedimetric and electrochemical biosensors have remarked sensitivity and have the potential to be developed as portable sensors for on-site applications. However, such biosensors could not prove visual signals and depend on expensive instruments such as electrochemical stations. The nanofiber-based optical biosensors, especially nanofiber-based ELISA, are convenient and visible. However, the existing nanofiber-based ELISA just slightly improves the sensitivity because of the hindered diffusion of larger-biomolecules.

According to the current progresses in the development of highly sensitive biosensors and the need for on-site detection, I proposed to development and fabrication of highly sensitive colorimetric personal use biosensors by incorporating ELISA on nanofibrous membranes. For achieving the goal, the dissertation is comprised of three objectives in the following subsequence:

1) To design and fabricate a portable colorimetric biosensor with nanofibrous membranes.

2) To study the mass transfer and adsorption property of large biomolecules, including antibodies and enzymes, through micro-porous nanofibrous membranes.

3) To optimize the biosensors and dramatically increase the sensitivity for toxicant detection based on the knowledge obtained from Objective 2.

This dissertation will report the research achievement in six chapters. Chapter 1 and chapter 2 are introduction and literature review, respectively. Chapter 3 reports the fabrication of a naked-eye distinguishable colorimetric biosensor for toxin detection with nanofibrous membrane-based ELISA. In this chapter, an antibiotic, chloramphenicol (CAP), was selected as a model analyte because CAP is banned by EPA recently but potentially exists in import seafood products. (Aldeek, Hsieh et al. 2017) A poly (vinyl alcohol-co-ethylene) (PVA-co-PE) nanofibrous membrane was electrospun, modified with different crosslink agents, and immobilized with anti-CAP antibodies. The antibody capacity was dramatically increased, and the signal intensity was dramatically increased. Consequently, a low concentration of CAP (0.3 ppb) could reveal a naked-eye detectable color change. A “Yes or No” biosensor was fabricated to determine whether the concentration of CAP is beyond the benchmark concentration or not. The successful design and fabrication of the nanofiber ELISA provide new paths towards the development of field-deployable biosensors without assistance from any instruments. Chapter 4 reports the diffusion property of protein molecules through microporous nanofibrous membranes. Since the specific surface area of the nanofibrous membrane is hundreds or thousands of times higher than the plate materials, the amount of antibody immobilized on the nanofibers and sensitivity of nanofiber ELISA should be improved accordingly. However, both antibody capacity and sensitivity of all the existing nanofiber biosensors were significantly lower than their theoretical values. For instance, in chapter 3, the amount of incorporated antibody increased by 7 times, and the sensitivity of the

sensor only increased by twice. After analysis, we found the large biomolecules have hindered diffusion behavior in the nanofibrous media, resulting in the accumulation of antibodies on the surface but not diffusing into the membranes, significantly reducing the benefits provided by the nanofibrous membranes. The classical diffusion model of protein molecules through porous media is based on the research of 3-dimensional homogenous matrices. But nanofibrous membranes have heterogeneous structures possessing much smaller effective pore sizes than the measured pore sizes, which was ignored by previous researchers. Thus, the diffusion coefficient of proteins inside a nanofibrous membrane is around tens or hundreds of times lower than the predicted results from a classical diffusion model, and the diffusion property of the protein is predictable only when the pore size of the nanofibrous membrane is at least 1000 times higher than the protein size. The results of this fundamental study provide insights into designing and optimizing the pore structure of nanofibrous membrane for further improving the sensitivity of nanofiber ELISA. Chapter 5 reports the development of an ultra-highly sensitive colorimetric biosensor on the nanofibrous membrane for toxin detection by improving the diffusion properties of large-biomolecules inside nanofibrous media. Not only we fabricated a novel nanofiber device in this objective, but also it is the first document about the influence of nanofiber microstructure on biosensor behavior which was ignored by previous researchers. Based on the results from chapter 4, we fabricated large pore size nanofibrous membranes as support materials for ELISA. The nanofibrous membrane with proper micro-structure avoids the hindered diffusion issue of large biomolecules inside a nanofibrous membrane. The sensitivity of the properly designed nanofiber ELISA could be dramatically improved with a limit of detection (LOD) for CAP detection at 0.005ppb. The successful design and

fabrication of the ultra-highly sensitive nanofiber biosensor prove the hypothesis of chapter 4 and provide insight into remarkedly improving the performance of nanofiber ELISA by optimizing the microstructure. Lastly, chapter 6 is the executive conclusion.

2.5 References

Abbott, S. R. (1980). Practical aspects of normal-phase chromatography. Journal of chromatographic science, 18(10), 540-550.

Alim, S., Kafi, A. K. M., Rajan, J., & Yusoff, M. M. (2019). Application of polymerized multiporous nanofiber of SnO2 for designing a bienzyme glucose biosensor based on HRP/GOx. International journal of biological macromolecules, 123, 1028-1034.

Almetwally, A. A., El-Sakhawy, M., Elshakankery, M. H., & Kasem, M. H. (2017). Technology of nano-fibers: Production techniques and properties-Critical review. Journal of Textiles Association, 78(1), 5-14.

Azimi, B., Nourpanah, P., Rabiee, M., & Arbab, S. (2014). Poly (∈-caprolactone) Fiber: an overview. Journal of Engineered Fibers and Fabrics, 9(3), 155892501400900309.

Baumgarten, P. K. (1971). Electrostatic spinning of acrylic microfibers. Journal of colloid and interface science, 36(1), 71-79.

Bhardwaj, N., & Kundu, S. C. (2010). Electrospinning: a fascinating fiber fabrication technique. Biotechnology advances, 28(3), 325-347.

Bockstahler, L. E., Li, Z., Nguyen, N. Y., Van Houten, K. A., Brennan, M. J., Langone, J. J., & Morris, S. L. (2002). Peptide nucleic acid probe detection of mutations in Mycobacterium tuberculosis genes associated with drug resistance. Biotechniques, 32(3), 508-514.

Bondavalli, P. (2019). Nanomaterials for biosensors: fundamentals and applications. MRS Bulletin, 44, 317.

Campbell, K., Huet, A. C., Charlier, C., Higgins, C., Delahaut, P., & Elliott, C. T. (2009). Comparison of ELISA and SPR biosensor technology for the detection of paralytic shellfish poisoning toxins. Journal of Chromatography B, 877(32), 4079-4089.

Casper, C. L., Stephens, J. S., Tassi, N. G., Chase, D. B., & Rabolt, J. F. (2004). Controlling surface morphology of electrospun polystyrene fibers: effect of humidity and molecular weight in the electrospinning process. Macromolecules, 37(2), 573-578.

Çetin, M. Z., & Camurlu, P. (2018). An amperometric glucose biosensor based on PEDOT nanofibers. RSC advances, 8(35), 19724-19731.

Chandra, S., Bharadwaj, R., & Mukherji, S. (2017). Label free ultrasensitive optical sensor decorated with polyaniline nanofibers: Characterization and immunosensing application. Sensors and Actuators B: Chemical, 240, 443-450.

Chen, A., Wang, G., Cao, Q., Wang, Y., Zhang, Z., Sun, Y., ... & Cheng, J. (2009). Development of an antibody hapten-chip system for detecting the residues of multiple antibiotic drugs. Journal of forensic sciences, 54(4), 953-960.

Chen, Y. J., Chen, M., Hsieh, Y. C., Su, Y. C., Wang, C. H., Cheng, C. M., ... & Chuang, K. H. (2018). Development of a highly sensitive enzyme-linked immunosorbent assay (ELISA) through use of poly-protein G-expressing cell-based microplates. Scientific reports, 8(1), 1-11.

Cheng, C. M., Martinez, A. W., Gong, J., Mace, C. R., Phillips, S. T., Carrilho, E., ... & Whitesides, G. M. (2010). Paper-based ELISA. Angewandte Chemie International Edition, 49(28), 4771-4774.

Cheng, J., Jun, Y., Qin, J., & Lee, S. H. (2017). Electrospinning versus microfluidic spinning of functional fibers for biomedical applications. Biomaterials, 114, 121-143.

Chu, X., Wu, L., Liu, X., Li, N., & Li, D. (2008). Detection of broad-spectrum aminoglycoside antibiotics through fluorescence-labeling aminoglycoside acetyltransferase (6′)-Ii. Analytical biochemistry, 376(1), 144-150.

Cooley, J. F. (1900). Improved methods of and apparatus for electrically separating the relatively volatile liquid component from the component of relatively fixed substances of composite fluids. United Kingdom Patent, 6385, 19.

Crowther, J. R. (2001). The ELISA guidebook (Vol. 149). Springer Science & Business Media.

Damborský, P., Švitel, J., & Katrlík, J. (2016). Optical biosensors. Essays in biochemistry, 60(1), 91-100.

Mustafov, S. D., Mohanty, A. K., Misra, M., & Seydibeyoğlu, M. Ö. (2019). Fabrication of conductive Lignin/PAN carbon nanofibers with enhanced graphene for the modified electrodes. Carbon, 147, 262-275.

Doshi, J., & Reneker, D. H. (1995). Electrospinning process and applications of electrospun fibers. Journal of electrostatics, 35(2-3), 151-160.

El-Aneed, A., Cohen, A., & Banoub, J. (2009). Mass spectrometry, review of the basics: electrospray, MALDI, and commonly used mass analyzers. Applied Spectroscopy Reviews, 44(3), 210-230.

Engvall, E., Jonsson, K., & Perlmann, P. (1971). Enzyme-linked immunosorbent assay. II. Quantitative assay of protein antigen, immunoglobulin G, by means of enzyme-labelled antigen and antibody-coated tubes. Biochimica et Biophysica Acta (BBA)-Protein Structure, 251(3), 427-434.

Falcucci, S., Paolini, F., Mileo, A. M., Franconi, R., Massa, S., Rinaldi, A., & Venuti, A. (2021). ePCL Electrospun Microfibrous Layers for Immune Assays: Sensitive ELISA for the Detection of Serum Antibodies Against HPV16 E7 Oncoprotein. ACS omega, 6(13), 8778-8783.

Fenn, J. B., Mann, M., Meng, C. K., Wong, S. F., & Whitehouse, C. M. (1989). Electrospray ionization for mass spectrometry of large biomolecules. Science, 246(4926), 64-71.

Fernandez, F., Pinacho, D. G., Sanchez-Baeza, F., & Marco, M. P. (2011). Portable surface plasmon resonance immunosensor for the detection of fluoroquinolone antibiotic residues in milk. Journal of agricultural and food chemistry, 59(9), 5036-5043.

Foong, C. Y., Wirzal, M. D. H., & Bustam, M. A. (2020). A review on nanofibers membrane with amino-based ionic liquid for heavy metal removal. Journal of Molecular Liquids, 297, 111793.

Gardas, A., & Lewartowska, A. (1988). Coating of proteins to polystyrene ELISA plates in the presence of detergents. Journal of immunological methods, 106(2), 251-255.

Gaudin, V., Cadieu, N., & Sanders, P. (2005). Results of a European proficiency test for the detection of streptomycin/dihydrostreptomycin, gentamicin and neomycin in milk by ELISA and biosensor methods. Analytica chimica acta, 529(1-2), 273-283.

Gokce, Z. G., Akalın, P., Kok, F. N., & Sarac, A. S. (2018). Impedimetric DNA biosensor based on polyurethane/poly (m-anthranilic acid) nanofibers. Sensors and Actuators B: Chemical, 254, 719-726.

Goode, J. A., Rushworth, J. V. H., & Millner, P. A. (2015). Biosensor regeneration: a review of common techniques and outcomes. Langmuir, 31(23), 6267-6276.

Greiner, A., & Wendorff, J. H. (2007). Electrospinning: a fascinating method for the preparation of ultrathin fibers. Angewandte Chemie International Edition, 46(30), 5670-5703.

Hammack, W., Carson, M. C., Neuhaus, B. K., Hurlbut, J. A., Nochetto, C., Stuart, J. S., ... & Heller, D. N. (2003). Multilaboratory validation of a method to confirm chloramphenicol in shrimp and crabmeat by liquid chromatography-tandem mass spectrometry. Journal of AOAC International, 86(6), 1135-1143.

Harris, D. C. (2010). Quantitative chemical analysis. Macmillan.

Hawkes, R., Niday, E., & Gordon, J. (1982). A dot-immunobinding assay for monoclonal and other antibodies. Analytical biochemistry, 119(1), 142-147.

Hejazi, F., & Mirzadeh, H. (2016). Novel 3D scaffold with enhanced physical and cell response properties for bone tissue regeneration, fabricated by patterned electrospinning/electrospraying. Journal of Materials Science: Materials in Medicine, 27(9), 1-17.

Huang, A. T., Garcia-Carreras, B., Hitchings, M. D., Yang, B., Katzelnick, L. C., Rattigan, S. M., ... & Cummings, D. A. (2020). A systematic review of antibody mediated immunity to coronaviruses: kinetics, correlates of protection, and association with severity. Nature communications, 11(1), 1-16.

Huang, Z. M., Zhang, Y. Z., Kotaki, M., & Ramakrishna, S. (2003). A review on polymer nanofibers by electrospinning and their applications in nanocomposites. Composites science and technology, 63(15), 2223-2253.

Impens, S., Reybroeck, W., Vercammen, J., Courtheyn, D., Ooghe, S., De Wasch, K., ... & De Brabander, H. (2003). Screening and confirmation of chloramphenicol in shrimp tissue using ELISA in combination with GC–MS2 and LC–MS2. Analytica Chimica Acta, 483(1-2), 153-163.

Jeong, G., Oh, J., & Jang, J. (2019). Fabrication of N-doped multidimensional carbon nanofibers for high-performance cortisol biosensors. Biosensors and Bioelectronics, 131, 30-36.

Jiang, D., Ge, P., Wang, L., Jiang, H., Yang, M., Yuan, L., ... & Ju, X. (2019). A novel electrochemical mast cell-based paper biosensor for the rapid detection of milk allergen casein. Biosensors and Bioelectronics, 130, 299-306.

Karaseva, N. A., & Ermolaeva, T. N. (2012). A piezoelectric immunosensor for chloramphenicol detection in food. Talanta, 93, 44-48.

Kaufmann, A., Butcher, P., Maden, K., Walker, S., & Widmer, M. (2015). Determination of nitrofuran and chloramphenicol residues by high resolution mass spectrometry versus tandem quadrupole mass spectrometry. Analytica Chimica Acta, 862, 41-52.

Kessick, R., Fenn, J., & Tepper, G. (2004). The use of AC potentials in electrospraying and electrospinning processes. Polymer, 45(9), 2981-2984.

Khajavi, R., Abbasipour, M., & Bahador, A. (2016). Electrospun biodegradable nanofibers scaffolds for bone tissue engineering. Journal of Applied Polymer Science, 133(3).

Khongorzul, P., Ling, C. J., Khan, F. U., Ihsan, A. U., & Zhang, J. (2020). Antibody–drug conjugates: a comprehensive review. Molecular Cancer Research, 18(1), 3-19.

Kim, C., Ryu, H. D., Chung, E. G., Kim, Y., & Lee, J. K. (2018). A review of analytical procedures for the simultaneous determination of medically important veterinary antibiotics in environmental water: sample preparation, liquid chromatography, and mass spectrometry. Journal of environmental management, 217, 629-645.

Kim, M., Iezzi Jr, R., Shim, B. S., & Martin, D. C. (2019). Impedimetric biosensors for detecting vascular endothelial growth factor (VEGF) based on poly (3, 4-ethylene dioxythiophene)(PEDOT)/gold nanoparticle (Au NP) composites. Frontiers in chemistry, 7, 234.

Kumar, G. G., & Nahm, K. S. (2011). Polymer nanocomposites-fuel cell applications. IntechOpen.

Länge, K., Rapp, B. E., & Rapp, M. (2008). Surface acoustic wave biosensors: a review. Analytical and bioanalytical chemistry, 391(5), 1509-1519.

Lee, J. K., Park, M., Jose, J., Kang, M. J., & Pyun, J. C. (2012). Electrochemical ELISA based on Escherichia coli with autodisplayed Z-domains. Sensors and Actuators B: Chemical, 175, 46-52.

Leng, S. X., McElhaney, J. E., Walston, J. D., Xie, D., Fedarko, N. S., & Kuchel, G. A. (2008). ELISA and multiplex technologies for cytokine measurement in inflammation and aging research. The Journals of Gerontology Series A: Biological Sciences and Medical Sciences, 63(8), 879-884.

LF Nascimento, M., S Araujo, E., R Cordeiro, E., HP de Oliveira, A., & P de Oliveira, H. (2015). A literature investigation about electrospinning and nanofibers: historical trends, current status and future challenges. Recent patents on nanotechnology, 9(2), 76-85.

Li, D., & Xia, Y. (2004). Electrospinning of nanofibers: reinventing the wheel?. Advanced materials, 16(14), 1151-1170.

Li, M., Wang, D., Xiao, R., Sun, G., Zhao, Q., & Li, H. (2013). A novel high flux poly (trimethylene terephthalate) nanofiber membrane for microfiltration media. Separation and Purification Technology, 116, 199-205.

Li, Z., Liu, Y., Chen, X., Cao, H., Shen, H., Mou, L., ... & Cong, Y. (2020). Surface-modified mesoporous nanofibers for microfluidic immunosensor with an ultra-sensitivity and high signal-to-noise ratio. Biosensors and Bioelectronics, 166, 112444.

Lin, A. V. (2015). Direct ELISA. In ELISA (pp. 61-67). Humana Press, New York, NY.

Adigal, S. S., Rizvi, A., Rayaroth, N. V., John, R. V., Barik, A., Bhandari, S., ... & Chidangil, S. (2021). Human Tear Fluid Analysis for Clinical Applications: Progress and Prospects. Expert Review of Molecular Diagnostics, (just-accepted).

Ma, Y., Ramos, T. M., Amador, L., Nitin, N., & Sun, G. (2021). Durable and chlorine rechargeable biocidal composite material for improved food safety. Cellulose, 28(1), 503-515.

Ma, Y., Wisuthiphaet, N., Bolt, H., Nitin, N., Zhao, Q., Wang, D., ... & Sun, G. (2021). N-Halamine Polypropylene Nonwoven Fabrics with Rechargeable Antibacterial and Antiviral Functions for Medical Applications. ACS Biomaterials Science & Engineering.

Mahmoudifard, M., Soudi, S., Soleimani, M., Hosseinzadeh, S., Esmaeili, E., & Vossoughi, M. (2016). Efficient protein immobilization on polyethersolfone electrospun nanofibrous membrane via covalent binding for biosensing applications. Materials Science and Engineering: C, 58, 586-594.

Mallik, A. K., Qiu, H., Takafuji, M., & Ihara, H. (2018). High molecular-shape-selective stationary phases for reversed-phase liquid chromatography: A review. TrAC Trends in Analytical Chemistry, 108, 381-404.

Martins, A., Araújo, J. V., Reis, R. L., & Neves, N. M. (2007). Electrospun nanostructured scaffolds for tissue engineering applications.

Marx, S., Zaltsman, A., Turyan, I., & Mandler, D. (2004). Parathion sensor based on molecularly imprinted sol− gel films. Analytical Chemistry, 76(1), 120-126.

McNaught, A. D. (1997). Compendium of chemical terminology (Vol. 1669). Oxford: Blackwell Science.

Mertz, T. O., Kunduru, V., Patra, P. K., Vattipalli, K., & Prasad, S. (2011). Patterned polymer nanofibers based biosensors. MRS Online Proceedings Library, 1358(1), 30701-30706.

Migliorini, F. L., Sanfelice, R. C., Mercante, L. A., Andre, R. S., Mattoso, L. H., & Correa, D. S. (2018). Urea impedimetric biosensing using electrospun nanofibers modified with zinc oxide nanoparticles. Applied Surface Science, 443, 18-23.

Mohammadian, M., & Haghi, A. K. (2014). Study on the production of a new generation of electrospun nanofiber webs. Bulg. Chemical Communication, 46(3), 530-534.

Montiel, V. R. V., Campuzano, S., Conzuelo, F., Torrente-Rodríguez, R. M., Gamella, M., Reviejo, A. J., & Pingarrón, J. M. (2015). Electrochemical magnetoimmunosensing platform for determination of the milk allergen β-lactoglobulin. Talanta, 131, 156-162.

Nassau, E., Parsons, E. R., & Johnson, G. D. (1976). The detection of antibodies to Mycobacterium tuberculosis by microplate enzyme-linked immunosorbent assay (ELISA). Tubercle, 57(1), 67-70.

Nilghaz, A., & Lu, X. (2019). Detection of antibiotic residues in pork using paper-based microfluidic device coupled with filtration and concentration. Analytica chimica acta, 1046, 163-169.

Nisbet, D. R., Forsythe, J. S., Shen, W., Finkelstein, D. I., & Horne, M. K. (2009). A review of the cellular response on electrospun nanofibers for tissue engineering. Journal of biomaterials applications, 24(1), 7-29.

Pham, Q. P., Sharma, U., & Mikos, A. G. (2006). Electrospinning of polymeric nanofibers for tissue engineering applications: a review. Tissue engineering, 12(5), 1197-1211.

Pillay, V., Dott, C., Choonara, Y. E., Tyagi, C., Tomar, L., Kumar, P., ... & Ndesendo, V. M. (2013). A review of the effect of processing variables on the fabrication of electrospun nanofibers for drug delivery applications. Journal of Nanomaterials, 2013.

Pohanka, M., & Skládal, P. (2008). Electrochemical biosensors--principles and applications. Journal of applied biomedicine, 6(2).

Pohanka, M. (2017). The piezoelectric biosensors: Principles and applications. International Journal of Electrochemical Science, 12, 496-506.

Qureshi, A., Gurbuz, Y., & Niazi, J. H. (2012). Biosensors for cardiac biomarkers detection: A review. Sensors and Actuators B: Chemical, 171, 62-76.

Ramon-Marquez, T., Medina-Castillo, A. L., Fernandez-Gutierrez, A., & Fernandez-Sanchez, J. F. (2016). A novel optical biosensor for direct and selective determination of

serotonin in serum by solid surface-room temperature phosphorescence. Biosensors and Bioelectronics, 82, 217-223.

Rayleigh, L. (1882). On the equilibrium of liquid conducting masses charged with electricity. The London, Edinburgh, and Dublin Philosophical Magazine and Journal of Science, 14(87), 184-186.

Reneker, D. H., Yarin, A. L., Fong, H., & Koombhongse, S. (2000). Bending instability of electrically charged liquid jets of polymer solutions in electrospinning. Journal of Applied physics, 87(9), 4531-4547.

Rønning, H. T., Einarsen, K., & Asp, T. N. (2006). Determination of chloramphenicol residues in meat, seafood, egg, honey, milk, plasma and urine with liquid chromatography–tandem mass spectrometry, and the validation of the method based on 2002/657/EC. Journal of Chromatography A, 1118(2), 226-233.

Sadir, S., Prabhakaran, M. P., Wicaksono, D. H., & Ramakrishna, S. (2014). Fiber based enzyme-linked immunosorbent assay for C-reactive protein. Sensors and Actuators B: Chemical, 205, 50-60.

Sarbatly, R., Krishnaiah, D., & Kamin, Z. (2016). A review of polymer nanofibres by electrospinning and their application in oil–water separation for cleaning up marine oil spills. Marine pollution bulletin, 106(1-2), 8-16.

Schreuder-Gibson, H. L., Truong, Q., Walker, J. E., Owens, J. R., Wander, J. D., & Jones, W. E. (2003). Chemical and biological protection and detection in fabrics for protective clothing. Mrs Bulletin, 28(8), 574-578.

Scortichini, G., Annunziata, L., Haouet, M. N., Benedetti, F., Krusteva, I., & Galarini, R. (2005). ELISA qualitative screening of chloramphenicol in muscle, eggs, honey and milk: method validation according to the Commission Decision 2002/657/EC criteria. Analytica Chimica Acta, 535(1-2), 43-48.

Shaibani, P. M., Etayash, H., Jiang, K., Sohrabi, A., Hassanpourfard, M., Naicker, S., ... & Thundat, T. (2018). Portable nanofiber-light addressable potentiometric sensor for rapid Escherichia coli detection in orange juice. ACS sensors, 3(4), 815-822.

Sharifi, F., Sooriyarachchi, A. C., Altural, H., Montazami, R., Rylander, M. N., & Hashemi, N. (2016). Fiber based approaches as medicine delivery systems. ACS Biomaterials Science & Engineering, 2(9), 1411-1431.

Shih, C. M., Chang, C. L., Hsu, M. Y., Lin, J. Y., Kuan, C. M., Wang, H. K., ... & Cheng, C. M. (2015). based ELISA to rapidly detect Escherichia coli. Talanta, 145, 2-5.

Shin, Y. M., Hohman, M. M., Brenner, M. P., & Rutledge, G. C. (2001). Experimental characterization of electrospinning: the electrically forced jet and instabilities. Polymer, 42(25), 09955-09967.

Si, Y., Fu, Q., Wang, X., Zhu, J., Yu, J., Sun, G., & Ding, B. (2015). Superelastic and superhydrophobic nanofiber-assembled cellular aerogels for effective separation of oil/water emulsions. ACS nano, 9(4), 3791-3799.

Simons, H. L. (1966). U.S. Patent No. 3,280,229. Washington, DC: U.S. Patent and Trademark Office.

Snyder, M. L., & Ritchie, J. C. (2010). Quantification of busulfan in plasma using liquid chromatography electrospray tandem mass spectrometry (HPLC-ESI-MS/MS). In Clinical Applications of Mass Spectrometry (pp. 129-136). Humana Press.

Song, K. M., Jeong, E., Jeon, W., Jo, H., & Ban, C. (2012). A coordination polymer nanobelt (CPNB)-based aptasensor for sulfadimethoxine. Biosensors and Bioelectronics, 33(1), 113-119.

Sparkman, O. D. (2000). Mass spectrometry desk reference 2. Journal of the American Society for Mass Spectrometry, 12(11), 1144.

Steinitz, M. (2000). Quantitation of the blocking effect of tween 20 and bovine serum albumin in ELISA microwells. Analytical biochemistry, 282(2), 232-238.

SternesjÖ, Å., & Gustavsson, E. (2006). Biosensor analysis of β-lactams in milk using the carboxypeptidase activity of a bacterial penicillin binding protein. Journal of AOAC International, 89(3), 832-837.

Taylor, G. I. (1964). Disintegration of water drops in an electric field. Proceedings of the Royal Society of London. Series A. Mathematical and Physical Sciences, 280(1382), 383-397.

Thavarungkul, P., Dawan, S., Kanatharana, P., & Asawatreratanakul, P. (2007). Detecting penicillin G in milk with impedimetric label-free immunosensor. Biosensors and Bioelectronics, 23(5), 688-694.

Thevenot, D. R., Toth, K., Durst, R. A., & Wilson, G. S. (1999). Electrochemical biosensors: recommended definitions and classification. Pure and applied chemistry, 71(12), 2333-2348.

Tighe, P. J., Ryder, R. R., Todd, I., & Fairclough, L. C. (2015). ELISA in the multiplex era: potentials and pitfalls. PROTEOMICS–Clinical Applications, 9(3-4), 406-422.

Tucker, N., Stanger, J. J., Staiger, M. P., Razzaq, H., & Hofman, K. (2012). The history of the science and technology of electrospinning from 1600 to 1995. Journal of engineered fibers and fabrics, 7(2_suppl), 155892501200702S10.

Vasita, R., & Katti, D. S. (2006). Nanofibers and their applications in tissue engineering. International Journal of nanomedicine, 1(1), 15.

Veach, B. T., Baker, C. A., Kibbey, J. H., Fong, A., Broadaway, B. J., & Drake, C. P. (2015). Quantitation of chloramphenicol and nitrofuran metabolites in aquaculture products using microwave-assisted derivatization, automated SPE, and LC-MS/MS. Journal of AOAC International, 98(3), 588-594.

Venugopal, J., & Ramakrishna, S. (2005). Applications of polymer nanofibers in biomedicine and biotechnology. Applied biochemistry and biotechnology, 125(3), 147-157.

Vo-Dinh, T., & Cullum, B. (2000). Biosensors and biochips: advances in biological and medical diagnostics. Fresenius' journal of analytical chemistry, 366(6), 540-551.

Vonnegut, B., & Neubauer, R. L. (1952). Production of monodisperse liquid particles by electrical atomization. Journal of colloid science, 7(6), 616-622.

Walker, J. M. (2009). The ELISA guidebook. In Series Springer Protocols. Methods in Molecular Biology (Vol. 516). New Jersey: Humana Press.

Wang, J. (2018). Near infrared optical biosensor based on peptide functionalized single-walled carbon nanotubes hybrids for 2, 4, 6-trinitrotoluene (TNT) explosive detection. Analytical biochemistry, 550, 49-53.

Wang, N., Si, Y., Wang, N., Sun, G., El-Newehy, M., Al-Deyab, S. S., & Ding, B. (2014). Multilevel structured polyacrylonitrile/silica nanofibrous membranes for high-performance air filtration. Separation and Purification Technology, 126, 44-51.

Wang, W. Q., Yue, H. Y., Yu, Z. M., Huang, S., Song, S. S., Gao, X., ... & Wang, Z. (2019). Synthesis and Application of MoS 2 Nanosheet Arrays/Carbon Nanofibers for Simultaneous Electrochemical Determination of Levodopa and Uric Acid. IEEE Sensors Journal, 19(15), 5988-5994.

Wang, X., Yang, D., Jia, S. T., Zhao, L. L., Jia, T. T., & Xue, C. H. (2020). Electrospun nitrocellulose membrane for immunochromatographic test strip with high sensitivity. Microchimica Acta, 187(12), 1-10.

Wang, X., Yu, J., Sun, G., & Ding, B. (2016). Electrospun nanofibrous materials: a versatile medium for effective oil/water separation. Materials today, 19(7), 403-414.

Wu, X., Kuang, H., Hao, C., Xing, C., Wang, L., & Xu, C. (2012). Paper supported immunosensor for detection of antibiotics. Biosensors and Bioelectronics, 33(1), 309-312.

Xiao, Y., & Isaacs, S. N. (2012). Enzyme-linked immunosorbent assay (ELISA) and blocking with bovine serum albumin (BSA)—not all BSAs are alike. Journal of immunological methods, 384(1-2), 148-151.

Xu, N., Bai, J., Peng, Y., Qie, Z., Liu, Z., Tang, H., ... & Ning, B. (2017). Pretreatment-free detection of diazepam in beverages based on a thermometric biosensor. Sensors and Actuators B: Chemical, 241, 504-512.

Yagati, A. K., Park, I., Cho, S., & Min, J. (2017). Impedimetric Horseradish Peroxidase Sensor Based on Polyaniline-Nanofiber-Modified Microdisk Electrode Arrays. Science of Advanced Materials, 9(9), 1595-1602.

Yalow, R. S., & Berson, S. A. (1960). Immunoassay of endogenous plasma insulin in man. The Journal of clinical investigation, 39(7), 1157-1175.

Yang, D., Niu, X., Liu, Y., Wang, Y., Gu, X., Song, L., ... & Jiang, X. (2008). Electrospun nanofibrous membranes: A novel solid substrate for microfluidic immunoassays for HIV. Advanced Materials, 20(24), 4770-4775.

Yang, X. H., He, P., & Xia, Y. Y. (2009). Preparation of mesocellular carbon foam and its application for lithium/oxygen battery. Electrochemistry Communications, 11(6), 1127-1130.

Yanilmaz, M., Dirican, M., Asiri, A. M., & Zhang, X. (2019). Flexible polyaniline-carbon nanofiber supercapacitor electrodes. Journal of Energy Storage, 24, 100766.

Ye, W. W., Ding, Y. T., Sun, Y., Tian, F., & Yang, M. (2017). A nanoporous alumina membrane-based impedance biosensor for histamine detection with magnetic nanoparticles separation and amplification. Procedia Technology, 27, 116-117.

Zander, N. E. (2013). Hierarchically structured electrospun fibers. Polymers, 5(1), 19-44.

Zhang, K., Zhang, L. L., Zhao, X. S., & Wu, J. (2010). Graphene/polyaniline nanofiber composites as supercapacitor electrodes. Chemistry of Materials, 22(4), 1392-1401.

Zhang, L., Chae, S. R., Hendren, Z., Park, J. S., & Wiesner, M. R. (2012). Recent advances in proton exchange membranes for fuel cell applications. Chemical Engineering Journal, 204, 87-97.

Zhang, S., & Pan, N. (2015). Supercapacitors performance evaluation. Advanced Energy Materials, 5(6), 1401401.

Zhang, S., Zhang, Z., Shi, W., Eremin, S. A., & Shen, J. (2006). Development of a chemiluminescent ELISA for determining chloramphenicol in chicken muscle. Journal of Agricultural and Food Chemistry, 54(16), 5718-5722.

Zhang, Y., Zuo, P., & Ye, B. C. (2015). A low-cost and simple paper-based microfluidic device for simultaneous multiplex determination of different types of chemical contaminants in food. Biosensors and Bioelectronics, 68, 14-19.

Zhang, Z., El-Moghazy, A. Y., Wisuthiphaet, N., Nitin, N., Castillo, D., Murphy, B. G., & Sun, G. (2020). Daylight-Induced Antibacterial and Antiviral Nanofibrous Membranes Containing Vitamin K Derivatives for Personal Protective Equipment. ACS Applied Materials & Interfaces, 12(44), 49416-49430.

Zhu, J., & Sun, G. (2012). Lipase immobilization on glutaraldehyde-activated nanofibrous membranes for improved enzyme stabilities and activities. Reactive and Functional Polymers, 72(11), 839-845.

Zhu, J., & Sun, G. (2015). Bio-functionalized nanofibrous membranes as a hybrid platform for selective antibody recognition and capturing. RSC Advances, 5(36), 28115-28123.

Zhu, J., Yang, J., & Sun, G. (2011). Cibacron Blue F3GA functionalized poly (vinyl alcohol-co-ethylene)(PVA-co-PE) nanofibrous membranes as high efficient affinity adsorption materials. Journal of membrane science, 385, 269-276.

Chapter 3. Design and fabrication of a highly sensitive and naked-eye distinguishable colorimetric biosensor for chloramphenicol detection by using ELISA on nanofibrous membranes

3.1 Introduction

Antibiotics are widely applied in the medical treatments of human infections and prevention of diseases in stock and aquaculture farming. (Witte 1998; Lipsitch, Singer et al. 2002; Chang, Wang et al. 2015) Due to their broad applications in agriculture and aquaculture production, residual antibiotics could exist in food products. (Chang, Wang et al. 2015; Khachatourians 1998) Frequent exposure to residual antibiotics could lead to the development of antibiotic-resistant bacteria. Approximately 2 million people acquire infections caused by antibiotic-resistant pathogens each year in the United States. (CDC 2014) The cost of associated with antibiotic-resistant bacterial treatment has doubled over the past few decades and reached $2 billion in 2014. (CDC 2014) As a result, the United States Department of Agriculture (USDA) and the US Food and Drug Administration (FDA) have established strict regulations on tolerant concentrations for specific antibiotics in aquaculture and farmed products. Although precise and selective measurements of antibiotics are available by mass-spectrometry, the routine analysis is currently cost-prohibitive due to the complexity of the analytical methods involved. Thus, rapid, accurate, and on-site detection is needed to track residual antibiotics in the food supply.

The conventional detection methods for antibiotics in foods include Liquid Chromatography or Gas Chromatography-Mass Spectrometry (LC/GC-MS) and Enzyme-Linked Immunosorbent Assay (ELISA). (Mungroo and Neethirajan 2014; Kümmerer 2009) The LC/GC-MS is a reliable, sensitive, and selective technique but has limitations such as the use of expensive apparatus, complicated procedures, the need of trained operators, and long preparation time, which limit their uses in on-site inspections and instant examinations. (Hirsch, Ternes et al. 1998; Haller, Müller et al. 2002) Contrarily, ELISA is a relatively convenient analytical technique with good selectivity. Firstly, the analytical targets are specifically captured by antibodies that are pre-loaded on surface of solid supports; Then, the dye substrate reveals colorimetric signal after reacting with the enzyme conjugation of analytical targets. Thus, the concentration of analytical targets could be analyzed by measuring the intensity of colorimetric signal. However, the conventional ELISA could not generate naked-eye distinguishable color at detection of low concentration of the targets. Thus, the conventional ELISA process is dependent on the use of plate readers or instruments to detect targets in low concentrations, which limits its application for on-site detection of a trace number of targets. (Wang, Lin et al. 2019; Xie, Wen et al. 2019; Wu, Liu et al. 2019; Huang, Zhang et al. 2019; Wu, Huang et al. 2020) For achieving naked-eye detection, the color intensity needs to be improved via replacing the conventional dye substrates by intensified chromogenic agents, such as gold nanoparticles or quantum dots. (De La Rica, & Stevens 2012; Wang, Lin et al. 2019; Xie, Wen et al. 2019) Furthermore, the sensitivity could be further increased by functionally modifying gold nanoparticles to assist particle aggregation and amplify the signal. (Wu, Liu et al. 2019; Huang, Zhang et al. 2019; Wu, Huang et al. 2020; Liu, Dou

et al. 2020) However, the gold nanoparticles may increase the cost and have protentional environmental issues. On the other hand, the colorimetric signals also could be increased via capturing more analytical targets on a solid surface such as developing new antibodies or nanobodies with high affinity. (Niu, Zhang et al. 2019; Ji, Dong et al. 2020) However, this developing process is time-costing and may slightly improve the sensitivity. To meet the demand for on-site and instrument-independent detection, we report the development of a highly sensitive and naked-eye distinguishable paper-based ELISA biosensor by employing microporous and nanofibrous membranes as solid support media of antibodies. The ultrahigh surface of the nanofibers in the paper-like membranes could dramatically increases the areas and improves the number of immobilized antibodies incorporated onto the surfaces, which can quickly capture analytes in the environment, leading to dramatically intensified colorimetric signals enough for human eye detection. The poly(vinyl-co-ethylene) (PVA-co-PE) was selected as polymer to fabricating nanofibrous membranes because it possesses abundant hydroxyl groups which could be modified by

The electrospun nanofibrous membranes were modified by glutaraldehyde solution (GA), cyanuric chloride (CC), and N, N’-disuccinimidyl carbonate (DSC), respectively, which possess different reactivities to the hydroxyl group and hydrophilicity to interact with proteins

In this study, we focus on (CAP) because it is banned in the USA but may present in imported US aquaculture products. (CDC 2014) The developed immunoassay biosensor demonstrated high sensitivity for detecting CAP with naked eyes..

3.2 Materials and Methods

3.2.1 Materials

Glutaraldehyde solution 25% (GA), cyanuric chloride (CC), N, N'-disuccinimidyl carbonate (DSC), triethylamine (TEA), 1,4-dioxane, acetone, hydrogen peroxide (30 wt%), pH 6.4 citric acid buffer, phosphate-buffered saline (PBS), Pierce™ BCA Protein Assay Kit, Millipore column and high-binding 96-well plates were purchased from Thermo Fisher Scientific (USA). Poly(vinyl-co-ethylene) (PVA-co-PE, PE content of 27%, MWn =90,000), chloramphenicol (CAP), florfenicol (FF), thiamphenicol (TAP), penicillin (PCN), 3,3',5,5'-tetramethylbenzidine (TMB), fluorescein isothiocyanate labeled immunoglobulin G (FITC-IgG), and bovine serum albumin (BSA) were obtained from Sigma-Aldrich (USA). Anti-CAP antibody (Ab) and CAP labelled horseradish peroxidase (CAP-HRP) were purchased from Abcam (Cambridge, MA, USA). Nitrocellulose membrane (0.45μm) was purchased from Bio-Rad (USA).

3.2.2 Fabrication of PVA-co-PE nanofibrous membranes

PVA-co-PE nanofibrous membrane was fabricated according to the literature. (Si, Zhang et al. 2018; El-Moghazy, Zhao et al. 2018) PVA-co-PE (Mn = 90,000) was added into a mixture of isopropanol and water (weight ratio 7:3) with stirring at 80℃ for 2 hours to prepare electrospinning solutions. The concentration of PVA-co-PE in the electrospinning solution was 8 wt%. Then, the solution was transferred into 20mL syringes, capped by a 6-gauge needle and loaded onto a programmable syringe pump (Kats Scientific Co.). The solution was fed at a constant rate of 2mL per hour. A high

voltage of 25 kV (EQ30, Matsusada Inc.) was employed on needle tips generating a continuous polymer jet stream. The PVA-co-PE nanofiber membranes were deposited on a copper grid covered the rotating receiver with a fixed distance of 20 cm. Residual isopropanol/water solvent was removed by drying the produced nanofibrous membranes in a vacuum oven at 50 ℃ for 1 hour.

3.2.3 Modification of nanofibrous membranes.

For CC modified nanofibrous membranes, 0.1g of PVA-co-PE nanofibrous membranes were immersed into 3M NaOH aqueous solution at 5℃ for 30 mins and then were immersed into 0.1 g/mL CC solution (prepared by dissolving 5g CC in 50 mL of 1,4-Dioxane) at room temperature for 2 hours. The resulting membranes were removed out, washed with water and acetone, and vacuum dried. For GA modified membranes, 50mL of 25 wt% GA aqueous solution was prepared, and then 0.1g of PVA-co-PE nanofibrous membranes were immersed into the GA solution at room temperature for 2 hours. The resulting membranes were washed with water and acetone, and vacuum dried. For DSC modified membranes, 5 g of DSC and 0.2 g TEA were dissolved in 50 mL of 1,4-dioxane solvent, then 0.1 g PVA-co-PE membranes were added into this as-prepared solution. The mixture was stirred at 80℃ for 2 hours. The resulting membranes were washed with 1,4-dioxane and acetone, and vacuum dried.

3.2.4 Immobilization of antibody

The antibody stock solution was diluted to concentrations of 0.1g/L, 1g/L, and 2g/L in a PBS buffer. Then 10μL of each antibody solution was dropwise added to the center of pre-punched 1cm^2 modified PVA-co-PE membranes. Then, the membranes were incubated into a bio-oven at 25℃ for 20 mins. After that, unreacted antibodies on the membranes was washed-off using a PBS buffer. The number of the immobilized proteins was determined by bicinchoninic acid (BCA) protein assay via UV-vis spectroscopy with three replicates for each experiment. The absorption intensity at wavelength 562 nm was recorded for representing the number of antibodies. The protein immobilization reaction efficiency was calculated by dividing the number of immobilized proteins by the number of injected proteins. The resulting membranes were immersed into a 1 wt% BSA solution to block any unreacted sites, and rinsed by a washing buffer (PBS solution containing 0.05% Tween 20) to remove excess unbound proteins.

3.2.5 Analysis of colorimetric signals from ELISA

A competitive ELISA assay was used to detect antibiotics. A test solution was prepared by mixing 50μL of CAP solutions in varying concentrations (ranging between 0ng/mL to 100ng/mL) with 50μL of 500ng/mL CAP-HRP. Then, the antibody immobilized membranes were exposed to the mixture solution under gentle agitation for 20 mins. Then, the membranes were washed with the PBS buffer and dried in air. A TMB substrate was prepared by mixing 100μL of 0.6 wt% TMB solution, 25μL of 1 wt% H_2O_2 aqueous solution, and 6.25 mL of citric acid buffer together. 20 μL of the as-prepared TMB substrate was

added onto the membranes, and the membranes were placed in an LED lightbox (E mart) for 15 mins. A colorimetric signal was observed under the LED light (Lux 10,000). The colorimetric signal was captured by a smartphone (iPhone 6s) and quantitatively analyzed by Image J software. The smartphone camera was kept at the top of nanofibrous membranes with the fixed distance at 50cm to record the digital images of membranes. Then, the red, green, and blue values (RGB values) in the red channel (R value) could be scanned by an installed imaging app (such as *ColorAssist*) or by a software (such as *Image J*) after transferring digital images to a computer. Moreover, the R values were further analyzed and utilized to analyze the concentration of CAP. The sample size is three for all experiments.

3.2.6 Analysis of colorimetric signals from conventional ELISA

The CAP solutions in varying concentrations were analyzed by both the 96-wells plate-based and nitrocellulose membrane-based ELISA, respectively. The antibody solution was diluted to concentrations of 2g/L and was added to each well or each membrane, respectively. The samples were incubated in a bio-oven at 37°C for 1 hour. Then, the procedures of blocking, rinsing, and addition of a test solution and TMB substrate were conducted as described in experimental section 2.5. The absorbance intensity of 96-wells plate-based ELISA was recorded by a microplate reader (ThermoFisher Inc.). A smartphone (iPhone 6s) was used to analyze the colorimetric signal from the nitrocellulose membrane-based ELISA.

3.2.7 Extraction of salmon sample

Wild-caught and farmed salmon samples were purchased from local supermarkets in Davis, CA. 1 g of salmon samples were mixed with 3 mL of PBS solution. The mixture was homogenized at a vortex oscillator and filtered by a Millipore column to remove solids and lipids. (Zhang, Richardson et al. 2017) Various concentrations of CAP were added into the filtered solution to make the spiked samples. Subsequently, the 50µL of the filtrate was mixed with 50µL of 500ng/mL CAP-HRP to prepare the test solution, which was directly added to the functional nanofibrous membranes.

3.3 Results and Discussion

3.3.1 Fabrication of nanofibrous membrane-based ELISA

In the present study, the incorporation of the antibody onto the surfaces of nanofiber membranes could increase sensitivity and produce color signals readable by naked eyes. Schematic design and workflow of the nanofiber membrane-based ELISA immunosensor are shown in Scheme 3.1. PVA-co-PE was selected as a polymer to produce nanofibrous membranes by electrospinning. The electrospinning process fabricates nano-size fiber and provides an ultra-high specific area for membranes. An SEM image of a PVA-co-PE nanofibrous membrane is shown in Figure 3.1a, with an average fiber diameter of approximately 400nm and micro-size pores. (Figure 3.1b) PVA-co-PE nanofibrous membranes were previously shown to provide desired reactions with proteins. (Zhu and Sun 2015) Here, hydroxy groups on the material could be activated by GA, CC or DSC for immobilization of antibodies. (Figure 3.1c)

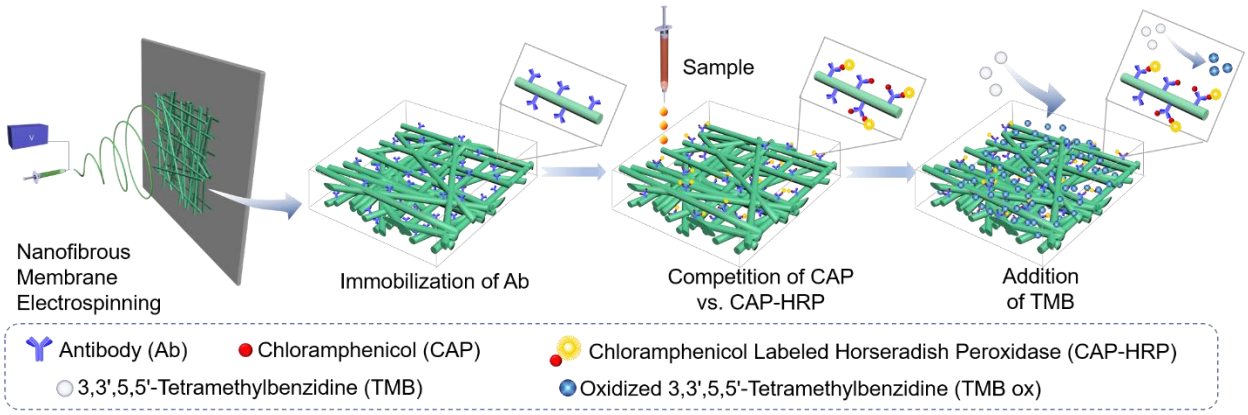

Scheme 3.1. Design, fabrication, and work mechanism of nanofibrous membrane-based ELISA.

The GA, CC, and DSC modified membranes possess different reactivities and hydrophilicity to interact with protein molecules. Among three reactive groups, CC is the least reactive and most hydrophobic one, while GA has medium reactivity and hydrophilicity, and DSC is the most reactive and most hydrophilic. Fourier-transform infrared spectroscopy (FTIR) proved successful incorporations of the reactive groups, including aldehyde peak of GA at 1722cm^{-1}, triazine peak of CC at 1547 cm^{-1}, and carbonate peak of DSC at 1730cm^{-1}. (Figure 3.1d) The chemically modified nanofibrous membranes retained the micro-porosity and nanofibrous structures (Figure 3.1e), reflecting the structural stability of the nanofibers and ensuring proper applications in further steps of reactions with biomolecules. Here, the CC modified nanofibers became swollen and adhesive because of alkali treatment of the PVA-co-PE membranes. The original nanofiber diameter of 449.57nm increased to 726.31nm after the CC modification as shown in Figure 3.1f. In contrast, the morphologies of the GA and DSC modified membranes were unchanged, with the nanofiber diameter slightly increased to 532.51nm and 547.19nm, respectively. Additionally, the GA, CC, and DSC reagents on the surfaces

of the fibers also improved hydrophilicity and wettability of PVA-co-PE fibers. The water contact angles of the membranes were measured after 1 second (1s) water contact as shown in Figure 3.1g. The original membranes were relatively hydrophobic with a water contact angle of 89.8°. Since CC is a non-polar reagent, the slight improvement of the membrane hydrophilicity (a water contact angle at 72°) may be attributed to polymer swelling during alkali treatment. In contrast, the more polar reagents (GA and DSC) modified membranes exhibited improved hydrophilic property with water contact angles at 31.1° and 22.8°, respectively. However, water could be fully adsorbed on the three modified membranes after 10s wetting time (0° water contact angle).

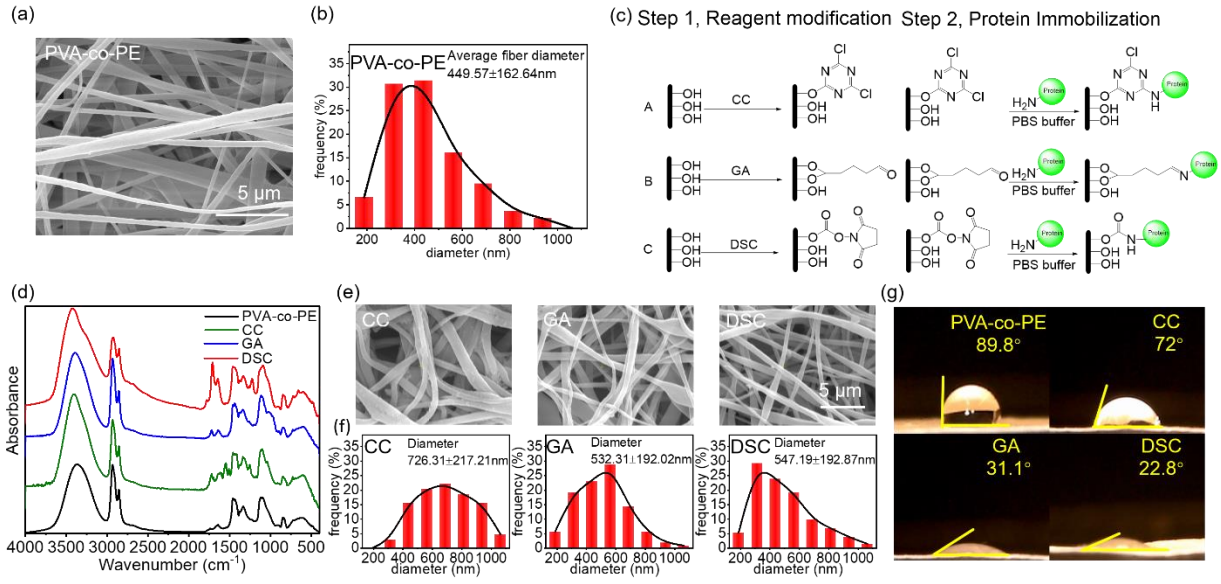

Figure 3.1. Microstructure and chemical modifications of nanofibrous membranes. a) SEM and b) Fiber diameter distribution of PVA-co-PE membrane; c) Reaction schemes of PVA-co-PE membrane with three reagents (CC, GA, and DSC) and proteins; d) FTIR spectra of PVA-co-PE membranes before and after modifications of CC, GA, and DSC;

e) SEM images and f) Fiber distributions of these nanofibrous membranes after reactions with CC, GA, and DSC; g) Water contact angles of these membranes.

3.3.2 Immobilization of protein onto nanofibrous membranes

The three modified membranes were then employed to immobilize antibodies as shown in Figure 3.1c. Here, FITC-IgG was used to qualitatively reveal the number of immobilized molecules by showing the intensities of fluorescence (brighter fluorescence indicates more immobilized proteins). The fluorescence images of each immobilized membranes are shown in Figure 3.2a. FITC-IgG diffused more homogenously into the more hydrophilic DSC and GA membranes than into the CC modified ones. An increase of the FITC-IgG solution concentration also improved the number of immobilized proteins on the CC membranes but not the GA and DSC membranes because the accessible reactive sites of the GA and DSC modified membranes may be saturated.

The number of immobilized antibodies and reaction efficiencies was quantitively measured by the bicinchoninic acid assay (BCA) test (Figure 3.2b and c). The CC modified membranes exhibited the lowest number of immobilized proteins, which was caused by the hydrophobic property and lower reactivity of the CC groups. Conversely, the hydrophilic and higher reactive reagents, GA and DSC, showed an increased number of immobilized proteins on the membranes. Besides, the CC modified membranes exhibited relatively low efficiency (20%). Contrarily, the immobilization efficiency on the GA and DSC treated membranes achieved at around 100% at the low FITC-IgG concentration but dramatically decreased with the protein concentration increased, which

confirmed the speculation that the reactive sites on these modified membranes were saturated. To compare the performance of reagents, the number of immobilized antibodies should be the same on each membrane. Thus, a concentration of 1g/L proteins was used in the immobilization reaction on the CC membranes, and a concentration of 0.5g/L proteins was applied to the GA or DSC membranes.

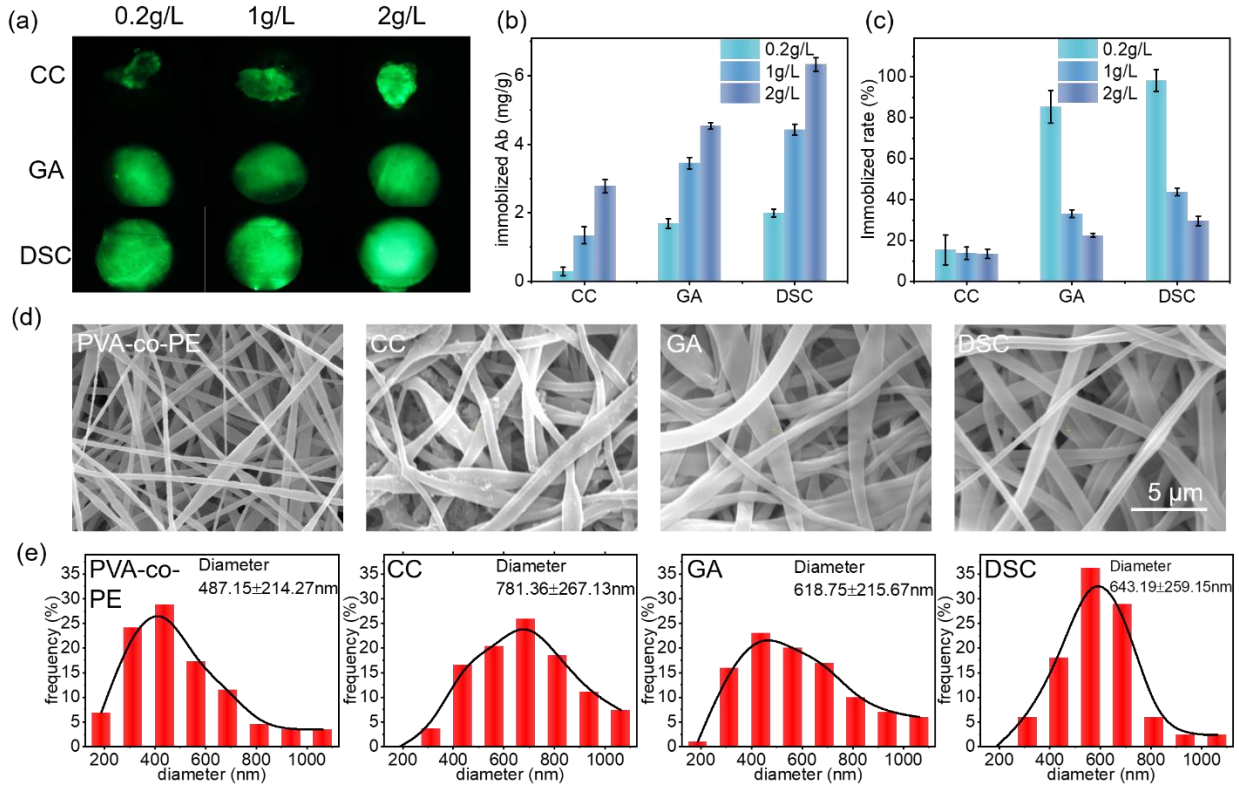

Figure 3.2. Immobilizing antibody onto nanofibrous membranes. a) Fluorescence images of three modified membranes immobilized with FITC-IgG; b) Immobilized antibody amounts on modified membranes; c) Immobilization reaction efficiency; d) SEM images of nanofibrous membranes after immobilization with the antibody; e) Fiber distributions of these membranes

Lastly, the impact of the immobilization reactions on the morphology of the nanofibrous membranes was studied by using an FE-SEM, as shown in Figure 3.2d. Compared with SEM images in Figure 3.1e, all fibers of three membranes revealed a slight swelling after being immobilized with the bio-macromolecule, but all fibers were still in the nanofiber level, which was further described by the slight changes of fiber diameter distributions as shown in Figure 3.2e.

3.3.3 Competitive ELISA on the nanofibrous membrane

Antibodies of CAP were immobilized on the chemically modified nanofibrous membranes, and the membranes were employed to detect CAP. The detection procedure is schematically described in Scheme 3.1. To find a proper concentration of CAP-HRP solution to be added onto the membranes, a checkerboard test was applied. A concentration of CAP-HRP at 250 ng/mL was identified as the optimal concentration.

Color signals could be observed under different concentrations of CAP solutions containing 250 ng/mL of CAP-HRP with various exposure times (Figure 3.3). TMB was used as an indicator of hydrogen peroxide generation via the catalytic effect of the peroxidase (CAP-HRP) enzyme. The oxidized TMB compound reveals a blue color (absorbance wavelength located at 605nm), indicating the number of CAP-HRPs conjugated with the antibodies on the membranes. The red channel value (R value) from red, green, and blue (RGB) results show the most significant change from the readings obtained with the smartphone. Thus, the R value was employed to represent the color intensity, with a lower R value indicating higher CAP concentration. As shown in Figure

3.3a, colorimetric signals were not homogenous on the CC modified membranes, causing relatively high error bars on R values in the plots. The blue color almost disappeared on the CC membranes at a low concentration of CAP at 0.3 ng/mL. The R value of the color signal reached a maximum value at 0.3ng/mL with 45 units higher than the R value at 0ng/mL and 30 units higher than that at 0.2ng/mL. These differences were easily visible by the naked eyes. On the contrary, although the GA and DSC treated membranes presented homogenous color signals (lower error bars), they could only distinguish higher CAP concentrations (0.5ng/mL by the GA modified membranes and 1ng/mL by the DSC modified membranes, respectively). Furthermore, the R values measured on the GA or DSC modified membranes could not achieve the maximum (155 units) at 1ng/mL of CAP because a considerable number of CAP-HRPs was likely bound to the immobilized antibodies on the membranes. The CAP molecules seem to have better competitive ability than CAP-HRP molecules with the antibody on the CC modified membranes, which is likely due to the conformation change after immobilization. For example, the conformation of loaded antibody may be affected by the membranes, and loaded antibody on CC membranes has a higher affinity with CAP than CAP-HRP. Therefore, more CAP could be captured on the CC modified membranes, and the sensitivity of the membrane was the highest. In general, all three membranes demonstrated varied abilities to detect trace amounts of CAP in solutions, with the CC modified membranes showing the highest sensitivity in the applications and being considered as the best substrate for the preparation of naked eye readable colorimetric sensors for CAP detection.

Besides, the exposure time also has the influence on the sensitivity. The oxidation of TMB by hydrogen peroxide and CAP-HRP is slow at the beginning of the reaction, due to

a lower concentration of generated hydroxyl radicals, becomes faster with the increase in reaction time, and gradually slows down again when the reagents are consumed. Thus, a membrane captured more CAP-HRPs (less CAP) should reveal a brighter color more rapidly than a membrane containing fewer CAP-HRPs (more CAP) in a short reaction duration. Finally, all membranes should exhibit the same color intensity at the end of the reaction theoretically because the same number of TMB molecules added. The CC modified membranes revealed distinct color change, as well as with significant R value difference, for solutions containing 0.2ng/mL and 0.3ng/mL CAP at a reaction time of 5mins, and the difference became more significant at 15mins. In contrast, the GA modified membranes exhibited a fast reaction with TMB, producing a more significant color difference within a short time (5mins) than at long reaction time (15mins). The corresponding R value difference between 0.2ng/mL and 0.3ng/mL was around 30 units at 5mins but decreased to 20 at 15mins. More CAP-HRPs on the GA-modified membranes prompt faster and possibly more sustained oxidation reaction of TMB, which can also explain why the color signal difference between 0.3ng/mL and 0.5ng/mL became significant with reaction time increase on the GA treated membranes. For the best use of the sensors in on-site detection for naked-eye observation, the color difference for a detectable range of a target should be significant and consistent for a reasonable duration. Hence, the GA treated membranes can be used for sensors to detect 0.5ng/mL CAP but may not be suitable to distinguish 0.3ng/mL CAP. Similarly, the sensors made from the DSC treated membranes would be useful in the detection of higher concentration CAP because the color difference between 0.5ng/mL and 1ng/mL of CAP became less significant within the duration.

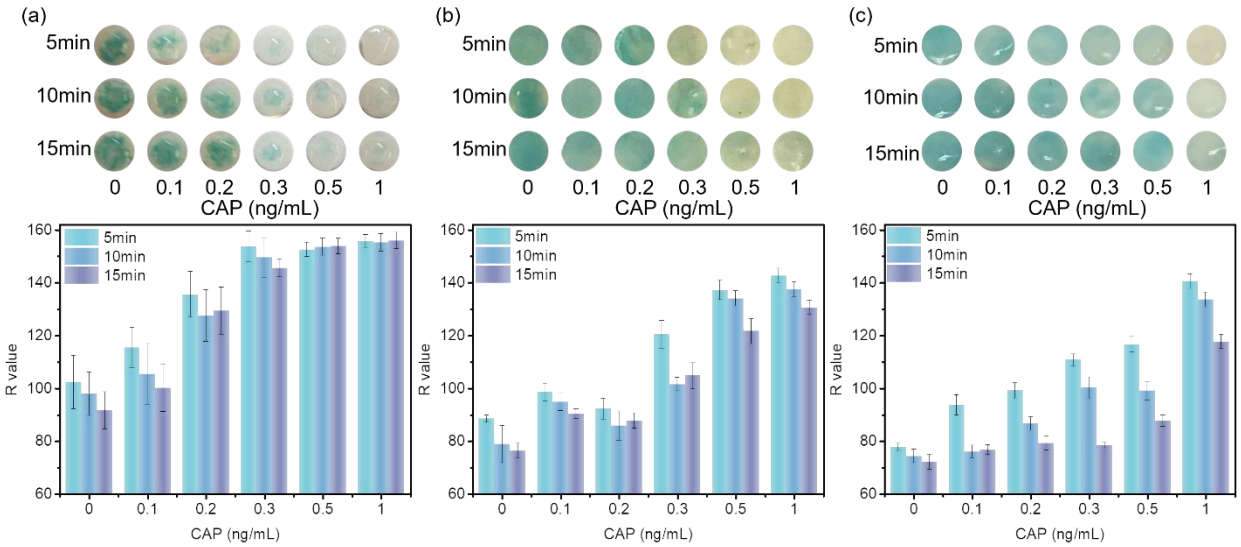

Figure 3.3. Optical images and color intensities (R values) of membranes modified by a) CC; b) GA; and c) DSC in the detection of CAP

3.3.4 Understanding naked-eye distinguishable sensor

By using microporous and nanofibrous membranes as solid media for ELISA assay, we achieved the goal of developing highly sensitive - colorimetric sensors for the antibiotic, CAP. A calibration curve of color intensity difference between the control and sample groups was established based on the following equation, and the results are presented in Figure 3.4.

$$\frac{B}{B_0} = \frac{(R_{max} - R_x)}{(R_{max} - R_0)}$$

Here, R_{max} is the maximum R value, R_x is R value at specific CAP concentration, and R_0 represents the R value at 0ng/mL of CAP. A higher ratio represents the concentration of CAP close to 0ng/mL of CAP, and a lower ratio means more CAP in

solutions. The concentrations of CAP varied from 0.01ng/mL to 100ng/mL in the calibration curve (Figure 3.4). Thus, the concentration of CAP in a solution was quantitively measured by determining the color intensity and deriving it from the calibration curve. The limitation of detection (LOD) was 0.1ng/mL, and the linear range was located between 0.1ng/mL to 0.4ng/mL. The linear relation equation could be described as B/B0=(-140.2)*log(Concentration of CAP)-54.5 (R^2=0.989). The narrow linear range may be due to the color intensity recorded by RGB value rather than optical density with conventional ELISA. Furthermore, the linear range is probably extended, and the LOD could decrease when employing specific devices to record absorbance intensity.

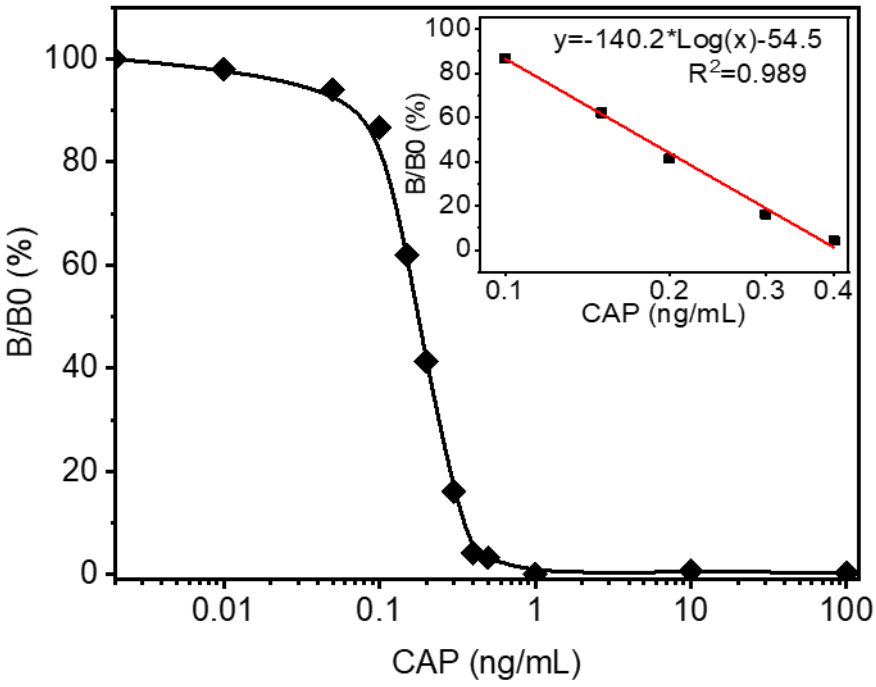

Figure 3.4. Competitive ELISA intensity ratio. Color intensity ratio is plotted against CAP concentration.

Besides the LOD and linear range, the lowest naked-eye distinguishable concentration is also a critical factor for portable devices, especially at where it is not convenient to use

smartphones or cameras. For example, although 0.1ng/mL of CAP could be detected and below 0.3ng/mL of CAP could be measured quantitatively, the membranes treated by low concentrated CAP could only reveal a slight color change which is hardly distinguished by naked eyes. The color changes of sensors at a benchmark concentration, such as a government regulation limit, should be the most significant and confirmative to the naked eyes. Based on the optical images shown in Figure 3a and plot in Figure 3.4, we estimated that at the benchmark concentration of 0.3ng/ml CAP, the CC treated membrane could result in a fade blue color significant enough for the naked eyes.

Then we compared the performance of nanofibrous membrane-based ELISA with other ELISA devices. Here, a 96 well plate was applied as support media for commercial ELSA, and a nitrocellulose membrane was applied as support media for conventional paper-based ELISA. (Figure 3.5). Although UV-vis absorbance intensity from 96-wells plate-based ELISA represented the LOD at 0.1ng/mL, the naked-eye distinguishable color change could only be observed between 1ng/mL of CAP and 10ng/mL of CAP. (Figure 3.5a) Meanwhile, the conventional paper-based ELISA revealed a high LOD (10ng/mL) and a slight color difference between 10ng/mL and 100ng/mL, probably because the extra enzymes were stuck in the pores and hardly washed off. (Figure 3.5b) Compared to published results of other developed ELISA sensors for CAP, nanofibrous membrane-based ELISA has certain advantages at the sensitivity of naked eye distinction. (Table 3.1) Thus, the use of the nanofibrous membranes with ultrahigh surface area indeed intensified colorimetric signal of the ELISA and produced sensors for rapid and sensitive detection without employing any instruments.

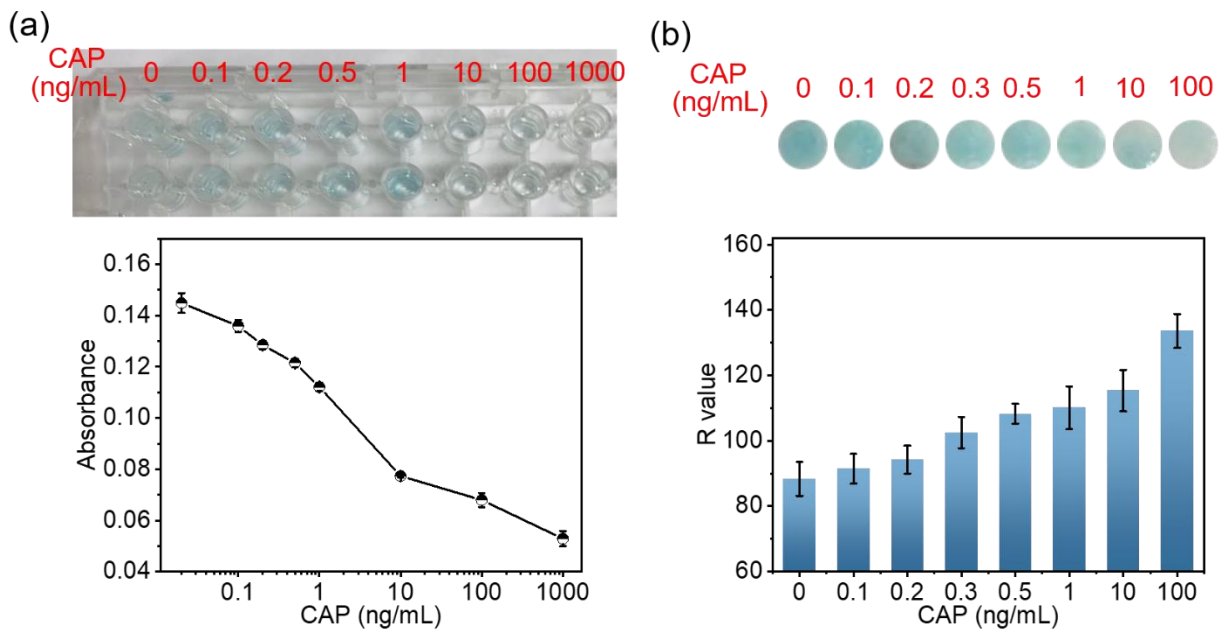

Figure 3.5. Optical images and color intensities (Absorbance or R values) of conventional ELISA. a) 96 well plate-based ELISA; b) nitrocellulose-based ELISA

Table 3.1. Comparison of lowest distinguishable CAP concentration among competitive ELISA from literature.

Solid Substrate	Signal Amplifying	Lowest instrument distinguishable concentration (ng/mL)	Lowest naked-eye distinguishable concentration (ng/mL)	reference
96 well plates	NA	0.1	NA	Wesongah, Murilla et al. 2007
96 well plates	Fluoro-immunoassays	0.05	NA	Shen, Zhang et al. 2006
96 well plates	Biotin-Streptavidin Amplified	0.042	NA	Wang, Zhang et al. 2010
96 well plates	Biotin-Streptavidin Amplified	0.10	NA	Chughtaiet, Maqbool et al. 2017

lateral flow assay	Colloidal Gold Particles	0.3	10	Byzova, Zvereva et al. 2010
96 well plates	Gold Nanoparticles	0.3	5	Wang, Chen et al 2016
Paper-based	NA	100	800	Duyen, Matsuura et al. 2017
Lateral flow assay	Quantum Dots	0.016	0.625	Xie, Wen et al. 2019
Solution	Ion amplified GNP	1.9	9.4-31.3	Wu, Liu et al. 2019
Solution	DNAzyme-functionalized gold nanoprobe	0.00013	NA	Huang, Zhang et al 2019
Solution	DNA amplified GNP	2.2	150	Wu, Huang et al. 2020
96 well plates	NA	0.1	10	This work
Nitrocellulose membranes	NA	1	10	This work
Nanofibrous membrane	NA	0.1	0.3	This work

3.3.5 Selectivity and the impact of interference

Antibiotics with similar structures to CAP, such as florfenicol (FF), thiamphenicol (TAP) and penicillin (PCN), may interfere with the high-sensitivity of nanofibrous membrane-based ELISA, resulting in false positives. To test whether FF, TAP and PCN bind to the CC-activated nanofibrous membrane sensor with CAP antibodies, each antibiotic was tested at a concentration of 100 ng/mL alongside a control group that did not contain any antibiotics. CAP showed a dramatical color change, but the other three antibiotics presented unchanged colors to the control group (Figure 3.6a). The selectivity of the competitive ELISA usually is described by a cross-reactivity ratio (CR%) which is calculated by the ratio of 50% inhibition concentration (IC_{50}) between other antibiotics and

CAP. Here, 100 ng/mL FF, TAP and PCN exhibited 92.85%, 97.31% and 100% color intensity of the control group respectively, but the IC_{50} of CAP is around 0.2ng/mL, indicating that the CR% values of the sensor to other antibiotics were lower than 0.5%. Thus, the results suggest that the antibody is specific to the target antibiotic, CAP, with high selectivity.

As a test for practical applications, farmed and wild-caught salmon samples were tested with the CC nanofibrous membrane-based immunosensor (Figure 3.6b and c). 0 ng/mL and 100 ng/mL CAP solutions were used as the reference in the tests. The brightest blue color was achieved on the 0 ng/mL treated membrane, while the 100 ng/mL treated membrane exhibited a white color. Three pieces of wild-caught salmons were extracted. The wild samples revealed bright color suggesting that the wild-caught salmons did not contain any CAP or contain CAP at a concentration lower than the detection limit of 0.1ng/mL. The R value of the wild samples was 91.55±4.13, which was close to the membrane treated by 0 ng/mL of CAP (92.0±4.64). Then, a known quantity of CAP was spiked into the wild salmon filtrate. The samples spiked with 0.1ng/mL CAP revealed a bright blue color (no significant color change from the reference), but the samples spiked with 0.3ng/mL and 0.5ng/mL exhibited white color close to the membrane treated by 100ng/ml CAP, and the color difference is distinguishable by naked eyes. The R values of the spiked salmon samples were 100.10±3.52, 145.04±1.81 and 155.92±2.36, respectively, which were close to R values of these concentrated CAP in PBS buffer (Figure 3.3a). 0.0967ng/mL of CAP was detected in 0.1ng/mL spiked salmon sample with recovery at 96.7% and standard deviation at 6.09% (n=3); 0.289ng/mL of CAP was detected in 0.3ng/mL spiked salmon sample with recovery at 96.3% and standard

deviation at 4.5% (n=3). Three pieces of farmed salmon samples were collected. The immunoassay test results exhibited farmed samples contained CAP, and the residual CAP amount was above 0.5ng/mL.

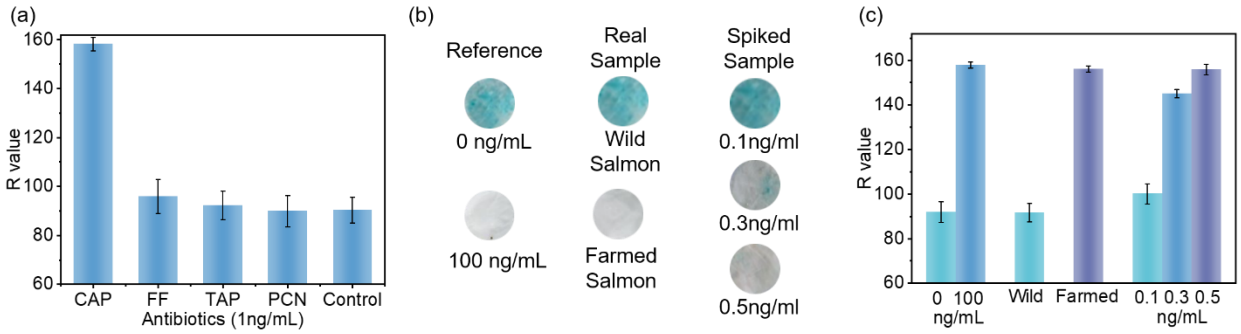

Figure 3.6. Sensitivity and practicality of the sensor. a) interferences of varied antibiotics; b) optical images and c) R values of the reference, wild-caught salmon, farmed salmon and spiked salmon samples

3.4 Conclusions

In conclusion, we have developed a highly sensitive and naked-eye distinguishable immunoassay biosensor using microporous nanofibrous membranes as supported ELISA media. The ultrahigh surface area of the nanofibrous membranes and abundant reactive sites on surfaces of the nanofibers significantly increased antibody immobilization, enhanced colorimetric signal, and improved sensitivity of the membrane-based sensors. The PVA-co-PE nanofibrous membranes were successfully modified by different reactive agents, including CC, GA and DSC, without damaging the structure of membranes. Although all modified membranes revealed homogenous and bright color after capturing CAP-HRP and reacting with dye substrate, CC treated membranes had higher sensitivity

and kept stable colorimetric signal with time-consuming. Compared with conventional ELISA and present studies, the nanofibrous membrane-based biosensor could achieve highly sensitivity and lower naked-eye distinguish limitation. The sensor also demonstrated a desired selectivity to the target antibiotic. A test with salmons proved that the sensor could accurately quantitively measure CAP in spiked samples and could detect a trace amount CAP in real farmed salmon samples.

3.5 References

Byzova, N. A., Zvereva, E. A., Zherdev, A. V., Eremin, S. A., & Dzantiev, B. B. (2010). Rapid pretreatment-free immunochromatographic assay of chloramphenicol in milk. Talanta, 81(3), 843-848.

CDC https://www.cdc.gov/drugresistance/index.html.

Chang, Q., Wang, W., Regev-Yochay, G., Lipsitch, M., & Hanage, W. P. (2015) Antibiotics in agriculture and the risk to human health: how worried should we be? Evolutionary applications, 8 (3), 240-247.

Chughtai, M. I., Maqbool, U., Iqbal, M., Shah, M. S., & Fodey, T. (2017). Development of in-house ELISA for detection of chloramphenicol in bovine milk with subsequent confirmatory analysis by LC-MS/MS. Journal of Environmental Science and Health, Part B, 52(12), 871-879.

De La Rica, R., & Stevens, M. M. (2012). Plasmonic ELISA for the ultrasensitive detection of disease biomarkers with the naked eye. Nature nanotechnology, 7(12), 821-824.

Duyen, T. T. M., Matsuura, H., Ujiie, K., Muraoka, M., Harada, K., & Hirata, K. (2017). based colorimetric biosensor for antibiotics inhibiting bacterial protein synthesis. Journal of bioscience and bioengineering, 123(1), 96-100.

El-Moghazy, A. Y., Zhao, C., Istamboulie, G., Amaly, N., Si, Y., Noguer, T., & Sun, G. (2018). Ultrasensitive label-free electrochemical immunosensor based on PVA-co-PE nanofibrous membrane for the detection of chloramphenicol residues in milk. Biosensors and Bioelectronics, 117, 838-844.

Haller, M. Y., Müller, S. R., McArdell, C. S., Alder, A. C., & Suter, M. J.-F. (2002) Quantification of veterinary antibiotics (sulfonamides and trimethoprim) in animal manure by liquid chromatography–mass spectrometry. Journal of Chromatography A, 952 (1-2), 111-120.

Hirsch, R., Ternes, T. A., Haberer, K., Mehlich, A., Ballwanz, F., & Kratz, K.-L. (1998) Determination of antibiotics in different water compartments via liquid chromatography–electrospray tandem mass spectrometry. Journal of chromatography A, 815 (2), 213-223.

Huang, W., Zhang, H., Lai, G., Liu, S., Li, B., & Yu, A. (2019). Sensitive and rapid aptasensing of chloramphenicol by colorimetric signal transduction with a DNAzyme-functionalized gold nanoprobe. Food chemistry, 270, 287-292.

Ji, L., Dong, C., Fan, R., & Qi, S. (2020). A high affinity nanobody against endothelin receptor type B: a new approach to the treatment of melanoma. Molecular biology reports, 47(3), 2137-2147.

Khachatourians, G. G. (1998) Agricultural use of antibiotics and the evolution and transfer of antibiotic-resistant bacteria. Canadian Medical Association Journal,159 (9), 1129-1136.

Kümmerer, K. (2009) Antibiotics in the aquatic environment–a review–part II. Chemosphere, 75 (4), 435-441.

Lipsitch, M., Singer, R. S., & Levin, B. R. (2002) Antibiotics in agriculture: When is it time to close the barn door? Proceedings of the National Academy of Sciences, 99 (9), 5752-5754.

Liu, S., Dou, L., Yao, X., Zhang, W., Zhao, B., Wang, Z., ... & Wang, J. (2020). Polydopamine nanospheres as high-affinity signal tag towards lateral flow immunoassay for sensitive furazolidone detection. Food chemistry, 315, 126310.

Mungroo, N., & Neethirajan, S. (2014) Biosensors for the detection of antibiotics in poultry industry—a review. Biosensors, 4 (4), 472-493.

Niu, Y., Zhang, P., Wang, L., Li, N., Lin, Q., Liu, L., ... & Fu, X. (2020). Development of double-antibody sandwich ELISA for rapidly quantitative detection of antigen concentration in inactivated SCRV vaccine. Aquaculture, 520, 734671.

Shen, J., Zhang, Z., Yao, Y., Shi, W., Liu, Y., & Zhang, S. (2006). A monoclonal antibody-based time-resolved fluoroimmunoassay for chloramphenicol in shrimp and chicken muscle. Analytica chimica acta, 575(2), 262-266.

Si, Y., Zhang, Z., Wu, W., Fu, Q., Huang, K., Nitin, N., ... & Sun, G. (2018). Daylight-driven rechargeable antibacterial and antiviral nanofibrous membranes for bioprotective applications. Science advances, 4(3), eaar5931.

Wang, J. J., Lin, Y., Jiang, Y. Z., Zheng, Z., Xie, H. Y., Lv, C., ... & Pang, D. W. (2019). Multifunctional Cellular Beacons with in Situ Synthesized Quantum Dots Make Pathogen Detectable with the Naked Eye. Analytical chemistry, 91(11), 7280-7287.12.

Wang, L., Zhang, Y., Gao, X., Duan, Z., & Wang, S. (2010). Determination of chloramphenicol residues in milk by enzyme-linked immunosorbent assay: improvement by biotin− streptavidin-amplified system. Journal of agricultural and food chemistry, 58(6), 3265-3270.

Wang, S., Chen, Z., Choo, J., & Chen, L. (2016). Naked-eye sensitive ELISA-like assay based on gold-enhanced peroxidase-like immunogold activity. Analytical and bioanalytical chemistry, 408(4), 1015-1022.

Wesongah, J. O., Murilla, G. A., Guantai, A. N., Elliot, C., Fodey, T., & Cannavan, A. (2007). A competitive enzyme-linked immunosorbent assay for determination of chloramphenicol. Journal of veterinary pharmacology and therapeutics, 30(1), 68-73.

Witte, W. (1998) Medical consequences of antibiotic use in agriculture. American Association for the Advancement of Science.

Wu, Y. Y., Huang, P., & Wu, F. Y. (2020). A label-free colorimetric aptasensor based on controllable aggregation of AuNPs for the detection of multiplex antibiotics. Food chemistry, 304, 125377.

Wu, Y. Y., Liu, B. W., Huang, P., & Wu, F. Y. (2019). A novel colorimetric aptasensor for detection of chloramphenicol based on lanthanum ion–assisted gold nanoparticle aggregation and smartphone imaging. Analytical and bioanalytical chemistry, 411(28), 7511-7518.

Xie, S., Wen, K., Wang, S., Wang, J., Peng, T., Mari, G. M., Li, J., Wang, Z., Yu, X., & Jiang, H. (2019) Quantitative and rapid detection of amantadine and chloramphenicol based on various quantum dots with the same excitations. Analytical chemistry, 411 (10), 2131-2140.

Zhang, Z., Richardson, C. E., Hennebelle, M., & Taha, A. Y. (2017). Validation of a one-step method for extracting fatty acids from salmon, chicken and beef samples. Journal of food science, 82(10), 2291-2297.

Zhu, J., & Sun, G. (2015). Bio-functionalized nanofibrous membranes as a hybrid platform for selective antibody recognition and capturing. RSC Advances, 5(36), 28115-28123.

Chapter 4. A study on diffusion of protein molecules through microporous nanofibrous membranes

4.1 Introduction

Electrospun nanofibrous membranes possess ultrahigh specific surface areas and have become promising materials in air filtration, chemical separation, and protein purification. (Sundarrajan, Tan et al. 2014; Ge, Zong et al. 2018; Zhu and Sun 2014; Tang, Zhang et al. 2019) The membranes have found increased applications in sensors, enzyme immobilizations, drug delivery, and protein separations. (Zhao, Si et al. 2020; Zhu and Sun 2012; Yu, Zhu et al. 2009) Because of the ultrahigh specific surface areas, the nanofibrous membranes could immobilize enormous amounts of proteins on surfaces of nanofibers by either physical adsorption or chemical covalent bonding. Theoretically, the surface areas of the nanofibers could be hundreds or thousands of times higher than that of macro-sized fibrous materials, and the expected performance of the nanofibrous membranes should be increased accordingly. However, experimental results on the membranes were lower than the theoretically speculated values. (Haider, Haider et al. 2018; Rezaei, Ghani et al. 2016; Fu, Duan et al. 2018) After analyzing the structural features of the nanofibrous membranes, inhibited diffusion of large biomolecules in the micro-porous nanofibrous membrane is considered to be caused by several factors. (Garcia-Galan, Berenguer-Murcia et al. 2011; Taniguchi, Kobayashi et al. 1989) When large biomolecules flow through the porous materials, the diffusion of the molecules could be significantly decreased due to potential steric inhibition and solute-to-polymer interactions. (Cannell and Rondelez 1980; Davidson and Deen 1988; Deen 1987; Yao

and Lenhoff 2006) As a result, the number of loaded proteins inside the membranes could be lower than the theoretically expected values.

The diffusion of solutes in polymer network membranes was studied by assuming cylinder pore structures in the materials, and the influence of material structural properties on the diffusion of solutes was revealed. (Lustig and Peppas 1988) Then, the impact of polymer properties, such as hydrophilicity and swelling ratios, on the diffusion of solutes in hydrogels was investigated. (Liu, Kotsmar et al. 2013; Vagias, Sergelen et al. 2017) However, the hypothesized cylindrical pore structure may not fit the structural features of the electrospun microporous nanofibrous membranes, where randomly distributed pores exist in differently stacked layers of horizontal fiber webs. A hindered diffusion of spherical molecules through fibrous materials was investigated, and a correlation between fiber volume fraction and the diffusion coefficient was established. (Clague and Phillips 1996) Furthermore, the performance of the fibrous matrix in solute sieving was optimized by comparing the transport of spherical particles through the fibrous media and a row of parallel cylinders. (Punyaratabandhu, Kongoup et al. 2017) These results explained well on diffusions of inert molecules through fenestrated systems having weak interactions with the open and homogenous fibrous matrices. The diffusion of proteins in varied hydrogels or polymer solutions revealed the influence of matrix structures on diffusion coefficiency. (Vermonden, Censi et al. 2012; Masaro and Zhu 1999; Dechadilok and Deen 2006; Gutenwik, Nilsson et al. 2004)

The microstructures of the nanofibrous membranes are dramatically different from these polymeric materials. The hydrogels and polymer solutions are homogenous systems in three dimensions (3D), but the electrospun nanofibrous membranes are

structures formed with a layer-by-layer accumulation of randomly oriented horizontal nanofiber webs. The pores in the top layer of the fibrous webs could be blocked by another layer of similar webs underneath, leading to the fact that the measured pore size of a membrane could be significantly larger than the pore size that a molecule diffusing through the membrane will encounter. Here, we define this pore size of the membrane as the effective pore size of the membrane, which could be significantly smaller than the measured pore sizes of membranes. This is a special structural feature of the nanofibrous membranes, which has not been addressed in the literature.

The special structural feature could affect the transport of large molecules such as proteins through the vertical direction of the nanofibrous membranes. Such a feature makes the nanofibrous membranes excellent filter media for ultrafiltration, (Chen, Du et al. 2018) but potentially reducing the loading of enzyme molecules to surfaces of nanofibers inside the membranes and consequently lowering desired sensitivity of the biosensors. Meanwhile, the ultrahigh specific surface areas of the nanofibrous materials could enhance interactions with biomolecules during the diffusion process. Thus, the transport behavior of larger biomolecules through the system should be investigated systematically.

In this work, microporous nanofibrous membranes were prepared by electrospinning a diluted polyacrylonitrile (PAN) solution and employed to investigate the diffusion of proteins through the fibrous media. The PAN membranes are structurally stable in aqueous systems. The membrane morphologies were controlled with varied sizes of fiber diameter and membrane pore prepared by adjusting electrospinning conditions. A side-by-side diffusion chamber was used to measure diffusion coefficients of proteins in the

fibrous membranes with varied porosity and fiber diameters, which also simulate the loading of biomolecules on the membranes during the preparation of biosensors. (Zhao, Si et al. 2020) The diffusions of proteins in this system were affected by a size ratio between protein and measured pores, protein-polymer interactions, and properties of proteins employed in diffusion studies. Diffusions of proteins in the nanofibrous membranes were analyzed using theoretical models applied for 3-dimensionally homogenous polymer systems. The results revealed that only the membrane with very large pores could match the modeled diffusion behavior of large molecules and the heterogeneous structures of the membranes in the diffusion direction significantly reduced the diffusion of large molecules inside the nanofibrous membrane materials.

4.2 Materials and method

4.2.1 Materials.

Polyacrylonitrile (PAN, M_n=150,000), bovine serum albumin (BSA), lysozyme, human immunoglobulin G (IgG), and horseradish peroxidase (HRP) were obtained from Sigma-Aldrich (USA). N, N-Dimethylformamide (DMF), phosphate-buffered saline (PBS pH=7.4) citrate buffer (pH=4.4), sodium bicarbonate ($NaHCO_3$), and sodium carbonate (Na_2CO_3) were supplied by Fischer Scientific (USA). Pierce™ BCA protein assay kit was purchased from Thermo Fisher Scientific (USA).

4.2.2 Fabrication of fibrous membranes

PAN was dissolved in DMF at 80 ℃ to prepare varied concentrations of PAN in 6, 7, 8, 10, 12 wt. %, respectively. Then, the PAN solutions were transferred into 20mL syringes and loaded on infusion single-channel syringe pumps (Kats Scientific Co.). A 6/G needle was caped on a syringe, and the feeding rate was set at 2 mL/hr. A high voltage of 20 kV was employed on the needle tip, generating a continuous jet stream. The relevant PAN nanofibers were deposited on an aluminum foil-covered rotating receiver with a fixed distance of 20 cm. In controlling pore sizes of the membranes, the humidity of the electrospinning chamber was adjusted to 30%, 40%, 50%, 60%, and 70% relative humidity, respectively, by using a humidifier (Urpower Co.). The temperature was controlled at 25 ±1 ℃ for all PAN solution. Residual DMF solvent was removed by drying the produced PAN nanofibrous membranes in a vacuum oven at 80 ℃ for 2 hours.

4.2.3 Characterization of fibrous membranes

Morphologies of the PAN nanofibrous membranes were obtained by a scanning electron microscope (SEM, Quattro ESEM, Thermo Scientific™). The pore size and the distribution of fiber sizes of the membranes were measured with a capillary flow porometer (Porous Media Inc., Ithaca, NY). Fiber diameter was measured from SEM images with the help of a photoshop program. The thickness of the PAN membranes was measured through an electronic micrometer thickness gauge (Neoteck). The fiber volume fraction and porosity of the membranes could be calculated by the mass, apparent volume and density of PAN polymer.

4.2.4 Measurement of protein diffusion in fibrous membranes

Protein diffusion in the fibrous membrane was measured by using a side-by-side diffusion chamber (PerneGear Co.) which consists of two 3.4 mL chambers with a 9mm orifice. A PAN fibrous membrane was mounted between two chambers, and chambers were well sealed and placed in a water bath to maintain the temperature at 25 ℃. Then, 3 mL of a PBS solution was added to each chamber respectively for prewetting the membranes. After 2 hours, 0.3 mL of a protein solution (10g/L in PBS buffer) was injected into the donor chamber, while the same amount of the PBS solution was added into the receptor chamber at the same time. Stirring bars were placed in both chambers and maintained at 750 rpm rate during the experiments. 20 μL of the sample solution was taken from each chamber at regular intervals and replaced with the same amount of the PBS buffer solution for at least 5 hours; then, the samples were diluted with 80 μL of the PBS buffer. The protein concentration was measured with the Pierce BCA protein assay kit (Thermo Fisher™). The working agent was prepared by mixing 50-parts Bicinchoninic acid (BCA) reagent A with 1-part Cu_2SO_4 reagent B. 100 μL of diluted protein sample was added into a test tube, mixing with 2 mL of the working agent, and the test tube was placed in a 37 ℃ oven for 30 mins. Protein concentration can be obtained with a UV-vis spectrophotometer (Thermo Scientific™) by calibration curves. Then, the protein concentration in the receptor chamber at increment time could be used to quantitatively determine protein diffusion property inside membranes.

4.2.5 Measurement of loaded protein ratio in fibrous membranes

Loaded protein ratio is defined as the ratio of protein concentration in a membrane to protein concentration in a solution at the equilibrium of protein adsorption and desorption. Protein concentration in the membrane can be obtained by the amount of protein in the membrane divided by the volume of the membrane. For measuring protein amount in a membrane, the PAN membrane was removed from the chambers and dried in a vacuum oven for 10 mins after the diffusion experiment. Then, the membrane was placed in 10mL working agents following the BCA process, and the concentration of the protein desorbed from the membranes was measured. The fibrous membrane volume was obtained by the measured membrane area and thickness. Meanwhile, protein concentration in a solution can be obtained by measuring protein concentration in both donor and acceptor chamber after the diffusion experiment.

4.3 Results and Discussion

4.3.1 Fabrication of PAN nanofibrous membranes

The fiber diameters of the prepared fibrous membranes were varied from tens of nanometers to sub-micrometers, while the pore sizes were in micrometer scales. The influence of the membrane morphology on protein diffusion can be described in **Error! R eference source not found.**. Firstly, proteins can be blocked by the porous fibrous matrices if the protein sizes are close to the average pore sizes (**Error! Reference s ource not found.**a), but the membranes containing large pore exhibits less hindrance to protein molecules to pass through (**Error! Reference source not found.**b). Secondly,

when a protein molecule passes through a pore, its motion may be hindered by the interactions between the protein molecules and surfaces of the fibers and hydrodynamic drag (**Error! Reference source not found.**c). Thus, the morphology of the membrane e xhibits a significant influence on protein diffusion.

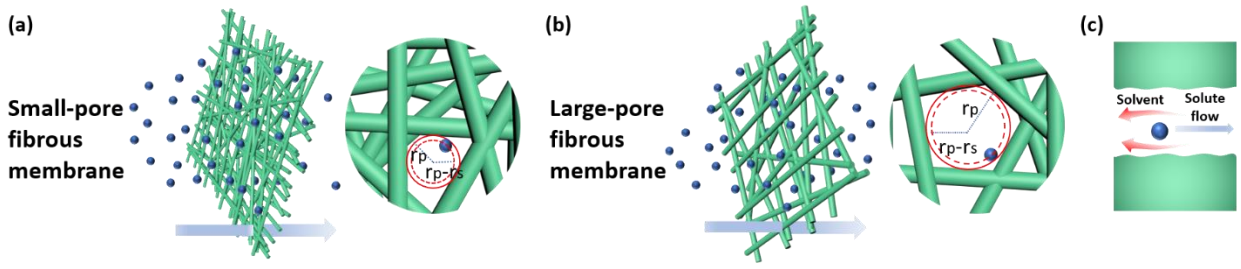

Scheme 4.1. The dynamic transport of proteins in small-pore (a) and large-pore (b) fibrous membranes; (c) diffusion of protein through a pore. Where rp is the average measured pore size, and rs is a radius of a spherical protein molecule.

The PAN nanofibrous membranes in different morphologies were fabricated by adjusting two parameters during electrospinning, polymer concentration and relative humidity. The SEM images of the corresponding nanofibrous membranes are shown in Figure 4.1a. All the membranes revealed layered microporous fibrous structures with fibers randomly distributed horizontally and gradually reduced pore sizes from top to inside through the membranes. The fiber diameters and measured pore sizes show significant differences among these membranes, affected by the polymer concentration and relative humidity during the electrospinning (Figure 4.1b, c and d). The fiber diameter increased almost linearly to the increase of polymer concentration in spinning solutions (Figure 4.1b). As shown in Figure 4.1c-d, the measured pore size distributions ranged

from 0.19 to 3.4 μm, and the measured pore sizes gradually increased from the membranes produced in polymer solutions of 6-12 wt%. The measured maximum pore size and average pore size both followed the same increase tendency as fiber diameter increased. As relative humidity increased from 30% to 60%, the measured pore size distribution gradually increased from 0.9 to 3.8 μm, but the pore size dramatically jumped to 9 μm at 70% RH, even though the nanofiber diameter linearly increased as the relative humidity was raised (Figure 4.1e-g). These different nanofibrous membranes were employed in the following protein diffusion studies.

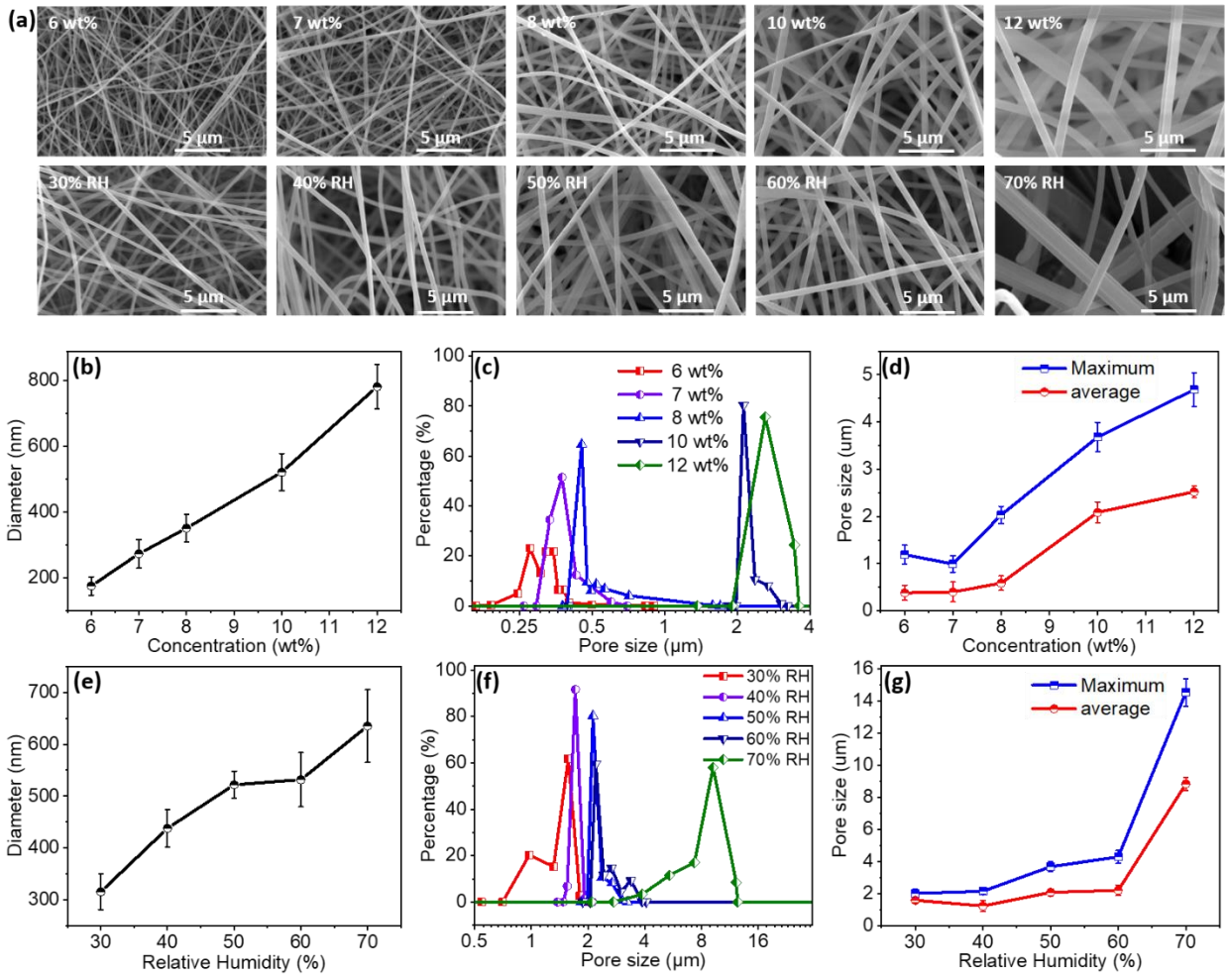

Figure 4.1. (a) SEM images of PAN nanofibrous membranes made under different polymer concentrations and relative humidity; and fiber diameters, pore distributions, pore sizes of as-prepared membranes: (b) and (e) fiber diameter, (c) and (f) measured pore distribution, and (d) and (g) measured maximum pore size and average pore size.

4.3.2 Derivation for protein diffusion in fibrous membranes

A side-by-side diffusion chamber was employed to measure protein transport in the PAN nanofibrous membranes (Figure 4.2a). Fick's Law was applied to calculate the diffusion of proteins in each membrane (Equation 1). (Durbin and Kobayashi 1962; Fanous, Swed et al. 2015)

$$J = -D_{eff}\frac{dC}{dx} \quad (1)$$

Where J is diffusion flux, which can be converted to the change of protein amount in each chamber at the membrane boundary at each chamber side, D_{eff} is the effective diffusion coefficient of protein in membranes, C is protein concentration, and x is the diffusion distance.

The morphology and pore structure of the membranes were not affected by PBS buffer solutions, which were supported by the SEM images (Figure 4.2 b and c). Thus, the protein concentration in the membranes can be hypothesized as linearly decreasing from the donor chamber boundary to the receptor chamber boundary at a pseudo steady-state. (Stringer and Peppas 1996) And the protein could be considered as diffusing in a consistent porous system.

The diffusion coefficient could be determined by the following equation at the pseudo steady-state (Equation 2) (Stringer and Peppas 1996):

$$\ln\left(1-\frac{2c_2}{c_0}\right)=-\frac{2D_{eff}k_dA}{V\Delta x} \quad (2)$$

Where C_0 and C_2 are the initial protein concentration in the donor chamber and protein concentration in the receptor chamber at a specific time. D_{eff} is the effective or apparent diffusion coefficient, and K_d is the partition coefficient of the protein. A is the protein diffusion area, V is the donor chamber volume, and Δx is the thickness of the membrane.

The effective diffusion coefficient could be calculated from a slope yielded by a plot of $\Delta x * \ln(1-2c_2/c_0)$ versus t with a known partition coefficient. As mentioned in the experimental section, the partition coefficient of a protein is defined as the ratio of protein concentration in the membrane (c_m) to protein concentration in solution (c_s), which can be obtained by measuring the amount of protein (Q_m) in membrane and protein concentration in the donor chambers (c_1) and receptor chamber (c_2), respectively (Equation 3).

$$k_d=\frac{c_m}{c_s}=\frac{Q_m/A\Delta x}{(c_1V+c_2V)/2V} \quad (3)$$

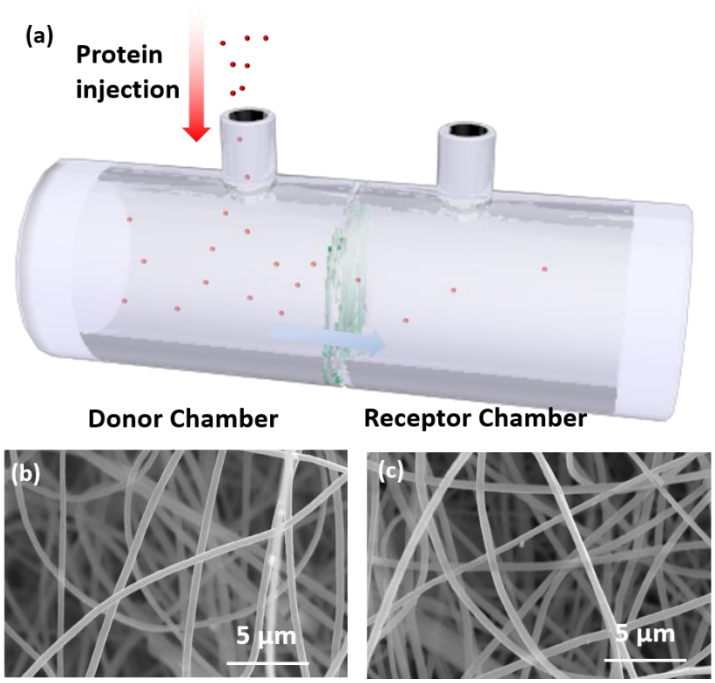

Figure 4.2. (a) A scheme of a side-by-side chamber used in this study; (b-c) SEM images of the membrane before and after the diffusion test.

4.3.3 Diffusion of BSA in various nanofibrous membranes

The as-prepared nanofibrous membranes were employed to investigate the influence of pore structure and fiber diameter on the diffusion and partition coefficient of BSA (Figure 4.3). The morphology of the membranes has a significant influence on the adsorption of the protein on the surface of the nanofibers. As shown in Figure 3a, the partition coefficient of the protein on the membrane increased as the relative humidity (RH) in the electrospinning chamber increased from 30% to 50%, which are the same as the increment of fiber diameter and pore size (Figure 4.1e and 1g). Then, the partition coefficient decreased after RH reached 60% and dramatically reduced at 70% RH due to

large pore size and reduced interactions of the protein with surfaces of the nanofibers. The same tendency of the partition coefficient was observed in the membranes prepared with different polymer concentrations (Figure 4.3b). The partition coefficient increased as the pore size increases from 6 wt % to 10 wt% of PAN and reached a peak at 10 wt% and slightly decreased at 12 wt% because of the oversized nanofiber diameter and reduced surface areas of the membranes (Figure 4.1b and d). Here, the loaded protein ratios per mass of membranes could better represent the amounts of the proteins adsorbed onto the membranes, which were obtained by taking the loaded protein ratios (c_m/c_s) divided by apparent densities of the membranes (d). The loaded protein ratios per mass of membrane increase with the increase of humidity and polymer concentration and reach peaks at proper parameters. The smaller nanofiber diameter represents a higher specific surface area and prompts more adsorption of the protein. Meanwhile, the amount of the loaded protein onto the surfaces of the fibers is also limited by the measured pore size of the membranes because protein molecules cannot reach fiber surfaces inside the membranes efficiently in the small pore samples.

The plots of the cumulative amounts of the protein in the receptor chamber versus time are shown in Figure 4.3 c and d. The amounts of the diffused protein revealed a significant difference among different membranes. A pseudo steady-state of diffusion of the protein could be maintained more than four hours in a membrane with smaller fiber diameter and pores, prepared under 30% RH, and a gentle slope in the linear range representing slow diffusion of the protein inside the membrane. However, it took almost 60 minutes to reach the pseudo steady-state during the diffusion process. Then, the time to reach pseudo steady-state diffusion dramatically reduced, and the slopes of curves became steeper

with increased fiber diameter and pore sizes, controlled by increased relative humidity from 30%-70%. Especially, the diffusion of the protein through a membrane prepared under 70% RH could achieve pseudo steady-state in a very short time, representing the membrane has negligible hindrance to protein diffusion. Similarly, the pseudo steady-state diffusion of the protein through the membranes with varied fiber and smaller pore using different polymer concentrations duplicated the pattern. Overall, large measured pores dramatically reduced the times to reach pseudo steady-state diffusion in the membranes.

The diffusion of protein in all membranes could achieve the pseudo steady-state representing the concentration of protein inside pores should maintain constant. Although the concentration of the adsorbed protein may change at pseudo steady-state, this protein has no contribution to the diffusion. Thus, the effective diffusion coefficient could be calculated by Equation 2 with the slop in the linear range. The ratios between the effective diffusion coefficient to the bulk diffusion coefficient (D_{eff}/D_0), which could be obtained by the reference, are shown in Figure 4.3 e and f. (Putnam, Prealbumin et al. 1975) The trends of the changes are consistent with the measured pore sizes and fiber diameters (Figure 4.1 b, d, e, and g). However, the increases of the diffusion coefficient of the membranes with the increases in humidity and polymer concentration all correlate to the increase of measured pore sizes in the membranes. The membranes with similar pore size but different fiber diameter (such as the membranes prepared under 50% RH and 10% wt) exhibited similar diffusion coefficients. Contrarily, the membranes with similar fiber diameters but different pore sizes (such as the membranes made under 70% RH

and 12% wt) present significant differences. Overall, the protein diffusion coefficient increased as the measured pore size of the membranes was enlarged.

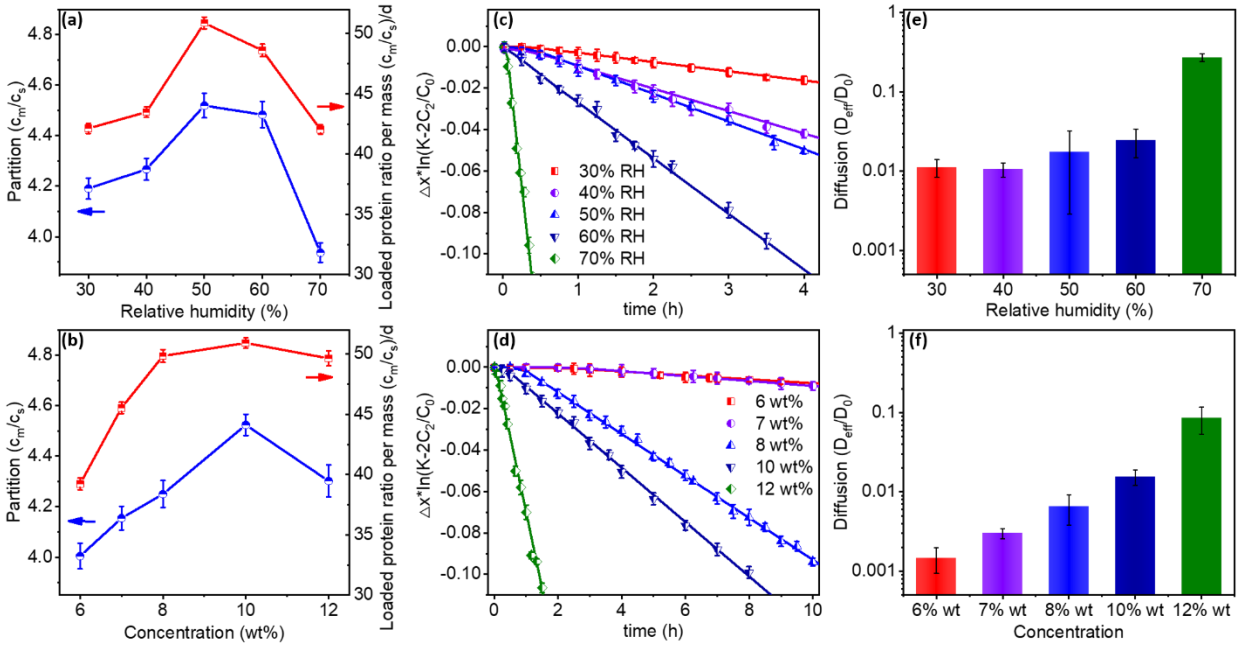

Figure 4.3. Partition coefficient of proteins inside membranes prepared (a) under different relative humidity conditions and (b) with different polymer concentrations; cumulative amounts of protein in receptor chamber versus time: (c) PAN membranes prepared under different relative humidity (RH) conditions, (d) membranes prepared with different polymer concentrations; and effective diffusion coefficients of membranes prepared (e) under different relative humidity conditions and (f) with different polymer concentrations.

4.3.4 Modeled diffusion of protein through nanofibrous membranes

Both humidity and concentration of the polymer solution of electrospinning affected fiber diameter and pore size of the membranes. Here, we would like to assign two ratios (r_s/r_p, r_s/r_f) of the membranes to represent the relative ratios of average measured pore size (r_p) and fiber diameter (r_f) to the size of protein (r_s), respectively, which could be used to find the relationship to effective diffusion pattern of the protein. A correlation between the protein size (r_s) to the measured pore size (r_p) ratio (r_s/r_p) or the protein size(r_s) to fiber diameter (r_f) ratio(r_s/r_f) with diffusion coefficient ratios (D_{eff}/D_0) is shown in Figure 4.4. The diffusion coefficient ratios dramatically decreased when the r_s/r_p ratio increased from 0 to 0.002, then reduced to hundreds of times lower as the r_s/r_p ratio further increased to 0.01. These results indicate that protein diffusion behaviors are different in nanofibrous membranes versus other polymer media. In general, the diffusion of proteins may be mainly affected by the steric hindrance and hydrodynamic interactions in a classical polymer network material, such as a hydrogel. And the protein adsorption on the polymeric media was negligibly considered in the literature. (Boschetti 1994; Farnan, Frey et al. 2002; Liu, Kotsmar et al. 2013) Firstly, the D_{eff} inside a classical fibrous membrane would be similar to the D_0 when the r_s/r_p ratio is lower than 0.01. (Dechadilok and Deen 2006; Beck and Schultz 1970; Yang, Liu et al. 2017) But the diffusion coefficients inside the nanofibrous materials are significantly lower than diffusion coefficients in other classical systems, indicating that the strong adsorption of proteins on the surfaces or potential blockage of the protein by the nanofibrous membranes occurs here. (Zhou, Li et al. 2017; Hettiaratchi, Schudel et al. 2018; Wu, Xiao et al. 2016) Since the physically adsorbed or blocked proteins have no contribution to the diffusion, the protein diffusing

through pores and protein adsorbed onto the fiber need to be discriminated, which could be calculated by following Equation 4,

$$C = \varphi * n + (1 - \varphi) * C^L \quad (4)$$

Where C is the total protein concentration in the membrane, C^L is the concentration of non-adsorbed protein in the pores, n is the amount of adsorbed protein on fiber surfaces inside the membrane, and φ is the volume fraction of fiber inside the membranes. Then, the diffusion equation (Equation 2) could be extended to account for the adsorbed protein as distinct from the protein in the pores (Equation 5).

$$\frac{\partial C(t,x)}{\partial t} + \left(\frac{\varphi}{1-\varphi}\right)\frac{\partial n(t,x)}{\partial t} = D\frac{\partial^2 C^L(t,x)}{\partial x^2} \quad (5)$$

Where D is the solute diffusion coefficient through the pores. To calculate the diffusion coefficient, the kinetics of protein adsorption need to be described. Here, we impose a simplest approach by assuming local equilibrium with Henry's adsorption, (Liu, Kotsmar et al. 2013; Kotsmar, Sells et al. 2012; Liu, Dursch et al. 2016) or Equation 6.

$$n = KC^L \quad (6)$$

Where K is Henry's adsorption constant of protein on fibers. The local equilibrium represents the protein adsorption is reversible and the rates of adsorption and desorption are faster than the rate of diffusion. Based on the literature, the kinetic adsorption constant of BSA on the PAN surface is at 10^{-4} cm/s, (Wang, Fu et al. 2019) but the diffusion constant of BSA in PBS buffer is at 10^{-7} cm^2/s range. (Putnam 1975) Meanwhile, D.E. Liu et al. also proved that the local equilibrium could be achieved when the solute-polymer

interactions are modest. (Liu, Dursch et al. 2016) Substitution of Equation 6 into Equation 5 yields the effective diffusion coefficient (D_{eff}) in Equation 7.

$$D_{eff} = \frac{D}{1+\frac{\varphi}{1-\varphi}K} \tag{7}$$

Henry's adsorption constant is required to solve Equation 7. However, since the adsorption proceeds with diffusion simultaneously, the direct measurement of the kinetic adsorption constant is complicated. (Dursch, Taylor et al. 2014; Shin, Yu et al. 2017; Silva, Azevedo et al. 2017) Here, we employed D.E. Liu's method: calculating adsorption constant by using the partition coefficient following Equation 8. (Sells et al. 2012; Liu, Dursch et al. 2016)

$$\frac{k_d}{1-\varphi} = E_{ex}E_{ad} \tag{8}$$

Where E_{ex} indicates a size-exclusion factor, or the volume of liquid available to the protein in the membrane divided by the total pore volume of membrane; and E_{ad} designates protein adsorption factors. For protein in a matrix with randomly oriented fibers, the E_{ex} could be presented by the classical Ogston equation (Equation 9). (Ogston 1958; Lazzara, Blankschtein et al. 2000)

$$E_{ex} = \exp\left[-\varphi(1+\frac{r_s}{r_f})^2\right] \tag{9}$$

Where r_s and r_f indicate the diameters of protein and fiber, respectively. The pore size was measured by a capillary flow porometer, where the pores among the fibrous membranes are equivalent to the capillary pores. Thus, the size exclusion factor also could be represented by the solute in capillary pores (Equation 10). (Pappenheimer, Renkin et al. 1951)

$$E_{ex} = \varphi(1 - \frac{r_s}{r_p})^2 \quad (10)$$

Where r_p is the diameter of the measured pore sizes. Based on Equation 6, the E_{ad} could be represented by the Henry adsorption constant (Equation 11).

$$E_{ad} = (1 + \frac{\varphi}{1-\varphi} K) \quad (11)$$

Thus, the kinetic adsorption constant could be solved by combining Equations 8-11. The adsorption constants (E_{ad}) of the membranes are about 40, indicating a strong interaction between protein and the fibrous matrix.

For a better understanding of the unique property of the transport of proteins inside the nanofibrous membrane, the experimental data were compared with the modelling results. Table 4.1 shows classical physical interaction-based diffusion theories that could predict the hindered diffusion of solutes in fibrous membranes. The effective diffusion coefficient (D_{eff}) of each model could be calculated via Equation 7 with obtained Henry's adsorption constants. The predicted results from each model overestimated the experimental results (represented as the line in Figure 4.4). The large discrepancy between measured effective diffusion coefficients and predicted results indicates the classical hindered diffusion theories are not fully suitable to the electrospun nanofibrous membranes. Different from the classical 3D homogenous fibrous membrane, the electrospun nanofibrous membranes are layer-by-layer assemblies and heterogeneous in the vertical direction from the planar areas. The SEM images of the top view and cross-section of the electrospun nanofibrous membrane indicate the different morphology between horizontal direction and vertical direction. Thus, the tortuosity of the nanofibrous membranes is dramatically high, making the classical modelling unfit to the nanofibrous membranes.

From the images, the measured pore sizes of every nanofibrous layer were blocked by the top and bottom layers of nanofibers, resulting in much smaller effective pores in the vertical direction of the nanofibrous membranes. Therefore, only very large pored nanofibrous membranes may still retain a real large effective pore size (r'_p) and small protein size (r_s) to pore size (r'_p) (r_s/r'_p) ratio. In fact, the effective diffusion coefficient of the membrane with the largest measured pore size (70%RH membrane) matched well with theoretical results, indicating the modelling analysis was meaningful but most nanofibrous membrane structures are not homogeneous in the diffusion direction and unfit for the model. Similar results were also obtained by measuring the diffusion coefficient of BSA in a nitrocellulose membrane in the literature. (Ahmad, Low et al. 2010) The diffusion coefficient of BSA in that membrane is hundreds of times lower than the bulk diffusion coefficient even when the pore size is over 1 μm.

Table 4.1. The classical diffusion models of molecular through fibrous media

Model type	expression[a]	ref
steric	$\frac{D}{D_0} = \exp(-\sqrt{\sigma})$	Ogston 1958
hydrodynamic	$\frac{D}{D_0} = [1 + (\frac{{r_s}^2}{k})^{\frac{1}{2}} + \frac{1}{3}\frac{{r_s}^2}{k}]^{-1}$	Phillips, Deen et al. 1989
effective media model	$\frac{D}{D_0} = \exp[-0.84\varphi(\sigma)]^{1.09}$	Johansson, Elvingson et al.1991
combined	$\frac{D}{D_0} = \frac{\exp[-0.84\varphi(\sigma)]^{1.09}}{[1 + \left(\frac{{r_s}^2}{k}\right)^{\frac{1}{2}} + \frac{1}{3}\frac{{r_s}^2}{k}]}$	Johnson, Berk et al. 1996

hindered transport	$\frac{D}{D_0} = (1 - \frac{r_s}{r_p})^2[1 - 2.10\frac{r_s}{r_p} + 2.09(\frac{r_s}{r_p})^3 - 0.95(\frac{r_s}{r_p})^5]$	Renkin 1954 Pappenheimer 1953

[a] $\sigma = \varphi(1 + \frac{r_s}{r_f})^2$; $k = 0.31{r_f}^2\varphi^{-1.17}$

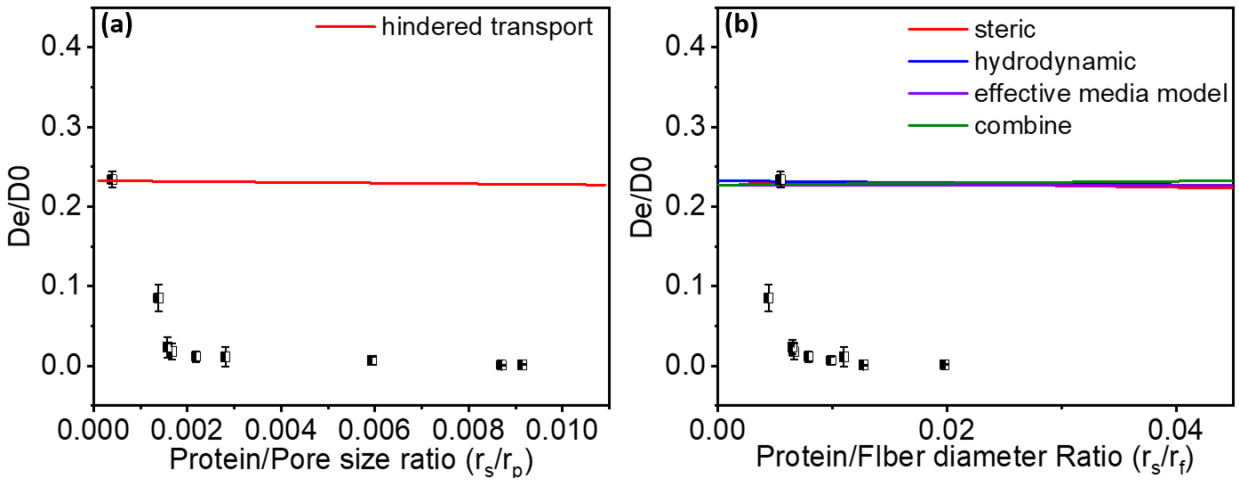

Figure 4.4. Measured and predicted results of effective diffusion coefficient ratios of proteins in membranes with different a) protein to measured pore size ratios, and b) protein to fiber diameter ratios

4.3.5 Influence of protein-polymer interaction on protein diffusion

Besides the morphology of the membranes, adsorption (partition) and diffusion of proteins in the systems are also affected by the chemical structures of fiber forming polymers. Generally speaking, the protein-polymer interactions consist of ionic force, hydrophobic force, dipole-dipole interactions, and hydrogen bonds. Among them, hydrogen bonds, hydrophobic and polar interactions are the dominating forces between

proteins and PAN polymer because acrylonitrile unit has a highly polar nitrile group and a lone pair of electrons on the nitrogen, potentially forming hydrogen bonds with proteins and possessing negative charges on fiber surfaces in solutions. Such interactions can be adjusted by applying different pH buffers, as shown in Figure 4.5. Since BSA (isoelectric point=5.4) possesses more negative charges as pH values of the buffer solutions are above its isoelectric point, the diffusion of the protein was prompted due to increased repulsion between the protein and the nanofiber at pH values of 5.5-10.4. (Bulk diffusion coefficient of BSA at varied pH buffer was obtained at ref). (Schmitz 1983) The low diffusion coefficient ratio of BSA at pH = 5.4 was probably due to the low solubility of the protein close to the isoelectric point. Afterward, as the pH increases, the diffusion coefficient of the protein increased. But the increased repulsion reduced adsorption amounts of BSA on the fiber surfaces. Based on the above results, both the adsorption and diffusion of the protein in the fibrous membranes are highly determined by the protein-fiber interactions as well. The stronger protein-fiber repulsion prompts protein diffusion but sacrifices protein adsorption of the membranes.

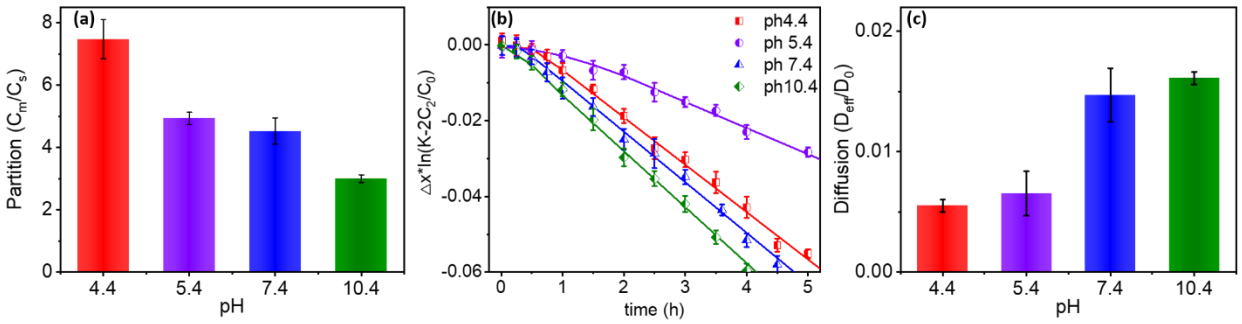

Figure 4.5. The impact of pH value on (a) partition coefficient, (b) cumulative amount of BSA in the receptor chamber versus time, and (c) diffusion coefficient of BSA in same PAN nanofibrous membrane

4.3.6 Diffusion of different proteins in nanofibrous membranes

Considering actual applications of the nanofibrous membranes in protein separation and purification applications, protein properties, such as protein size and isoelectric point (pI), on their diffusion performances also were investigated. Four proteins were selected to study their corresponding protein diffusion performances. (Table 4.2) Since the concentration of each protein in the side-by-side chamber is low, protein molecules could be simplified as spherical particles diffusing in the nanofibrous membranes, and radiuses of the proteins were estimated based on literature data. (Farnan, Frey et al. 2002; Yang, Liu et al. 2017; Wu, Xiao et al. 2016; Liu, Dursch et al. 2016) A nanofibrous membrane made from 10 wt% of PAN DMF solution under 50% RH was selected in this study, and a PBS buffer served as the media.

Table 4.2. Parameters of four different proteins: BSA, Lysozyme, IgG and HRP

Protein	pI	r_s (nm)	D_0 (cm^2/s)
BSA	5.4 [a]	3.48 [b]	$5.9*10^{-7}$ [c]
Lysozyme	11.35 [d]	1.85 [e]	$1.11\pm0.05*10^{-6}$ [f]
IgG	6.6 - 7.2 [g]	5.4 [h]	$4.4\pm1.3*10^{-7}$ [h]
HRP	8.8 [i]	3.0 [j]	$7.57*10^{-7}$ [k]

(Ge, Kojio et al. 1998[a]; Axelsson 1978[b]; Putnam, Prealbumin et al. 1975[c]; Wetter and Deutsch 1951[d]; Parmar and Muschol 2009[e]; Brune and Kim 1993[f]; Chiodi, Sidén et al. 1985[g]; Saltzman, Radomsky et al. 1994[h]; Lavery, MacInnis et al. 2010[i]; Engberg and Frank 2011[j])

Partition and diffusion coefficients of the proteins are shown in Figure 4.6. Lysozyme (pI=11.35) reveals the highest partition coefficients on the membrane among all proteins

because it carries more positive charge at the PBS buffer and prompts the strongest protein-fiber attraction. The strong protein-fiber attraction hinders the diffusion of lysozyme in the nanofibrous membrane and provided the lowest diffusion coefficient even with the smallest size among all proteins. Immunoglobulin G (IgG) is a large size protein but has a similar loaded protein ratio as BSA. And it presents a lower diffusion coefficient in the membranes as speculated due to the large IgG protein size (5.4nm) hindering the diffusion. Horseradish peroxidase (HRP) contains more positive charge than BSA at the PBS buffer; thus, it has a higher partition coefficient but a similar diffusion coefficient as BSA.

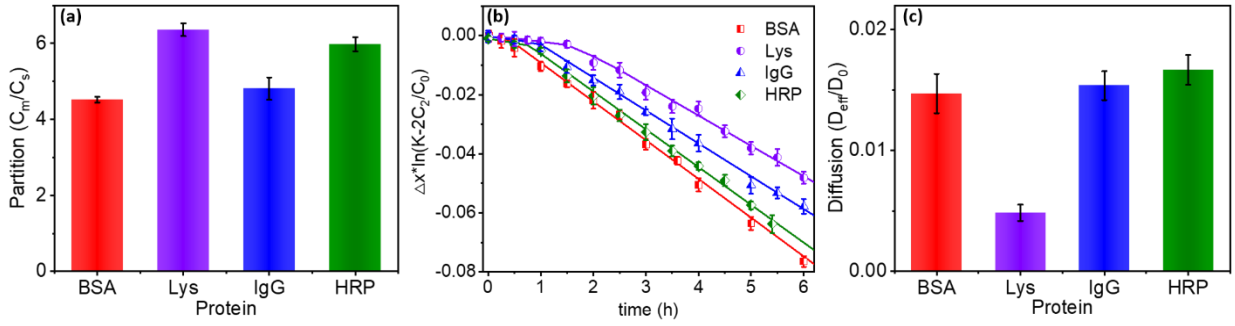

Figure 4.6. (a) Partition coefficient of proteins and (b) cumulative amount of protein in the receptor chamber versus time, and (c) diffusion coefficient of four proteins in the same PAN nanofibrous membrane

4.4 Conclusion

The protein diffusion and partition coefficient, the two vital factors describing protein transport behavior in nanofibrous membranes, were investigated in this study, which is the first step to reveal the impact of nanofibrous membrane structures on diffusions of

large biomolecules in the system. Different from classical solute diffusion models in a 3-D homogenous fibrous material, the electrospun nanofibrous membranes contain layered unparallel pores with large pore sizes in each layer, and the pores of each nanofiber layer are blocked by the top and bottom layers, resulting in smaller effective pore sizes in the membranes. The protein diffusion is profoundly affected by the membrane morphology and protein-polymer interactions. The effective pore size of the membranes has a dominating impact on both protein diffusion and adsorption. The polymer-protein interactions significantly affect protein adsorption on fiber surfaces, but the repulsive inter-molecule force could enhance protein diffusion through the membranes. Overall, the diffusion of protein and loaded protein ratios on membranes is determined by effective pore sizes of the membranes, protein sizes and buffer pH conditions in the media.

4.5 References

Ahmad, A. L., Low, S. C., Shukor, S. A., Fernando, W. J. N., & Ismail, A. (2010). Hindered diffusion in lateral flow nitrocellulose membrane: Experimental and modeling studies. Journal of Membrane Science, 357(1-2), 178-184.

Axelsson, I. (1978). Characterization of proteins and other macromolecules by agarose gel chromatography. Journal of Chromatography A, 152(1), 21-32.

Beck, R. E., & Schultz, J. S. (1970). Hindered diffusion in microporous membranes with known pore geometry. Science, 170(3964), 1302-1305.

Boschetti, E. (1994). Advanced sorbents for preparative protein separation purposes. Journal of Chromatography A, 658(2), 207-236.

Brune, D., & Kim, S. (1993). Predicting protein diffusion coefficients. Proceedings of the National Academy of Sciences, 90(9), 3835-3839.

Cannell, D. S., & Rondelez, F. (1980). Diffusion of polystyrenes through microporous membranes. Macromolecules, 13(6), 1599-1602.

Chen, Z., Du, X. A., Liu, Y., Ju, Y., Song, S., & Dong, L. (2018). A high-efficiency ultrafiltration nanofibrous membrane with remarkable antifouling and antibacterial ability. Journal of Materials Chemistry A, 6(31), 15191-15199.

Chiodi, F., Sidén, Å., & Ösby, E. (1985). Isoelectric focusing of monoclonal immunoglobulin G, A and M followed by detection with the avidin‐biotin system. Electrophoresis, 6(3), 124-128.

Clague, D. S., & Phillips, R. J. (1996) Hindered diffusion of spherical macromolecules through dilute fibrous media. Phys. Fluids, 8 (7), 1720-1731.

Davidson, M. G., & Deen, W. M. (1988). Hindered diffusion of water-soluble macromolecules in membranes. Macromolecules, 21(12), 3474-3481.

Dechadilok, P., & Deen, W. M. (2006). Hindrance factors for diffusion and convection in pores. Industrial & Engineering Chemistry Research, 45(21), 6953-6959.

Deen, W. M. (1987). Hindered transport of large molecules in liquid‐filled pores. AICHE journal, 33(9), 1409-1425.

Durbin, L., & Kobayashi, R. (1962). Diffusion of Krypton‐85 in Dense Gases. The Journal of Chemical Physics, 37(8), 1643-1654.

Dursch, T. J., Taylor, N. O., Liu, D. E., Wu, R. Y., Prausnitz, J. M., & Radke, C. J. (2014). Water-soluble drug partitioning and adsorption in HEMA/MAA hydrogels. Biomaterials, 35(2), 620-629.

Engberg, K., & Frank, C. W. (2011). Protein diffusion in photopolymerized poly (ethylene glycol) hydrogel networks. Biomedical Materials, 6(5), 055006.

Fanous, J., Swed, A., Joubran, S., Hurevich, M., Britan-Rosich, E., Kotler, M., ... & Hoffman, A. (2015). Superiority of the S, S conformation in diverse pharmacological

processes: Intestinal transport and entry inhibition activity of novel anti-HIV drug lead. International journal of pharmaceutics, 495(2), 660-663.

Farnan, D., Frey, D. D., & Horvath, C. (2002). Surface and pore diffusion in macroporous and gel-filled gigaporous stationary phases for protein chromatography. Journal of Chromatography A, 959(1-2), 65-73.

Fu, Q., Duan, C., Yan, Z., Si, Y., Liu, L., Yu, J., & Ding, B. (2018). Electrospun nanofibrous composite materials: a versatile platform for high efficiency protein adsorption and separation. Composites Communications, 8, 92-100.

Garcia-Galan, C., Berenguer-Murcia, Á., Fernandez-Lafuente, R., & Rodrigues, R. C. (2011). Potential of different enzyme immobilization strategies to improve enzyme performance. Advanced Synthesis & Catalysis, 353(16), 2885-2904.

Ge, J., Zong, D., Jin, Q., Yu, J., & Ding, B. (2018). Biomimetic and superwettable nanofibrous skins for highly efficient separation of oil-in-water emulsions. Advanced Functional Materials, 28(10), 1705051.

Ge, S., Kojio, K., Takahara, A., & Kajiyama, T. (1998). Bovine serum albumin adsorption onto immobilized organotrichlorosilane surface: influence of the phase separation on protein adsorption patterns. Journal of Biomaterials Science, Polymer Edition, 9(2), 131-150.

Gutenwik, J., Nilsson, B., & Axelsson, A. (2004). Determination of protein diffusion coefficients in agarose gel with a diffusion cell. Biochemical Engineering Journal, 19(1), 1-7.

Haider, A., Haider, S., & Kang, I. K. (2018). A comprehensive review summarizing the effect of electrospinning parameters and potential applications of nanofibers in biomedical and biotechnology. Arabian Journal of Chemistry, 11(8), 1165-1188.

Hettiaratchi, M. H., Schudel, A., Rouse, T., García, A. J., Thomas, S. N., Guldberg, R. E., & McDevitt, T. C. (2018). A rapid method for determining protein diffusion through hydrogels for regenerative medicine applications. APL bioengineering, 2(2), 026110.

Johansson, L., Elvingson, C., & Loefroth, J. E. (1991). Diffusion and interaction in gels and solutions. 3. Theoretical results on the obstruction effect. Macromolecules, 24(22), 6024-6029.

Johnson, E. M., Berk, D. A., Jain, R. K., & Deen, W. M. (1996). Hindered diffusion in agarose gels: test of effective medium model. Biophysical journal, 70(2), 1017-1023.

Kotsmar, C., Sells, T., Taylor, N., Liu, D. E., Prausnitz, J. M., & Radke, C. J. (2012). Aqueous solute partitioning and mesh size in HEMA/MAA hydrogels. Macromolecules, 45(22), 9177-9187.

Lavery, C. B., MacInnis, M. C., MacDonald, M. J., Williams, J. B., Spencer, C. A., Burke, A. A., ... & D'Cunha, G. B. (2010). Purification of peroxidase from horseradish (Armoracia rusticana) roots. Journal of agricultural and food chemistry, 58(15), 8471-8476.

Lazzara, M. J., Blankschtein, D., & Deen, W. M. (2000). Effects of multisolute steric interactions on membrane partition coefficients. Journal of colloid and interface science, 226(1), 112-122.

Liu, D. E., Dursch, T. J., Taylor, N. O., Chan, S. Y., Bregante, D. T., & Radke, C. J. (2016). Diffusion of water-soluble sorptive drugs in HEMA/MAA hydrogels. Journal of Controlled Release, 239, 242-248.

Liu, D. E., Kotsmar, C., Nguyen, F., Sells, T., Taylor, N. O., Prausnitz, J. M., & Radke, C. J. (2013). Macromolecule sorption and diffusion in HEMA/MAA hydrogels. Industrial & Engineering Chemistry Research, 52(50), 18109-18120.

Liu, D. E., Kotsmar, C., Nguyen, F., Sells, T., Taylor, N. O., Prausnitz, J. M., & Radke, C. J. (2013). Macromolecule sorption and diffusion in HEMA/MAA hydrogels. Industrial & Engineering Chemistry Research, 52(50), 18109-18120.

Lustig, S. R., & Peppas, N. A. (1988). Solute diffusion in swollen membranes. IX. Scaling laws for solute diffusion in gels. Journal of Applied Polymer Science, 36(4), 735-747.

Masaro, L., & Zhu, X. X. (1999). Physical models of diffusion for polymer solutions, gels and solids. Progress in polymer science, 24(5), 731-775.

Ogston, A. G. (1958). The spaces in a uniform random suspension of fibres. Transactions of the Faraday Society, 54, 1754-1757..

Pappenheimer, J. R. (1953). Passage of molecules through capillary walls. Physiological Reviews, 33(3), 387-423.

Pappenheimer, J. R., Renkin, E. M., & Borrero, L. M. (1951). Filtration, diffusion and molecular sieving through peripheral capillary membranes: a contribution to the pore theory of capillary permeability. American Journal of Physiology-Legacy Content, 167(1), 13-46.

Parmar, A. S., & Muschol, M. (2009). Hydration and hydrodynamic interactions of lysozyme: effects of chaotropic versus kosmotropic ions. Biophysical journal, 97(2), 590-598.

Phillips, R. J., Deen, W. M., & Brady, J. F. (1989). Hindered transport of spherical macromolecules in fibrous membranes and gels. AIChE journal, 35(11), 1761-1769.

Punyaratabandhu, N., Kongoup, P., Dechadilok, P., Katavetin, P., & Triampo, W. (2017). Transport of spherical particles through fibrous media and a row of parallel cylinders: applications to glomerular filtration. Journal of biomechanical engineering, 139(12).

Putnam, F. W. (1975). Alpha, beta, gamma, omega—the roster of the plasma proteins. In The plasma proteins (pp. 57-131). Academic Press.

Putnam, F. W. (1975). Alpha, beta, gamma, omega—the roster of the plasma proteins. In The plasma proteins (pp. 57-131). Academic Press.

Renkin, E. M. (1954). Filtration, diffusion, and molecular sieving through porous cellulose membranes. The Journal of general physiology, 38(2), 225-243.

Rezaei, B., Ghani, M., Shoushtari, A. M., & Rabiee, M. (2016). Electrochemical biosensors based on nanofibres for cardiac biomarker detection: A comprehensive review. Biosensors and Bioelectronics, 78, 513-523.

Saltzman, W. M., Radomsky, M. L., Whaley, K. J., & Cone, R. A. (1994). Antibody diffusion in human cervical mucus. Biophysical journal, 66(2), 508-515.

Schmitz, K. S., & Lu, M. (1983). Effect of titration charge on the diffusion of bovine serum albumin. Proceedings of the National Academy of Sciences, 80(2), 425-429.

Shin, K., Yu, H., & Kim, J. (2017). Determination of diffusion coefficient and partition coefficient of photoinitiator 2-hydroxy-2-methylpropiophenone in nanoporous polydimethylsiloxane network and aqueous poly (ethylene glycol) diacrylate solution. Journal of Industrial and Engineering Chemistry, 56, 443-449.

Silva, D. F. C., Azevedo, A. M., Fernandes, P., Chu, V., Conde, J. P., & Aires-Barros, M. R. (2017). Determination of partition coefficients of biomolecules in a microfluidic aqueous two phase system platform using fluorescence microscopy. Journal of Chromatography A, 1487, 242-247.

Stringer, J. L., & Peppas, N. A. (1996). Diffusion of small molecular weight drugs in radiation-crosslinked poly (ethylene oxide) hydrogels. Journal of Controlled Release, 42(2), 195-202.

Sundarrajan, S., Tan, K. L., Lim, S. H., & Ramakrishna, S. (2014). Electrospun nanofibers for air filtration applications. Procedia Engineering, 75, 159-163.

Tang, P., Zhang, M., Ji, B., Yong, T., & Sun, G. (2019). Hierarchical Nucleophilic Nanofibrous Membranes for Fast, Durable, and Bare‐Eye Visible Detoxification of Carcinogenic Alkylating Toxicants. Advanced Functional Materials, 29(50), 1905990.

Taniguchi, M., Kobayashi, M., & Fujii, M. (1989). Properties of a reversible soluble–insoluble cellulase and its application to repeated hydrolysis of crystalline cellulose. Biotechnology and bioengineering, 34(8), 1092-1097.

Vagias, A., Sergelen, K., Koynov, K., Košovan, P., Dostalek, J., Jonas, U., ... & Fytas, G. (2017). Diffusion and permeation of labeled IgG in grafted hydrogels. Macromolecules, 50(12), 4770-4779.

Vermonden, T., Censi, R., & Hennink, W. E. (2012). Hydrogels for protein delivery. Chemical reviews, 112(5), 2853-2888.

Wang, L., Fu, Q., Yu, J., Liu, L., & Ding, B. (2019). Nanoparticle-doped polystyrene/polyacrylonitrile nanofiber membrane with hierarchical structure as promising protein hydrophobic interaction chromatography media. Composites Communications, 16, 33-40.

Wetter, L. R., & Deutsch, H. F. (1951). Immunological studies on egg white proteins. J. biol. Chem, 192, 237-242.

Wu, J., Xiao, Z., He, C., Zhu, J., Ma, G., Wang, G., ... & Chen, S. (2016). Protein diffusion characteristics in the hydrogels of poly (ethylene glycol) and zwitterionic poly (sulfobetaine methacrylate)(pSBMA). Acta biomaterialia, 40, 172-181.

Yang, X., Liu, C., Li, Y., Marchesoni, F., Hänggi, P., & Zhang, H. P. (2017). Hydrodynamic and entropic effects on colloidal diffusion in corrugated channels. Proceedings of the National Academy of Sciences, 114(36), 9564-9569.

Yao, Y., & Lenhoff, A. M. (2006). Pore size distributions of ion exchangers and relation to protein binding capacity. Journal of Chromatography A, 1126(1-2), 107-119.

Yu, D. G., Zhu, L. M., White, K., & Branford-White, C. (2009). Electrospun nanofiber-based drug delivery systems. Health, 1(02), 67.

Zhao, C., Si, Y., Pan, B., Taha, A. Y., Pan, T., & Sun, G. (2020). Design and fabrication of a highly sensitive and naked-eye distinguishable colorimetric biosensor for chloramphenicol detection by using ELISA on nanofibrous membranes. Talanta, 217, 121054.

Zhou, Y., Li, J., Zhang, Y., Dong, D., Zhang, E., Ji, F., ... & Yao, F. (2017). Establishment of a physical model for solute diffusion in hydrogel: understanding the diffusion of proteins in poly (sulfobetaine methacrylate) hydrogel. The Journal of Physical Chemistry B, 121(4), 800-814.

Zhu, J., & Sun, G. (2012). Lipase immobilization on glutaraldehyde-activated nanofibrous membranes for improved enzyme stabilities and activities. Reactive and Functional Polymers, 72(11), 839-845.

Zhu, J., & Sun, G. (2014). Facile fabrication of hydrophilic nanofibrous membranes with an immobilized metal–chelate affinity complex for selective protein separation. ACS applied materials & interfaces, 6(2), 925-932.

Chapter 5. Improving sensitivity of nanofibrous membrane-based ELISA for on-site antibiotics detection

5.1 Introduction

Trace amount of pesticide chemicals and antibiotics are existing in soil, ground water, and foods, which are causing human safety and environmental concerns. The conventional detection methods, including liquid chromatography /gas chromatography mass spectrometry (LC/GC-MS) and enzyme-linked immunosorbent assay (ELISA), are reliable and selective, however, have limitations. These techniques are sensitive to detect trace number of toxicants in environment but are highly dependent on the use of sophisticated facilities and well-trained professionals, limiting their applications in the on-site detection. (Kümmerer 2009; Haller, Müller et al. 2002; Mungroo and Neethirajan 2014) Thus, sensors and sensing technologies possessing highly sensitive, selective and rapid on-site detection ability of these chemicals are desired and necessary for improving human and environmental protection.

In efforts of developing highly selective and sensitive sensors for on-site detection of toxic chemicals, ELISA on nanofibrous membrane sensors were prepared with demonstrated ability and capacity of rapid, selective, naked-eye, and on-site detection. (Zhao, Si et al. 2020, Russo, Ursino et al. 2020; Tawfik, Elmasry et al. 2020; Yagati, Chavan et al. 2018) A combination of sensitivity and selectivity of ELISA assay with ultra-high specific surface area and porous structures of nanofibrous membranes was considered as the best pathway to develop such unique personal use sensors. Specific surfaces area of a nanofibrous membrane should be at least three magnitude (1000 times)

higher than that of the conventional ELISA plates, and the numbers of loaded antibodies should be dramatically increased, subsequently improving the sensitivity of the ELISA on the nanofibrous membrane. However, previous research and literature results on ELISA on nanofibrous membranes only revealed several times increases in sensitivities, much lower than the expectation. (Zhao, Si et al. 2020; Yang, Niu et al. 2008; Li, Liu et al. 2020; Hersey, Meller et al. 2015; Mahmoudifard, Soleimani et al. 2017)

The nanofibrous membranes prepared by regular electrospinning processes possess dimensionally heterogenous porosity structures due to the layered nanofibrous structures. (Holzmeister, Rudisile et al. 2007) The pore sizes and distributions in the membranes vary significantly depending on different directions, mostly in the vertical direction. The pores along this direction of the membrane could have three different types, through pores, blind pores, and closed pores. (Jang, Kang et al. 2019) The through pores can allow micro-sized particles or large biomolecules to penetrate through the membrane, and the blind pores have closed ends that can block the diffusion of the particles. Closed pores are formed in the middle of the membranes without access to out layers, which have no contribution to diffusion or partition of chemicals into the membranes. (Jang, Kang et al. 2019) Our recent study of diffusion of large molecules through nanofibrous membranes found that only the measured pore size of the membrane is close to 1000 times larger than diffusant molecules, a normal diffusion pattern of the molecules could be observed through the membrane. (Zhao, Si et al. 2021) The effective pore could be significantly smaller than the measured pores of the microporous nanofibrous membranes, and subsequently, the protein molecules are hard to diffuse into or through the micro-porous membrane structures. As a result, the large enzyme molecules are mostly incorporated

on the outside surfaces of nanofibrous membranes not inside. (Hu, Liu et al. 2014; Yan, Li et al. 2009) Then, the hindered diffusion of large biomolecule may lead to increased ligand density on the surface of membranes resulting in a steric crowding effect and reduction of the analyte binding efficiency. As a result, the sensitivity of regular nanofibrous membrane-based ELISA is dramatically lower than the theoretical values, without presenting the benefits of the higher surface areas versus the conventional ELISA. (Bonanno and DeLouise 2007; Cooper and Williams 1999)

Theoretically speculated nanofibrous membranes for ELISA applications should be three-dimensional uniform with large pore size, in addition to the desired chemical reactivity and stability as membrane materials. Here, we report the newly progresses in improving the sensitivity of immunoassay biosensor by incorporating competitive ELISA onto structurally modified poly(vinyl-co-ethylene) (PVA-co-PE) nanofibrous matrices. The following modification measures were adopted on the membrane structures, including more through pores, stable nanofiber structure, hydrophilic modification agents and proper diffusion condition, increasing the number of antibodies interacting and immobilized on the membranes. First, the improved accessibility of the ultrahigh surface areas of the membranes dramatically increased the number of immobilized antibodies with reduced steric hindrance for reacting with target and other biomolecules. Improvement in hydrophilicity of the membranes facilitates the entrance and access of analytes and biomolecules, as well as the interaction with the pre-loaded antibodies, leading to significant increase in color signals while detecting targets in ultra-low concentrations. As a result, the sensor made of the novel membrane structures could

reveal a naked eye distinguishable color change at 0.01ng/mL of chloramphenicol (CAP), and the limitation of detection (LOD) is 0.005ng/mL with the help of a smartphone.

5.2 Materials and Methods

5.2.1 Materials

Poly(vinyl-co-ethylene) (PVA-co-PE, PE content of 27%, MWn =90,000), chloramphenicol (CAP), florfenicol (FF), thiamphenicol (TAP), penicillin (PCN), 3,3',5,5'-tetramethylbenzidine (TMB), Immunoglobulin G (IgG), fluorescein isothiocyanate (FITC), fluorescein isothiocyanate labeled immunoglobulin G (FITC-IgG), fluorescein isothiocyanate linked dextran (FITC-dextran) and bovine serum albumin (BSA) were obtained from Sigma-Aldrich (USA). Anti-CAP antibody (Ab) and CAP labeled horseradish peroxidase (CAP-HRP) were purchased from Abcam (Cambridge, MA, USA). Isopropanol, N, N'-disuccinimidyl carbonate (DSC), triethylamine (TEA), 1,4-dioxane, acetone, hydrogen peroxide (30 wt%), copper sulfate ($CuSO_4$), sodium carbonate (Na_2CO_3), sodium bicarbonate ($NaHCO_3$), citric acid, sodium citrate, phosphate-buffered saline (PBS), N-hydroxysuccinimide (NHS), polyethylene glycol (PEG), polydimethylsiloxane (PDMS) and its crosslinking agent, Pierce™ BCA Protein Assay Kit, high-binding 96-well plates were purchased from Thermo Fisher Scientific (USA).

5.2.2 Fabrication of PVA-co-PE nanofibrous membranes

PVA-co-PE nanofibrous membrane was fabricated according to our previous report. (Zhao, Si et al. 2020) PVA-co-PE (MWn = 90,000) isopropanol/water (70/30) solutions in

varied concentrations were prepared. During the electrospinning process, the relative humidity was controlled at 50% by a humidifier (Urpower Co.). The membrane morphology was analyzed by a field-emission scanning electron microscopy (Quattro ESEM, Thermo Scientific™), and the pore distribution of the membrane was measured with a capillary flow porometer (Porous Media Inc., Ithaca, NY). The thickness of the membranes was measured with an electronic micrometer thickness gauge (Neoteck).

5.2.3 Measurement of diffusion of biomolecules in PVA-co-PE nanofibrous membranes

Diffusion of biomolecules (FITC-dextran compounds or protein samples) through nanofibrous membranes was measured by using a side-by-side diffusion cell (PerneGear Co.) according to a previous report. (Zhao, Si et al. 2021) The FITC-dextran concentration in both chambers was measured by a plate reader (BioTek®) at regular intervals. And the protein concentration in both chambers could be measured with the BCA protein assay (Thermo Fisher™) and a UV-vis spectrophotometer (Thermo Scientific), according to the previous report. (Zhao, Si et al. 2021) The permeability coefficient and diffusion coefficient can be calculated by using Fick's law with biomolecule concentrations in the receptor chamber.

After 30min diffusion of FITC-Dextran samples, the membrane was removed from the side-by-side chamber and dried in a vacuum oven at 100 ℃ for 50s. Then, the membrane was frozen in liquid nitrogen, sliced and sealed by two pieces of glass and placed on a glass side. The cross-section images of the membranes were taken by a laser scanning

confocal microscopy (LSCM) (FluoView 1000 system, Olympus America, Center Valley, PA) at 520nm under the excitation of 488 nm. Then, the confocal fluorescence images were analyzed using the Olympus Fluoview 1.5 software.

5.2.4 Modification and characterization of nanofibrous membranes

The electrospun PVA-co-PE membrane was modified by reacting with DSC according to a previous procedure. (Zhao, Si et al. 2020) After the DSC reaction, a N-hydroxylsuccinimide (NHS) ester is formed on the membranes for further reaction with primary amines of proteins. The amount of the loaded NHS ester was determined by the color change of bicinchoninic acid (BCA) dye solution measured by a UV-vis spectroscopy. One milligram of the modified membrane was soaked in a BCA working agent, which was prepared, according to a previous report. (Zhao, Si et al. 2020) The number of loaded NHS esters was measured by a UV-vis spectroscopy based on a calibration curve which was established by measuring the color intensity of various concentration of NHS. In addition, these membranes were also characterized by a Fourier-transform infrared spectroscopy (FTIR) (Thermal Co) for proving the successful modification. The hydrophilicity of the membranes was represented by measuring water contact angle of loaded 50µL of water onto the surface with a microscope camera (Dino-lite Co). The morphology changes of the membranes were analyzed by using a field-emission scanning electron microscopy (FE-SEM), and the fiber diameter was measured based on the FE-SEM images. The pore sizes of the membranes were measured with a capillary flow porometer (Porous Media Inc., Ithaca, NY).

5.2.5 Immobilization of antibody

The modified PVA-co-PE nanofibrous membranes were punched to small pieces (circles with diameter=0.9cm). (Zhao, Si et al. 2020) Antibody stock solution was diluted to varied concentrations from 0.02g/L to 2g/L, respectively, in a PBS buffer, then 10μL of the as-prepared antibody solution was added onto the membranes. The membranes were incubated in a bio-oven at 37℃ for 30 mins with continuous shaking. Then, these treated membranes were placed into a PBS buffer to wash-off unreacted proteins. The number of immobilized antibodies could be measured by a standard BCA protein assay. Since NHS ester could reduce copper sulfate and make BCA colored, the residual NHS ester on the membrane needs to be hydrolyzed in an alkaline solution (pH 11.5 sodium carbonate buffer) containing 10%wt PEG. Then, the pre-treated membranes were soaked into the BCA mixture for the measurement of immobilized proteins. Meanwhile, the protein immobilization reaction efficiency could be calculated by dividing the number of the immobilized proteins by the total amount of injected antibodies. Then, the resulting membrane was soaked into a 1 wt% BSA solution to block unreacted sites, preventing the unspecific reaction between CAP-HRP and the membranes.

5.2.6 Analysis of colorimetric signals by nanofibrous membrane-based ELISA

Competitive ELISA assay was employed for testing the concentration of CAP. The test solution was prepared by mixing 25μL of a CAP solution with 25μL of a known

concentrated CAP-HRP solution. The antibody immobilized membranes were immersed into the as-prepared test solution for 10 mins. Then, the unreacted CAP-HRP was washed off by a PBS buffer. A TMB dye substrate was prepared according to the literature. (Zhao, Si et al. 2020) Then, 50 μL of the TMB dye substrate was added onto the CAP-HRP captured membranes, and the membranes was placed in a box under LED light (Lux 10,000). The color change could be recorded by a smartphone (iPhone 6s), and the concentration of CAP could be further quantitatively analyzed by using an Image J software. The red channel (R) from RGB value was used to represent the color intensity. Here, the red channel intensity change could be represented by ΔRGB value which was obtained by RGB value difference between background and each membrane, or:

$$\Delta RGB = RGB_{background} - RGB_{membranes} \quad (1)$$

5.3 Results and Discussion

5.3.1 Fabrication of nanofibrous membrane-based ELISA

The nanofibrous membranes possess unique porous structures including through pores, blind pores, and closed pores, and only the through pores can allow biomolecules to penetrate through the membranes, and both blind and through pores can let the molecules enter the membranes. In addition, the nanofibrous membranes have much smaller effective pore sizes than those measured by different instruments. (Zhao, Si et al. 2021) As a result, large biomolecules could be frequently blocked by the porous nanofibrous matrices, leading to a large number of proteins loaded on the surfaces instead of entire media of the membranes, subsequently resulting in a sterically crowding

effect and the decrease of binding efficiency. (Wang, Partridge et al. 2019) (Figure 5.1a) However, properly structured nanofibrous membranes could allow antibodies rapidly diffuse into the three-dimensional fibrous matrix, which can fully demonstrate the advantageous of the ultrahigh surface areas of the nanofibers and desired sensitivity of biosensors based on the membranes. (Figure 5.1b).

To further verify diffusion properties of biomolecules in varied sizes through the nanofibrous membranes, firstly, we fabricated nanofibrous membranes with large pores according to our previous report. All the membranes were fabricated under high relative humidity environment (50% RH) to ensure more through pores formed in the membranes with larger pore sizes. As shown in SEM images, all the membranes reveal varied fiber diameters and randomly distributed microporous structures (Figure 5.1c). The distribution of fiber diameters and pore sizes are presented in Figure 5.1d and e, and the average fiber diameter and pore size are shown in Figure 5.1f. The average pore sizes of the membranes prepared by using 6 wt% and 8 wt% polymer concentrations were at hundreds of nanometers, which is similar with the pore sizes of the previously fabricated membranes. (Zhao, Si et al. 2020) The pore size increased with the increase of the polymer concentration. When the concentration of the polymer solution increased to 12 wt%, the average pore size reached 4.1μm, which is nearly 1,000 time larger than the antibody size. Fibrous membranes in such large pore sizes could present a similar diffusion pattern as a 3-D porous matrix. However, the average fiber diameter increased with the increment of polymer concentration, leading to the decrease of specific surface area and reduction of the loaded antibody. Especially, the fiber diameter is nearly 1μm in the membrane made from 12 wt% polymer solution.

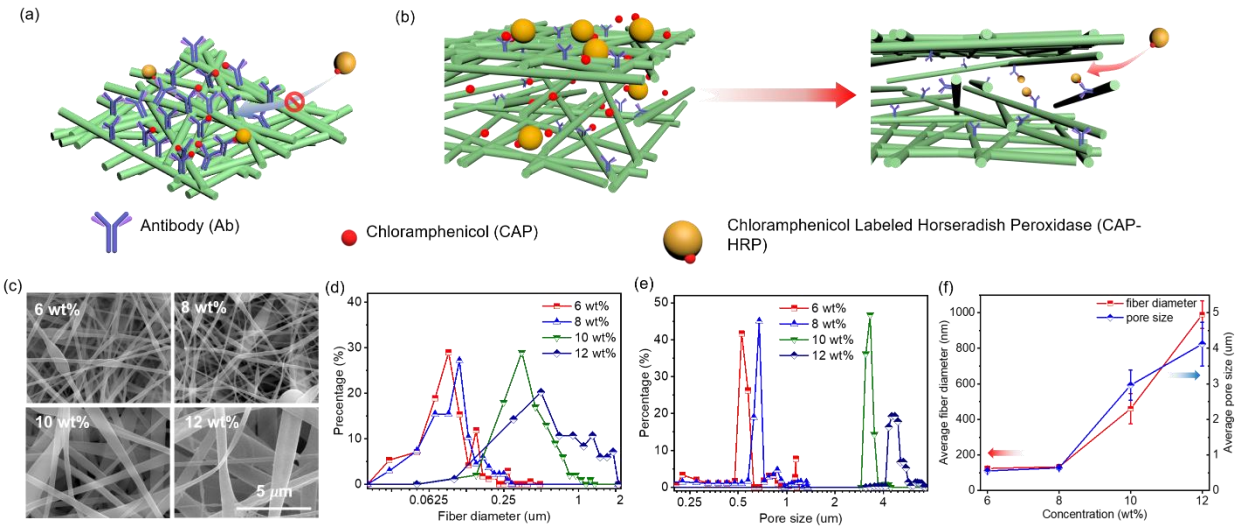

Figure 5.1. The scheme and microstructure of PVA-co-PE nanofibrous membranes. a) steric crowding effect of high density of biomolecule on the surface of regular nanofibrous membrane; and b) diffusion of biomolecule inside a hydrophilic and large porous nanofibrous membrane; c) SEM images of nanofibrous membranes made from different polymer concentrations, d) fiber diameter distribution, e) pore distribution, and f) average fiber diameter and pore size.

5.3.2 Diffusion property of the membranes

FITC linked dextran compounds in different molecular sizes were employed as the sample biomolecules to study the influence of pore structures of the membranes on their diffusivities. As reported in literature, concentrations of diffusants can be hypothesized as linearly decreasing inside the membrane from the boundary close to the donor side to the boundary near the receptor side at a pseudo steady-state, (Stringer and Peppas 1996) and the permeability coefficient of biomolecules inside the membranes could be determined by the equation 2:

$$\ln\left(1-\frac{2c_2}{c_0}\right)=-\frac{2PA}{V\Delta x} \quad (2)$$

Where C_0 is initial concentration of the biomolecules in donor chamber, C_2 is the concentration of the biomolecules in receptor chamber at a specific time. P is a permeability coefficient, A is the effective area for the diffusion, V is the volume of each chamber, and Δx is the thickness of the membrane. The plots of $\Delta x * \ln(1-2c_2/c_0)$ versus time are shown in Figure 5.2a and b. The FITC-dextran in size of 150KDa could reach pseudo steady-state of the diffusion inside membranes made by using 6wt% and 8wt% polymer solutions in around 2 hours, and gentle slopes in the linear range represent rather slow diffusion of the molecules (Figure 5.2a). With the pore size increase in the membranes made with more concentrated polymer solutions (10wt% and 12wt%), the times to reach to the pseudo steady-state diffusion reduced gradually, and the slopes in the linear range become steeper. Then, the diffusion properties of dextran molecules in different size were measured. The 150kDa and 40 kDa dextran molecules could represent IgG and horseradish peroxidase (HRP), while FITC itself can represent small molecules including CAP and TMB. The times to reach the pseudo steady-state for diffusion of the dextran molecules inside the membrane (8wt%) dramatically reduced with the decrease of the dextran size. The diffusion of the small FITC could reach pseudo steady-state in a very short time, and the slope in the linear range is extremely steep, representing the rapid diffusion of small molecule inside the fibrous membrane (Figure 5.2b). The permeability coefficients of the FITC linked dextran molecules versus dextran/pore size ratios were analyzed and are shown in Figure 5.2c. Here, the permeability coefficients of the FITC linked dextran molecules could be calculated by the slopes at the linear range (equation 2), and the hydrodynamic radii of the dextran molecules in dilute solution are

obtained from the literature. (Ioan, Aberle et al. 2000) The permeability coefficients decreased with the size ratio increase. Especially, the permeability of FITC is dramatically higher than the larger FITC-dextran molecules, revealing the varied hindrance of the membranes to diffusion of molecules in varied sizes. The confocal images were taken after 30min diffusion to visualize the differences. (Figure 5.2d and e) The fluorescence intensities of FITC inside membranes were measured and analyzed by Olympus Fluoview 1.5. The FITC linked dextran molecules diffused slowly into the membranes (6wt% and 8wt%) in smaller pores but more rapidly inside or through the membranes (10wt% and 12wt%) in larger pores, consistent with the measured permeability coefficients (Figure 5.2d). Similarly, the diffusion distances in the membranes increased with the molecule size decrease. Especially, the small molecule, FITC, could completely penetrate through and homogenously distribute inside the membrane in 30 mins (Figure 5.2e). The large size FITC-dextran (150kDa) diffused inside membranes very slowly, especially in membranes with smaller pores.

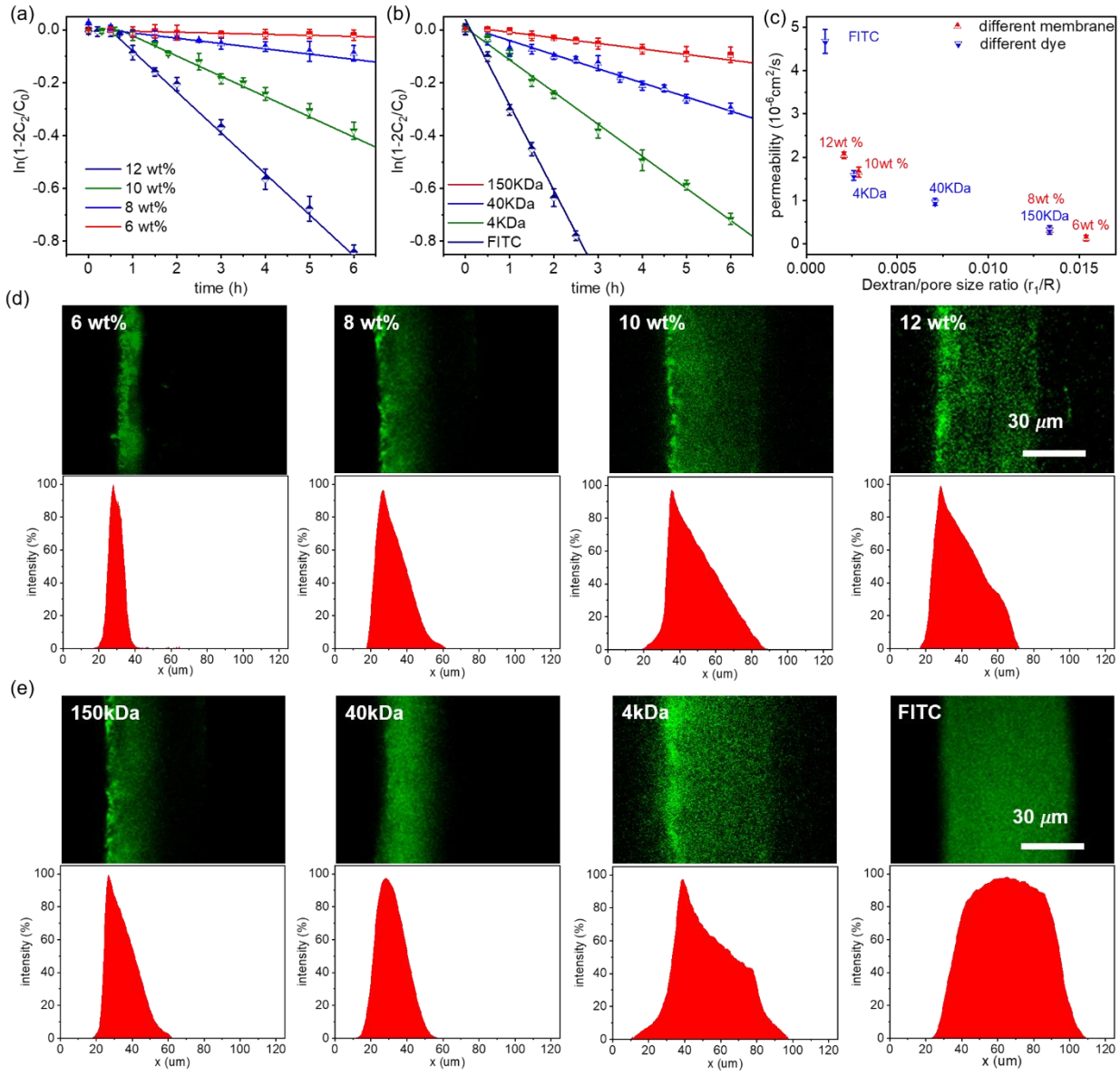

Figure 5.2. Diffusion behaviors of FITC linked dextran molecules inside membranes. a) diffusion patterns of 150kDa dextran through different membranes; b) diffusion behaviors of different dextran molecules through a representative membrane (8wt%); c) permeability coefficients of dextran molecules inside different membranes; d) confocal images and fluorescence intensity of 150kDa dextran inside different membranes; and e) confocal images and fluorescence intensity of different dextran inside an 8wt% membrane.

5.3.3 Hydrophilicity of nanofibrous membranes

In another effort of further improving the diffusion of biomolecule inside nanofibrous membranes, the hydrophilicity of the membranes was changed via chemical modifications. Hydrophilic surfaces of the nanofibers could reduce adsorption of proteins and facilitate the diffusion of proteins through the membranes. (Zhao, Si et al. 2021; Rabinow, Ding et al. 1995) Antibody proteins can be chemically immobilized onto nanofibrous membranes by using three different agents, including glutaraldehyde (GA), cyanuric chloride (CC), N, N-disuccinimidyl carbonate (DSC). (Zhao, Si et al. 2020; Zhu, Bahramian et al. 2012) Among them, DSC could provide improved hydrophilic surface than others and exhibit higher reactivities with the proteins, which was selected in the study. (Zhao, Si et al. 2020) The modification reaction and the following immobilization of antibodies are shown in Figure 5.3a. Varied DSC concentrations were employed to optimize the reaction conditions. The optical images of the modified membrane and measured NHS amounts loaded on the membranes are shown in Figure 5.3b. The NHS amount does not show significant difference among the membranes in different pore structures, which could be attributed to the fact that small molecules can easily diffuse through the membranes and be exposed to surfaces of nanofibers. The nanofibrous membranes revealed a significant yellowing effect at high concentration of DSC (15%), representing a potential change of their micro-morphology. Meanwhile, loaded NHS amount increased rapidly at low concentrations (0%-10%) but slowly at high concentrations (10%-15%) which could be attributed to gradual reduction of reactive surface areas of the nanofibers in high DSC concentration. Then, the membranes prepared with 10 wt% polymer concentration was

employed for FTIR and water contact angel characterizations. The NHS groups incorporated on the membrane are shown in FTIR with a carbonate peak at 1730cm^{-1}. And the intensity of carbonate peak increased with increasing DSC concentrations in the reactions. (Figure 5.3c). The hydrophilicity of the modified membranes is measured by water contact angle (WCA). The membranes become more hydrophilic with increasing DSC concentration in the reactions, represented by a decrease of WCA (Figure 5.3d). Although the modified membranes retained nanofiber morphology and micro-porous structure, the nanofibers became swollen obviously with the increase of DSC concentration, shown in the SEM image (Figure 5.3e). The original nanofiber diameter of 520.00nm increased to 742.80nm as the DSC concentration increased to 15% (Figure 5.3f). Since the membrane modified with 5wt% of DSC still revealed a relative hydrophobic (WCA = 89.2 at 3 seconds) surface and the membrane modified with 15wt% DSC showed significant swelling, 10% DSC solution was employed in the modification of the membranes to provide proper hydrophilicity (WCA=27.6) and moderate swelling (average diameter=616.95nm).

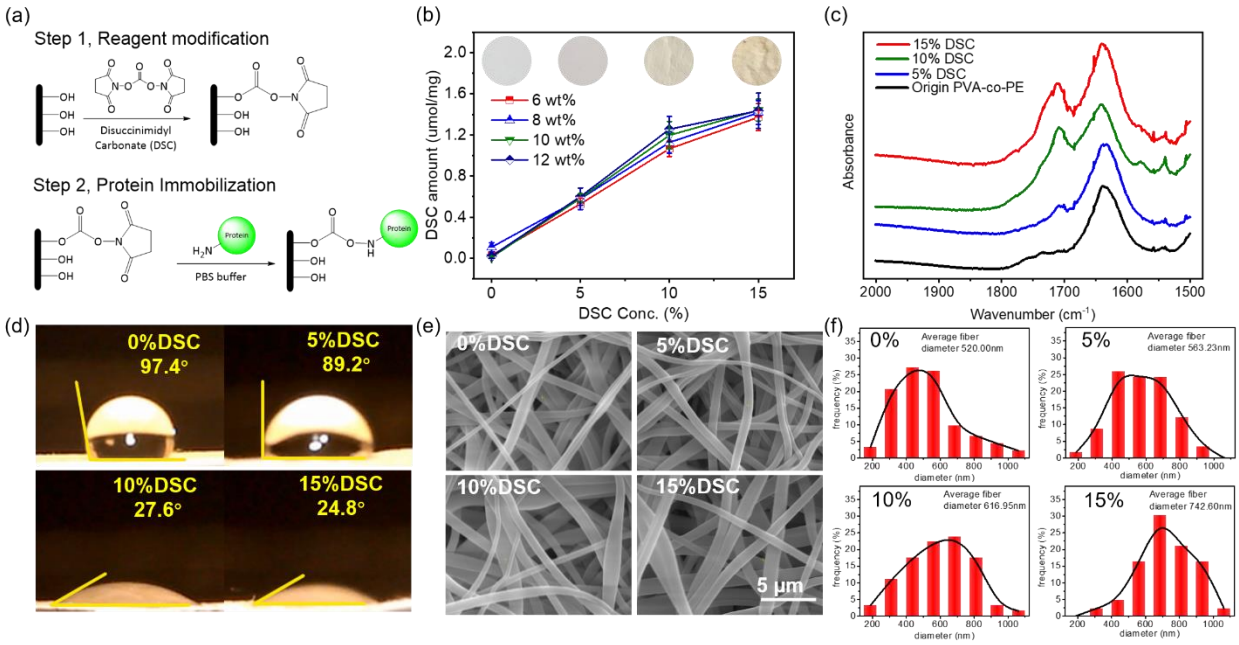

Figure 5.3. Chemical modification of nanofibrous membranes. a) Reaction of PVA-co-PE membrane with DSC and proteins; b) Optical images and loaded NHS amounts on membranes modified by DSC in varied concentrations; c) FTIR spectra of membranes before and after modification; d) Water contact angles of membranes after reactions; f) SEM images and g) Fiber diameter distributions of membranes after reactions

5.3.4 Immobilization of antibody

With the above results, the DSC modified nanofibrous membranes were employed for immobilization of antibodies (IgG), and the reaction is shown in Figure 5.3a (Step 2). The amounts of the immobilized IgG and reaction efficiencies are shown in Figure 5.4a and Figure 5.4b, respectively. At low antibody concentrations (below 100 mg/L), all protein molecules could be immobilized onto the nanofibers in the membranes, reaching the immobilization efficiency around 100%. Then, reaction efficiencies dramatically

decreased with high protein concentrations, which may be resulted from overloading the protein molecules above the maximum reactive sites of the modified nanofibrous membrane. Meanwhile, as speculated earlier the nanofibrous membranes having large pore sizes (made by 10 wt% and 12 wt% polymer solutions) show more antibodies immobilized inside the membranes and present higher reaction efficiencies than those of regular pore sizes (made with 6 wt% and 8 wt% polymer solutions) of electrospun nanofibrous membranes. These results can be attributed to the hindered diffusion behaviors of IgG in regular pore size membranes, causing high concentration of antibodies on the surface of membranes. Then, FITC-IgG was used to reveal the homogeneity of the immobilized protein on the membranes by mapping their fluorescence signals. (Figure 5.4c). The increase of the FITC-IgG concentration prompts more IgG immobilization on the nanofibrous membranes, and the fluorescent signals are brightness at 200mg/L of protein indicating homogenous immobilization. Thus, 200mg/L is the minimum injected concentration used in further studies.

IgG proteins can reach a pseudo steady-state of diffusion within 3 hours in all membranes (Figure 5.4d). The diffusion of IgG molecules in the membranes are faster than that of 150kDa dextran (Figure 5.2a) because IgG is more hydrophobic with a higher partition coefficient on the membranes. Then, the slopes at the linear ranger could be employed to calculating permeability coefficient (*P*) of IgG. The diffusion coefficient (*D*) could be calculated by the equation 3:

$$P = D * k_d \tag{3}$$

The k_d in the equation is partition coefficient of the protein in the membranes or represents the ratio of the concentration of non-adsorbed protein in the pores inside the

membrane to average concentration of protein in both chambers. The k_d could be obtained by measuring the number of proteins inside membrane after diffusion test according to previous reports. (Zhao, Si et al. 2021; Liu, Kotsmar et al. 2013) Then, the ratios between diffusion coefficient of IgG inside membranes to the bulk diffusion coefficient (D/D_0) are shown in Figure 5.4e, while the diffusion coefficient of IgG in the bulk solvent could be obtained following the method used in the reference. (Saltzman, Radomsky et al. 1994)

The diffusion coefficient of IgG increases with the decrease of IgG-pore size ratio (r_1/R), and the diffusion coefficient of IgG inside the largest pore membrane (12wt%) is around 10 times higher than the diffusion coefficient of IgG through the membrane prepared with 6wt% and 8wt%of PVA-co-PE. Such dramatic difference of diffusion behavior of the membranes further confirms the significant variance of distribution of immobilized protein inside membranes. Then, the measured results are compared with a classical diffusion theory, the Renkin equation, (Renkin 1954; Pappenheimer 1953) or

$$\frac{D}{D_0} = (1 - \frac{r_1}{R})^2[1 - 2.10\frac{r_1}{R} + 2.09(\frac{r_1}{R})^3 - 0.95(\frac{r_1}{R})^5] \quad (4)$$

Where r_1 and R represent the solute size and pore size of membranes, respectively. The diffusion coefficients of IgG inside the PVA-co-PE membranes could be overestimated by following the classical hindered diffusion theory. The heterogeneity of the nanofibrous membranes does not have much through pores in vertical direction and possesses much smaller effective pore sizes, making them the best filtration materials. Meanwhile, since PVA-co-PE could dramatically swell inside aqueous solvent, the effective pore size could further decrease in the diffusion test. (Zhu, Yang et al. 2011)

Then, the distribution of IgG could be predicted by the fundamental solutions of Fick's second law, or:

$$C(x,t) = \frac{1}{\sqrt{4\pi Dt}} e^{\left(-\frac{x^2}{4Dt}\right)} \quad (5)$$

Where x represents the distance between the location of diffused protein to the boundary at donor chamber. When an incubation time of 30 min is substituted into equation 5, the concentration distribution of IgG inside membranes could be predicted, as shown in Figure 5.4f. The predicted results show that the IgG could diffuse inside the lager pore size membrane, but hardly penetrate through regular pore size membranes after incubation. The predicted results confirm the confocal images of the membranes (Figure 5.4d).

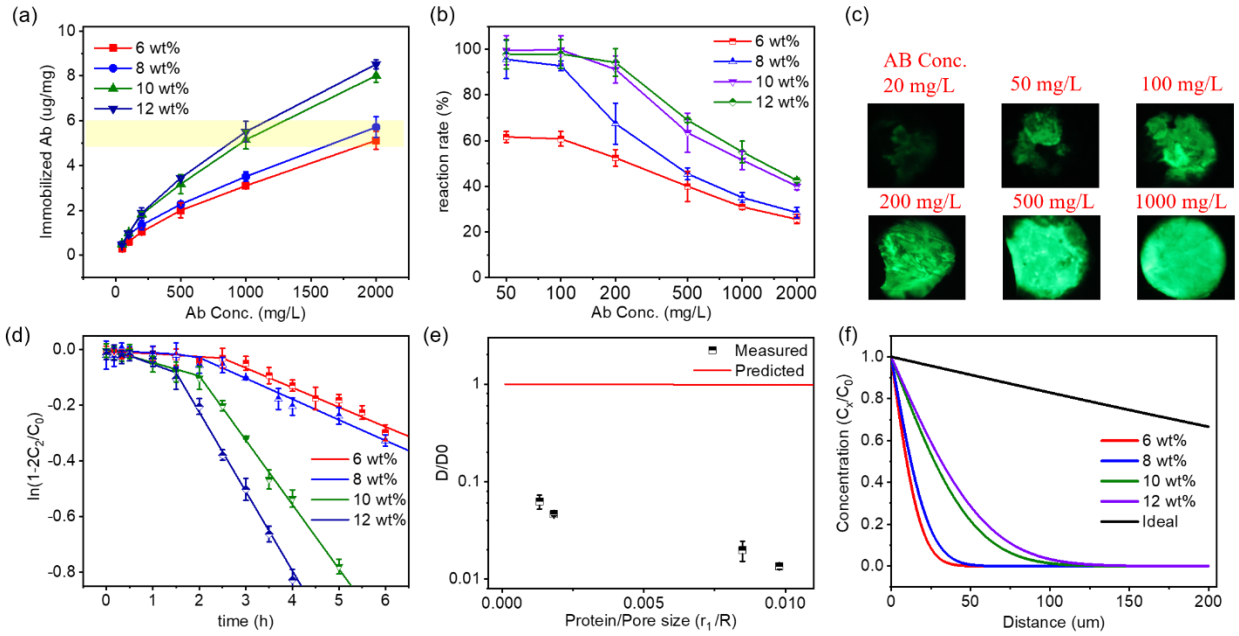

Figure 5.4. Immobilization and diffusion of IgG inside nanofibrous membranes. a) Immobilized antibody amounts on modified membranes; b) reaction efficiencies of antibody immobilization on modified membranes; c) Fluorescence images of FITC-IgG

loaded membranes; d) cumulative amounts of IgG in receptor chamber versus time, e) diffusion coefficients of IgG inside membranes, and f) the predicted IgG distribution inside membranes

5.3.5 Sensitivity comparison among varied membranes

Here, 2000mg/L of CAP antibody was incubated on the membranes prepared with regular pores (made with 6 wt% and 8 wt% of polymers), and 1000mg/L of the antibody was immobilized on the membranes prepared with large pores (made with 10 wt% and 12 wt% of polymers). The immobilized antibody was controlled at 6 μg per microgram of the membrane. Then, 75ng/mL CAP-HRP was mixed with a CAP solution, and the mixture was injected onto the as-prepared membranes. The optical images and ΔRGB values of membranes are shown in Figure 5.5a-d. The membranes treated by 0ng/mL CAP revealed a bright blue color, but membranes treated by other concentrations of CAP appeared in faded colors. And all membranes prepared with varied pore structures revealed significant color intensity difference while detecting 0ng/mL and 0.1ng/mL of CAP. However, the membranes with regular pore size did not show the difference of colorimetric intensity as significant as the membranes prepared with larger pores on the ΔRGB value, which could be a result from the difference of protein distribution inside each membrane (as shown in Figure 5.4f). Thus, pore size of the nanofibrous membranes has a significant influence on the sensitivity of competitive ELISA. Here, the membrane made with 12 wt% polymer did not show obvious enhancement on the sensitivity than the 10 wt% membrane, which could be the reduction of the specific surface area while the fiber

diameter was increased as well. Thus, the membrane prepared with 10 wt% of PVA-co-PE was employed for the following experiments.

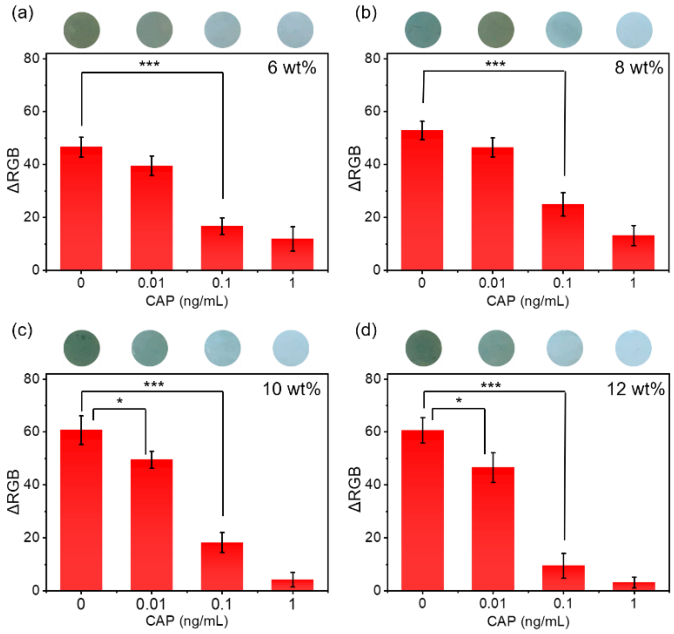

Figure 5.5. Optical images and color intensities of membranes for detecting varied concentration of CAP. The membranes were prepared with different polymer concentration a) 6 wt%, b) 8 wt%, c) 10 wt% and d) 12 wt%.

5.3.6 Improved sensitivity in detecting CAP

With all parameters, including the amount of immobilized antibody and the concentration of loaded CAP-HRP, optimized via a checkerboard test (Figure 5.6a), the sensitivity of the biosensor made from the nanofibrous membranes were further increased. The ΔRGB values of the membranes treated by 0ng/mL and 0.01ng/mL of CAP were measured, and the differences of ΔRGB value between the membranes treated by two concentrated CAP solutions were calculated. Here,10μg of loaded antibody and 50ng/mL

of CAP-HRP were selected as optimal parameters for detecting CAP. Then, the optical image and color intensity of the membranes treated by different concentrations of CAP solution are described in Figure 5.6b. The blue color on the membranes became faded and ΔRGB values decreased with the increasing concentrations of CAP. The color intensity at 0.01ng/mL of CAP (18.08±3.74) was dramatically lower than the color intensity at 0ng/mL of CAP (53.30±4.33), and the color difference could be observed by naked eyes. A linear range was located from 0.006ng/mL to 0.012 ng/mL with R^2 at 0.94. The limit of detection (LOD) of this membrane-based ELISA sensor reached to 0.005ng/mL, where the ΔRGB value of the membrane treated by 0.005ng/mL of CAP was 42.08±3.52, lower than two standard deviations of ΔRGB value of the membrane treated by 0ng/mL of CAP.

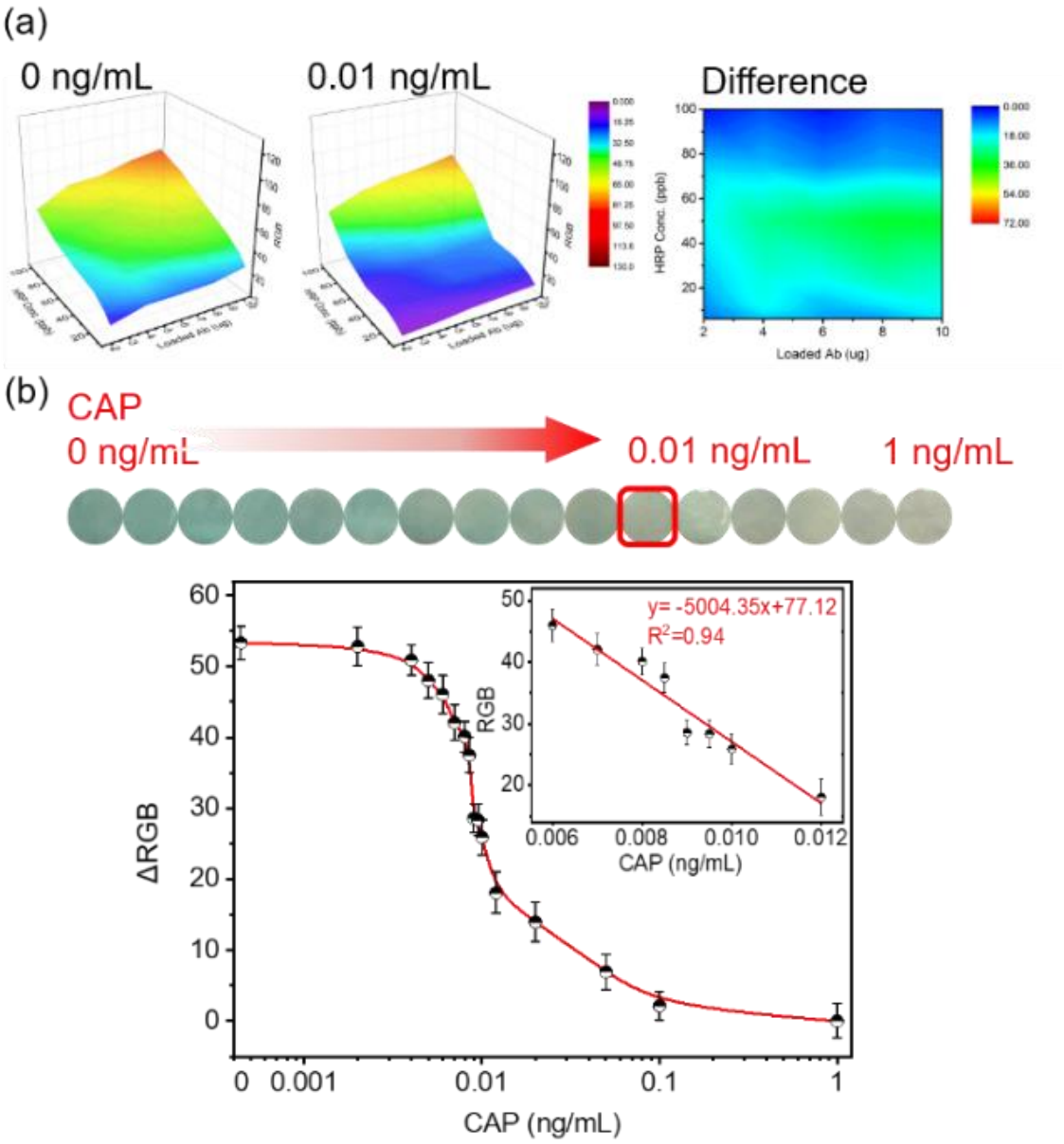

Figure 5.6. Quantitative detection of trace amount of CAP. a) checkerboard test; b) optical image and calibration curve of membranes treated by varied concentrations of CAP.

Comparing the previous published results of other developed ELISA sensors for CAP, the currently developed nanofibrous membrane-based ELISA reveals highly improved

sensitivity. (Table 5.1) In the previous report, the naked eye detection LOD of the previously fabricated nanofibrous membrane-based ELISA was close to the commercial 96 well plate-based ELISA and conventional paper-based ELISA. (Zhao, Si et al. 2020) This newly developed nanofibrous membranes significantly enhanced the sensitivity and decreased the LOD by 20 times. Meanwhile, compared with results from the ELISA sensors by using regular nanofibrous membranes in literature, the large pore size and hydrophilic nanofibrous membranes revealed a significant improvement of sensitivity. (Table 5.2)

Table 5.1. Comparison of LOD of CAP detection among various ELISA sensors from literature.

Solid Substrate	Signal Amplifying	LOD (ng/mL)	reference
96 well plates	NA	0.1	Wesongah, Murilla et al. 2007
96 well plates	Fluoro-immunoassays	0.05	Shen, Zhang et al. 2006
96 well plates	Biotin-Streptavidin Amplified	0.042	Wang, Zhang et al. 2010
96 well plates	Biotin-Streptavidin Amplified	0.10	Chughtai, Maqbool et al. 2017
96 well plates	Gold Nanoparticles	0.3	Wang, Chen et al. 2016
Paper-based	NA	100	Duyen, Matsuura et al. 2017
Solution	Ion amplified GNP	1.9	Wu, Liu et al. 2019
Solution	DNA amplified GNP	2.2	Wu, Huang et al. 2020
96 well plates	NA	0.1	Previous work
Nitrocellulose membranes	NA	1	Previous work

Nanofibrous membrane	NA	0.1	Previous work
Optimally developed nanofibrous membrane	NA	0.005	This work

Table 5.2. Comparison of sensitivity improvement among various nanofibrous membrane-based ELISA from literature

Polymer of nanofibrous membrane	Target molecule	Sensitivity improvement	Reference
polycarbonate	HIV	5 times	Yang, Niu et al. 2008
TiO2-based polyethersolfone	HIV & interleukin staphylococcus enterotoxin B	6.41-6.93 times 1.2 times	Li, Liu et al. 2020 Mahmoudifard, Soudi et al. 2016
poly(oxanorbornene)	mouse IgG	0.12 times	Hersey, Meller et al. 2015
polyacrylonitryle	mouse IgG	2-2.77 times	Mahmoudifard, Soleimani et al. 2017
poly-L-lactic acid & cellulose acetate	C-reactive protein	2.1 times	Sadir, Prabhakaran et al. 2014

phospholipid polymer	Human IgG	4.6 times	Chantasirichot, Ishihara et al. 2012
poly(styrene-alt-maleic anhydride)	Anti-IgG	3.33 times	Lee, Lee et al. 2011
poly(ε-caprolactone)	Human papilloma virus (HPV) type 16	5-6 times	Falcucci, Paolini et al. 2021
PVA-co-PE	CAP	1 time	Previous work
Large pore size & hydrophilic PVA-co-PE	CAP	20 times	This work

5.3.7 Selectivity and stability

The selectivity of the ELISA sensors on different antibiotics was measured by comparing colorimetric signals of penicillin (PCN), thiamphenicol (TAP) and florfenicol (FF) (Figure 5.7a). The spiked concentration of each antibiotic was 1ng/mL, and no antibiotic was presented in the control group. Here, the ΔRGB value of the membranes exposed to CAP was significantly lower than these to other three antibiotics. Color intensities of 1 ng/mL of CAP, PCN, TAP and FF were 6.71%, 98.64%, 99.27%, respectively, while the control revealed 100.33% color intensity. Thus, the ELISA on nanofibrous membrane sensor is specific to CAP with a high sensitivity. In addition, the selectivity could also be described by cross-reactivity ratios (CR%) which are measured

by the ratio of the 50% inhibition concentration (IC_{50}) between interferences and the target. The IC_{50} of the sensor in detecting CAP is around 0.009ng/mL (Figure 5.4b), but the IC_{50} for detecting other three antibiotics should be higher than 1ng/mL (Figure 5.7a). Thus, the CR% of the ELISA sensor to other three interferences is lower than 1%.

The stability of immobilized antibody is shown in Figure 5.7b. The antibody loaded nanofibrous membranes were stored in a refrigerator at 4℃ for varied durations and then employed for detecting CAP. The color intensity only decreased by 15.3% for detecting 0ng/mL CAP and 19.4% for detecting 0.01ng/mL CAP after a storage of 28 days. Significant signal intensity difference was maintained between 0ng/mL and 0.01ng/mL after the storage. Furthermore, based on the checkerboard test, over 70% of the initially loaded antibody retained their reactivity after 28-day storage, revealing a good storage stability of the sensors.

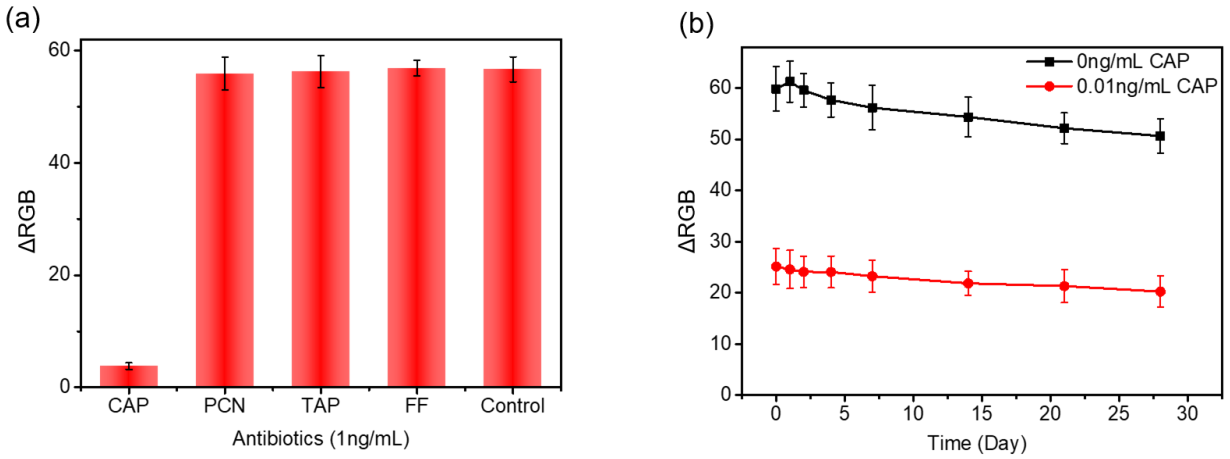

Figure 5.7. Elimination of interferences for CAP detection. a) Selectivity of ELISA; b) Stability of ELISA.

5.4 Conclusion

Structural features of electrospun nanofibrous membranes were investigated by diffusing various biomolecules in different sizes through the membranes in varied porous structures. The porous structures of the membranes were controlled by electrospinning PVA-co-PE in different polymer concentrations. In addition, hydrophilicity of the membranes was improved by using a more hydrophilic agent of N, N'-disuccinimidyl carbonate DSC in the chemical modification of the nanofibers. As a result, nanofibrous membrane with large pore sizes and hydrophilic surface demonstrated increased diffusion of the biomolecules inside the membranes. The ultrahigh surface areas of the nanofibers could indeed increase sensitivity in the fabrication of ELISA on nanofibrous membrane biosensors. An ultra-highly sensitive immunoassay biosensor by combing the advantages ELISA and microporous nanofibrous matrices was successfully developed. The sensors could achieve quantitative analysis of antibiotics in environment by measuring RGB value of optical images taking by a smartphone.

5.5 References

Bonanno, L. M., & DeLouise, L. A. (2007). Steric crowding effects on target detection in an affinity biosensor. Langmuir, 23(10), 5817-5823.

Chantasirichot, S., & Ishihara, K. (2012). Electrospun phospholipid polymer substrate for enhanced performance in immunoassay system. Biosensors and Bioelectronics, 38(1), 209-214.

Chughtai, M. I., Maqbool, U., Iqbal, M., Shah, M. S., & Fodey, T. (2017). Development of in-house ELISA for detection of chloramphenicol in bovine milk with subsequent confirmatory analysis by LC-MS/MS. Journal of Environmental Science and Health, Part B, 52(12), 871-879.

Cooper, M. A., & Williams, D. H. (1999). Kinetic analysis of antibody–antigen interactions at a supported lipid monolayer. Analytical biochemistry, 276(1), 36-47.

Duyen, T. T. M., Matsuura, H., Ujiie, K., Muraoka, M., Harada, K., & Hirata, K. (2017). based colorimetric biosensor for antibiotics inhibiting bacterial protein synthesis. Journal of bioscience and bioengineering, 123(1), 96-100.

Falcucci, S., Paolini, F., Mileo, A. M., Franconi, R., Massa, S., Rinaldi, A., & Venuti, A. (2021). ePCL Electrospun Microfibrous Layers for Immune Assays: Sensitive ELISA for the Detection of Serum Antibodies Against HPV16 E7 Oncoprotein. ACS omega, 6(13), 8778-8783.

Haller, M. Y., Müller, S. R., McArdell, C. S., Alder, A. C., & Suter, M. J. F. (2002). Quantification of veterinary antibiotics (sulfonamides and trimethoprim) in animal manure by liquid chromatography–mass spectrometry. Journal of Chromatography A, 952(1-2), 111-120.

Hersey, J. S., Meller, A., & Grinstaff, M. W. (2015). Functionalized nanofiber meshes enhance immunosorbent assays. Analytical chemistry, 87(23), 11863-11870.

Holzmeister, A., Rudisile, M., Greiner, A., & Wendorff, J. H. (2007). Structurally and chemically heterogeneous nanofibrous nonwovens via electrospinning. European polymer journal, 43(12), 4859-4867.

Hu, X., Liu, S., Zhou, G., Huang, Y., Xie, Z., & Jing, X. (2014). Electrospinning of polymeric nanofibers for drug delivery applications. Journal of controlled release, 185, 12-21.

Ioan, C. E., Aberle, T., & Burchard, W. (2000). Structure properties of dextran. 2. Dilute solution. Macromolecules, 33(15), 5730-5739.

Jang, E. S., Kang, C. W., & Jang, S. S. (2019). Pore characterization in cross section of yellow poplar (Liriodendron tulipifera) wood. Journal of The Korean Wood Science and Technology, 47(1), 8-20.

Kümmerer, K. (2009). Antibiotics in the aquatic environment–a review–part I. Chemosphere, 75(4), 417-434.

Lee, Y., Lee, H. J., Son, K. J., & Koh, W. G. (2011). Fabrication of hydrogel-micropatterned nanofibers for highly sensitive microarray-based immunosensors having additional enzyme-based sensing capability. Journal of Materials Chemistry, 21(12), 4476-4483.

Li, Z., Liu, Y., Chen, X., Cao, H., Shen, H., Mou, L., ... & Cong, Y. (2020). Surface-modified mesoporous nanofibers for microfluidic immunosensor with an ultra-sensitivity and high signal-to-noise ratio. Biosensors and Bioelectronics, 166, 112444.

Liu, D. E., Kotsmar, C., Nguyen, F., Sells, T., Taylor, N. O., Prausnitz, J. M., & Radke, C. J. (2013). Macromolecule sorption and diffusion in HEMA/MAA hydrogels. Industrial & Engineering Chemistry Research, 52(50), 18109-18120.

Mahmoudifard, M., Soleimani, M., & Vossoughi, M. (2017). Ammonia plasma-treated electrospun polyacrylonitryle nanofibrous membrane: the robust substrate for protein immobilization through glutaraldhyde coupling chemistry for biosensor application. Scientific reports, 7(1), 1-14.

Mahmoudifard, M., Soudi, S., Soleimani, M., Hosseinzadeh, S., Esmaeili, E., & Vossoughi, M. (2016). Efficient protein immobilization on polyethersolfone electrospun nanofibrous membrane via covalent binding for biosensing applications. Materials Science and Engineering: C, 58, 586-594.

Mungroo, N. A., & Neethirajan, S. (2014). Biosensors for the detection of antibiotics in poultry industry—a review. Biosensors, 4(4), 472-493.

Pappenheimer, J. R. (1953). Passage of molecules through capillary walls. Physiological Reviews, 33(3), 387-423.

Rabinow, B. E., Ding, Y. S., Qin, C., McHalsky, M. L., Schneider, J. H., Ashline, K. A., ... & Albrecht, R. M. (1995). Biomaterials with permanent hydrophilic surfaces and low

protein adsorption properties. Journal of Biomaterials Science, Polymer Edition, 6(1), 91-109.

Renkin, E. M. (1954). Filtration, diffusion, and molecular sieving through porous cellulose membranes. The Journal of general physiology, 38(2), 225-243.

Russo, F., Ursino, C., Avruscio, E., Desiderio, G., Perrone, A., Santoro, S., ... & Figoli, A. (2020). Innovative Poly (Vinylidene Fluoride)(PVDF) electrospun nanofiber membrane preparation using DMSO as a low toxicity solvent. Membranes, 10(3), 36.

Sadir, S., Prabhakaran, M. P., Wicaksono, D. H., & Ramakrishna, S. (2014). Fiber based enzyme-linked immunosorbent assay for C-reactive protein. Sensors and Actuators B: Chemical, 205, 50-60.

Saltzman, W. M., Radomsky, M. L., Whaley, K. J., & Cone, R. A. (1994). Antibody diffusion in human cervical mucus. Biophysical journal, 66(2), 508-515.

Shen, J., Zhang, Z., Yao, Y., Shi, W., Liu, Y., & Zhang, S. (2006). A monoclonal antibody-based time-resolved fluoroimmunoassay for chloramphenicol in shrimp and chicken muscle. Analytica chimica acta, 575(2), 262-266.

Stringer, J. L., & Peppas, N. A. (1996). Diffusion of small molecular weight drugs in radiation-crosslinked poly (ethylene oxide) hydrogels. Journal of Controlled Release, 42(2), 195-202.

Tawfik, S. M., Elmasry, M. R., Sharipov, M., Azizov, S., Lee, C. H., & Lee, Y. I. (2020). Dual emission nonionic molecular imprinting conjugated polythiophenes-based paper devices and their nanofibers for point-of-care biomarkers detection. Biosensors and Bioelectronics, 160, 112211.

Wang, L., Zhang, Y., Gao, X., Duan, Z., & Wang, S. (2010). Determination of chloramphenicol residues in milk by enzyme-linked immunosorbent assay: improvement by biotin− streptavidin-amplified system. Journal of agricultural and food chemistry, 58(6), 3265-3270.

Wang, S., Chen, Z., Choo, J., & Chen, L. (2016). Naked-eye sensitive ELISA-like assay based on gold-enhanced peroxidase-like immunogold activity. Analytical and bioanalytical chemistry, 408(4), 1015-1022.

Wang, Y., Partridge, A., & Wu, Y. (2019). Improving nanoparticle-enhanced surface plasmon resonance detection of small molecules by reducing steric hindrance via molecular linkers. Talanta, 198, 350-357.

Wesongah, J. O., Murilla, G. A., Guantai, A. N., Elliot, C., Fodey, T., & Cannavan, A. (2007). A competitive enzyme‐linked immunosorbent assay for determination of chloramphenicol. Journal of veterinary pharmacology and therapeutics, 30(1), 68-73.

Wu, Y. Y., Huang, P., & Wu, F. Y. (2020). A label-free colorimetric aptasensor based on controllable aggregation of AuNPs for the detection of multiplex antibiotics. Food chemistry, 304, 125377.

Wu, Y. Y., Liu, B. W., Huang, P., & Wu, F. Y. (2019). A novel colorimetric aptasensor for detection of chloramphenicol based on lanthanum ion–assisted gold nanoparticle aggregation and smartphone imaging. Analytical and bioanalytical chemistry, 411(28), 7511-7518.

Yagati, A. K., Chavan, S. G., Baek, C., Lee, M. H., & Min, J. (2018). Label-free impedance sensing of aflatoxin B1 with polyaniline nanofibers/Au nanoparticle electrode array. Sensors, 18(5), 1320.

Yan, S., Xiaoqiang, L., Lianjiang, T., Chen, H., & Xiumei, M. (2009). Poly (l-lactide-co-ε-caprolactone) electrospun nanofibers for encapsulating and sustained releasing proteins. Polymer, 50(17), 4212-4219.

Yang, D., Niu, X., Liu, Y., Wang, Y., Gu, X., Song, L., ... & Jiang, X. (2008). Electrospun nanofibrous membranes: A novel solid substrate for microfluidic immunoassays for HIV. Advanced Materials, 20(24), 4770-4775.

Zhao, C., Si, Y., Pan, B., Taha, A. Y., Pan, T., & Sun, G. (2020). Design and fabrication of a highly sensitive and naked-eye distinguishable colorimetric biosensor for chloramphenicol detection by using ELISA on nanofibrous membranes. Talanta, 217, 121054.

Zhao, C., Si, Y., Zhu, S., Bradley, K., Taha, A. Y., Pan, T., & Sun, G. (2021). Diffusion of protein molecules through microporous nanofibrous polyacrylonitrile membranes. ACS Applied Polymer Materials, 3(3), 1618-1627.

Zhu, J., Bahramian, Q., Gibson, P., Schreuder-Gibson, H., & Sun, G. (2012). Chemical and biological decontamination functions of nanofibrous membranes. Journal of Materials Chemistry, 22(17), 8532-8540.

Zhu, J., Yang, J., & Sun, G. (2011). Cibacron Blue F3GA functionalized poly (vinyl alcohol-co-ethylene)(PVA-co-PE) nanofibrous membranes as high efficient affinity adsorption materials. Journal of membrane science, 385, 269-276.

Chapter 6. Executive Conclusion

In this dissertation, a series of studies were conducted to develop an ultra-highly sensitive colorimetric biosensor by incorporating ELISA on nanofibrous membranes. Initial investigations began with designing a portable and naked-eye distinguishable sensor for on-site detection of antibiotics. The conventional chromatography methods have limitations at on-site and instant detection because expensive facilities and complicated procedures are necessary. And portable ELISA methods are less sensitive and depend on expensive detectors. Contrarily, possessing ultrahigh surface area and abundant reactive sites, nanofibrous membranes could enhance the sensitivity of ELISA and reveal a strong colorimetric signal for naked eye distinguishing. The PVA-co-PE

nanofibrous membranes were successfully modified by reactive agents, and antibodies were successfully immobilized onto the modified membranes. As-prepared membranes revealed homogenous and bright color while capturing CAP-HRP and reacting with dye substrate. Especially, the CC modified membranes exhibited higher sensitivity for naked-eye detection and stable colorimetric signal. The novel developed nanofibrous membrane-based biosensors exhibited high sensitivity for detecting CAP at 0.3ng/mL level with the naked eyes, while the conventional ELISA could detect above 10ng/mL of CAP with the naked eyes. The nanofibrous membrane-based biosensors were fabricated to rapidly determine whether the CAP residues were beyond the benchmark concentration or not. Meanwhile, the nanofibrous membrane biosensor could quantitively measure CAP via a smartphone, and a test with spiked salmon proved the sensor could detect a trace amount of CAP in the real seafood samples.

Then, to improve the antibody capacity and sensitivity of the nanofibrous membrane biosensors, the hindered diffusion behavior of large biomolecules inside membranes was studied. Different from 3-D homogenous material, the electrospun nanofibrous membranes possess vertically heterogeneous structures and layered unparallel pores resulting in smaller effective pore sizes in the membranes. The effective pore size has a dominating impact on molecule diffusion. Thus, the diffusion coefficients of large biomolecules inside nanofibrous membranes are hundreds of times lower than the predicted results from a classical diffusion model, which is based on the research of 3-dimensional homogenous matrices. And the proteins were blocked by the nanofibrous membrane, resulting in the reduction of the benefits provided by the nanofibrous membranes. Moreover, protein diffusion is profoundly affected by protein-polymer

interactions. The polymer-protein attractions improve protein adsorption onto fiber surfaces but hinder protein diffusion into the membrane. Overall, for improving the diffusion behavior of proteins inside nanofibrous membranes, the nanofibrous membranes need to possess larger effective pores and be more hydrophilic.

In addition, the sensitivity of the nanofibrous membrane ELISA biosensors was significantly improved by optimizing the diffusion properties of protein through the nanofibrous membranes. The pore sizes of electrospun nanofibrous membranes were enlarged by increasing the concentration of PVA-co-PE polymer. And, the hydrophilicity was improved by employing hydrophilic modification agents, such as N, N'-disuccinimidyl carbonate. The diffusion test and confocal results proved the antibodies could penetrate and homogenously distributed into the nanofibrous membranes. As a result, the sensitivity of as-fabricated nanofibrous membrane ELISA was dramatically improved. The LOD for CAP detection was 0.005ng/mL, around two hundred times lower than the LOD of a conventional paper-based biosensor. Meanwhile, the biosensors could achieve quantitative analysis by recording the RGB value of optical images taken by a smartphone. And, the biosensors exhibited the desired selectivity to target antibiotics and stability after long-term storage.

In conclusion, the nanofibrous membrane ELISA biosensors were successfully developed and fabricated with ultra-high sensitivity and naked-eye distinguishable colorimetric signal. Such biosensors have the potential to be applied for on-site inspection and rapid determination of trace toxicants in food and the environment.